Optical Network Design, Modelling and Performance Evaluation for the Upgraded LHC at CERN

A thesis submitted for the degree of Doctor of Philosophy (PhD)

by

Spyridon Papadopoulos

Communications and Information Systems Research Group

Department of Electronic and Electrical Engineering

University College London

April 2013

Statement of Originality

I, Spyridon Papadopoulos confirm that the work presented in this thesis is my own. Where information has been derived from other sources, I confirm that this has been indicated in the thesis.

Signed:

Date:

To the memory of my mother

"The secret of Happiness is Freedom, and the secret of Freedom, Courage." - Thucydides (460 BC - 395 BC)

"At his best, man is the noblest of all animals; separated from law and justice he is the worst." - Aristotle (384 BC - 322 BC)

Abstract

This thesis considers how advances in optical network and optoelectronic technologies may be utilised in particle physics applications. The research is carried out within a certain framework; CERN's Large Hadron Collider (LHC) upgrade. The focus is on the upgrade of the "last-tier" data links, those residing between the last information-processing stage and the accelerator. For that purpose, different network architectures, based on the Passive Optical Network (PON) architectural paradigm, are designed and evaluated. Firstly, a Time-Division Multiplexed (TDM) PON targeting timing, trigger and control applications is designed. The bi-directional, point-to-multipoint nature of the architecture leads to infrastructure efficiency increase. A custom protocol is developed and implemented using FPGAs. It is experimentally verified that the network design can deliver significantly higher data rate than the current infrastructure and meet the stringent latency requirements of the targeted application. Consequently, the design of a network that can be utilised to transmit all types of information at the upgraded LHC, the High-Luminosity LHC (HL-LHC) is discussed. The most challenging requirement is that of the high upstream data rate. As WDM offers virtual point-to-point connectivity, the possibility of using a Wavelength-Division Multiplexed (WDM) PON is theoretically investigated. The shortcomings of this solution are identified; these include high cost and complexity, therefore a simpler architecture is designed. This is also based on the PON paradigm and features the use of Reflective Electroabsorption Modulators (REAM) at the front-end (close to the particle collision point). Its performance is experimentally investigated and shown to meet the requirements of a unified architecture at the HL-LHC from a networking perspective. Finally, since the radiation resistance of optoelectronic components used at the front-end is of major importance, the REAM radiation hardness is experimentally investigated. Their radiation resistance limits are established, while new insights into the radiation damage mechanism are gained.

Acknowledgements

The work described in this thesis was carried out at CERN and UCL. It would not have been possible without the significant contribution of a number of people, to whom I am highly indebted.

Foremost, I would like to thank my academic supervisor, Prof Izzat Darwazeh, Head of the Communications and Information Systems Group of University College London, for his continuous support and guidance throughout the 4 years of my PhD. Izzat, apart from being an excellent supervisor from an academic perspective, has also been a real friend, supporting me during strenuous times. Furthermore, he is essentially the person who gave me the opportunity to realize my childhood dream of completing a PhD. By making me aware of the life-changing opportunity to join CERN and ACEOLE, Izzat enabled me to realize that dream.

I owe gratitude to Dr Francois Vasey, Leader of the PH-ESE-BE Section of CERN for his critical interventions at key points of my PhD without which its completion would not have been possible. Francois' skillful management have shaped the course of my PhD. I consider myself lucky to have worked with someone like Francois, who gave me the freedom to carry out my own research while intervening at the right time to steer my efforts to the correct direction. Francois, with his outstanding work ethics and wise decision-making has been a role model for me.

I would like to thank my CERN supervisor, Dr Jan Troska, for his help during the radiation damage tests, described in Chapter 7 of the thesis. His knowledge on the radiation damage mechanisms of optoelectronic devices has been very useful in explaining the outcome of the tests. I would also like to thank Jan for sharing his knowledge on LHC operation aspects, as well as on the LHC upgrade plans. The information he provided has been particularly useful during the requirements gathering phase, described in Chapter 2.

Special thanks go to Dr Ioannis Papakonstantinou, a former colleague at CERN, now a Lecturer at University College London, for providing me significant insights on how to carry out research and write scientific documents. I would also like to thank Ioannis for leading the work on the TDM PON, presented in Chapter 4, as well as for his friendship which made my stay at CERN pleasant.

I would particularly like to thank my CERN colleagues, Csaba Soos, Sarah Seif El-Nasr Storey and Christoph Sigaud. I would like to thank Csaba for the FPGA implementation of the ONU and OLT transceivers presented in Chapter 4 and Sarah and Christoph for their critical help in setting up the irradiation tests described in Chapter 7. I would like to thank all my CERN colleagues of the PH-ESE-BE Section for making my stay at CERN a pleasant experience. I would particularly like to thank Sarah, Csaba and Paul Anthony Haigh for being really good friends and supporting me throughout this period.

My project work was funded by ACEOLE, a Marie Curie mobility action at CERN; part of the European Commission's 7th Framework Programme. I am particularly grateful to Robert Andrew McLaren and Seamus Hegarty, who ably managed ACEOLE at CERN. Robert and Seamus offered me the possibility to attend high-quality courses that greatly enhanced my soft skills; I would like to thank them not only for the excellent selection of appropriate courses that were very suitable for my training needs, but also for the wonderful experiences I gained as a member of the ACEOLE team.

I would also like to thank my colleagues at UCL. Specifically, I would like to thank Dr Manoj Thakur of UCL for his help during the tests presented in Chapter 6 of the thesis. Special thanks go to Ryan Grammenos for his help with Latex during thesis writing. Ryan also offered me great support during the period of my mother's illness, for which I am grateful. I would also like to thank Ryan, along with Yu Chen and Pedro Moreira, for making my stay at UCL enjoyable and colorful.

Last but not least I would like to thank my parents and my sister. My parents for instilling in me the right values that enabled me to persist through all the challenges of the PhD journey and together with my sister for their support throughout this journey. I am particularly grateful to them for taking on their shoulders the bulk of the burden of my mother's illness during the last stages of the PhD. If this had not happened I believe that the outcome of the journey would not have been positive.

Finally, I would like to thank my partner, Ada Richman, for her patience and for the moral support she generously offered me throughout these years. I would also like to thank her for the many pleasant moments she offered me that made the journey enjoyable.

Contents

List of Figures

List of Tables

List of Abbreviations

AC	Alternating Current
ADC	analog-to-digital converter
ALICE	A Large Ion Collider Experiment
APD	Avalanche Photodiode
APON	ATM PON
ASE	Amplified Spontaneous Emission
ATLAS	A Toroidal LHC Apparatus
ATM	Asynchronous Transfer Mode
AWG	Arrayed Waveguide Grating
BAWG	Broadcast AWG
BER	Bit-Error Rate
BGP	Bandwidth Guaranteed Polling
BLS	Broadband Light Source
BPON	Broadband PON
BT	British Telecomms

CDMA	Code Division Multiple Access
CDR	Clock and Data Recovery
CMS	Compact Muon Solenoid
CO	Central Office
CW	Continuous-Wave
CWDM	Course Wavelength-Division Multiplexing
DAC	digital-to-analog converter
DAQ	Data Acquisition
DBA	Dynamic Bandwidth Allocation
DBR	Distributed Bragg Reflector
DBRu	Dynamic Bandwidth Report upstream
DC	Direct Current
DCA	Digital Communications Analyzer
DEB	Deterministic Effective Bandwidth
DFB	Distributed Feedback
DiffServ	Differentiated Services
DSL	Digital Subscriber Line
DSP	Digital-Signal Processing
DUT	device under test
DWDM	Dense Wavelength-Division Multiplexing
ECAL	Electromagnetic Calorimeter
ECL	External Cavity Laser

ECS	Experiment Control System
EDFA	Erbium-Doped Fiber Amplifier
EFM	Ethernet in the First Mile
EPON	Ethernet PON
FFT	Fast Fourier Transform
FIFO	First In First Out
FKE	Franz-Keldysh Effect
FM-to-AM	frequency modulation to amplitude modulation
FP-LD	Fabry-Perot Laser Diode
FPGA	Field-Programmable Gate Array
FSAN	Full Service Access Network
FSK	Frequency Shift Keying
FTTH	Fiber-To-The-Home
FTTx	Fiber-To-The-x
GBT	Gigabit Transceiver
GCSR	Grating-assisted Coupler with Sampled Reflector
GPIB	General Purpose Interface Bus
GPON	Gigabit PON
GTC	GPON Transmission Convergence
HCAL	Hadronic Calorimeter
HL-LHC	High-Luminosity Large Hadron Collider

IEEE	Institute of Electrical and Electronics Engineers
IFFT	Inverse Fast Fourier Transform
IntServ	Integrated Services
IP	Internet Protocol
IPACT	Interleaved Polling with Adaptive Cycle Time
ISI	Inter-Symbol Interference
ITU	International Telecommunications Union
L1A	Layer 1 Accept
LAr	Liquid Argon
LD	Laser Diode
LED	Light Emitting Diode
LHC	Large Hadron Collider
LHCb	LHC-beauty
MAC	Medium Access Control
MEMS	Micro-Electro-Mechanical Systems
MPCP	Multipoint Control Protocol
MPN	Mode Partition Noise
MQW	Multiple Quantum Wells
MZM	Mach-Zehnder modulator
OCDM	Optical Code Division Multiplexing

OCDMA	Optical CDMA
OFDM	Orthogonal Frequency Division Multiplexing
OFDMA	Orthogonal Frequency Division Multiple Access
OLT	Optical Line Terminal
ONU	Optical Network Unit
OSA	Optical Spectrum Analyzer
PCS	Physical Coding Sublayer
PISO	Parallel Input to Serial Output
PLL	Phase-Locked Loop
PMA	Physical Medium Attachment
PON	Passive Optical Network
PPM	Pulse Position Modulation
PRBS	Pseudo-Random Binary Sequence
QCSE	Quantum Confined Stark Effect
QD	Quantum-Dot
QD-LD	Quantum-Dot Laser Diode
QoS	Quality of Service
QW	Quantum Well
REAM	Reflective Electroabsorption Modulator
RIN	Relative Intensity Noise
rms	root mean square

RSOA	Reflective Semiconductor Optical Amplifier
SCM	Sub-Carrier Multiplexing
SCT	Semiconductor Tracker
SEE	Secondary Electron Emission
SG-DBR	Sampled Grating-Distributed Bragg Reflector
SLED	Superluminescent Light Emitting Diode
SNR	Signal-to-Noise Ratio
SOA	Semiconductor Optical Amplifier
SSC	Superconducting Super Collider
T-CONT	Transport Container
TDM	Time-Division Multiplexing
TDM PON	Time-Division Multiplexing Passive Optical Network
TDMA	Time Division Multiple Access
TODC	turn-on delay compensation
TRT	Transition Radiation Tracker
TTC	Timing, Trigger and Control
TTCex	TTC transmitter
TTCrx	TTC receiver
TTS	Trigger Throttling System
VCO	Voltage-Controlled Oscillator
VCSEL	Vertical Cavity Surface Emitting Laser

WDM	Wavelength-Division Multiplexing
WDM PON	Wavelength-Division Multiplexing Passive Optical Network
WDMA	Wavelength Division Multiple Access

List of Mathematical and Greek Symbols

$L_{AWG,insertion}$	AWG insertion loss
α_{AWG}	AWG loss
B_{br}	Chirping-induced spectrum broadening
$L_{Ch,B}$	Broadcast channel loss
B	Bit rate
$B_{BLS,3dB}$	BLS 3-dB linewidth
CRR	Channel Readout Ratio
C	Chirp parameter
C_L	Channel loss
Δv_{ch}	Channel spacing
$\alpha_{circulator}$	Circulator loss
C	Compression ratio
α_{con}	Connector losses
D	dispersion parameter
δ_d	Dispersion power penalty

$\alpha_{pen,ds}$	Downstream power penalty
$M_{S,ds}$	Downstream power margin
A_{eff}	Optical fiber effective core area
L_{eff}	Effective interaction length
$\bar{\alpha_H}$	Effective Henry parameter
C_{EPON}	EPON cost
$C_{ONU,EPON}$	EPON ONU cost
SR_{EPON}	EPON splitting ratio
δ_{ex}	Extinction ratio power penalty
B_{excess}	Excess required bandwidth
$\alpha_{excess,spl}$	Excess splitter loss
r_{ex}	Extinction ratio
α_f	Fiber loss per kilometer
α_{filter}	Filter loss
G	Amplifier gain
C_{GPON}	GPON cost
$C_{ONU,GPON}$	GPON ONU cost
SR_{GPON}	GPON splitting ratio
β_2	Fiber group-velocity dispersion
α_H	Henry's parameter
δ_X	Crosstalk-induced power penalty
T_1	Half-width at 1/e intensity point after transmission
T_0	Half-width at 1/e intensity point before transmission
k	Imaginary part of complex refractive index

X	Integrated transmittivity
L	Link length
T_{mn}	Transmittivity between channels m and n
N	Number of channels/users
C_{OLT}	OLT cost
$\bar{P}_{rec,ONU}$	ONU receiver sensitivity
B_o	Optical bandwidth
D	Overall aggregate data rate
OH	Overhead
P_{ch}	Power per channel
I_1	Average photocurrent at "mark" level
I_0	Average photocurrent at "space" level
P_{in}	Input light intensity
$P_{out}(V)$	Output light intensity
$P_{AWG,Input}(f)$	Power spectrum at the AWG input port
$P_{AWG,Output}$	Power at the AWG output port
$P_{ch,Seed}$	Required power per channel at light source
$P_{ch,Tx}$	Required power per channel
P_1	Power at "mark" level
α_{pen}	Power penalty
P_0	Power at "space" level
z	Propagation distance
P_{th}	Power threshold limit
S_R	Raman gain slope

δ_R	Raman scattering power penalty
D_R	Fractional power loss due to Raman scattering
$\alpha_{REAM,ins}$	REAM insertion loss
$\alpha_{ream,ER}$	REAM extinction ratio power penalty
$\alpha_{ream,overall}$	REAM overall power penalty
$R_{ONU,eff}$	Effective data transmission rate per ONU
R	Required number of bits per single channel readout
n	Real part of complex refractive index
R_{us}	Overall upstream data rate
$\bar{P}_{rec}$	Average received power
σ_1	Noise standard deviation at "mark" level
$L_{slicing}$	Spectrum slicing loss
σ_λ	Source linewidth
α_{spl}	Splitting losses
M_s	System margin
$T_{OH,8b/10b}$	Duration of 8b/10b encoding overhead
T_{cdr}	Clock recovery related overhead
$T(V)$	REAM transfer function
T_{gap}	Additional required time for receiver sensitivity recovery
T_{IFG}	Inter-frame gap
T_{off}	Duration of laser switch-off time overhead
$T_{OH,BM}$	Duration of burst-mode operation overhead
$T_{OH,Protocol}$	Duration of protocol-related overhead
T_{on}	Duration of laser switch-on time overhead

$T_{overhead}$	Duration required to transmit overhead information
$T_{preamble}$	Preamble duration
TR	Trigger rate
T_{switch}	Duration between subsequent ONU transmissions
T_{th}	Threshold recovery related overhead
$\bar{P}_{tr,OLT}$	Average OLT transmitted power
$\bar{P}_{tr}$	Average transmitted power
$\alpha_{pen,us}$	Upstream power penalty
$M_{S,us}$	Upstream power margin
r_X	Crosstalk-induced noise

Chapter 1

Introduction

The evolution of fundamental science has always been strongly coupled to technological advances. The expansion of the human knowledge frontier is, to a great extent, driven by the invention of new technologies. This is particularly evident in particle physics, where capturing snapshots of the outcomes of particle interactions with increasingly high time, position and energy resolution requires the use of highly sophisticated detectors. Reaching particle collision energies that allow emulating conditions that happened billions of years ago and discovering what happened at the early stages of the creation of the universe would not have been possible without the use of state-of-the-art technologies, such as advanced superconducting technologies, high speed communication systems and high power signal processing.

As much as it is true that fundamental science has greatly benefited from the use of state-of-the-art technologies, the opposite also holds. Technological advances, apart from being a driver of progress in fundamental science, were also fueled by this progress. Again, particle physics offers an abundance of examples where technological innovation was fueled by the need to meet the special requirements of particle physics experiments. The world wide web as we know it today was developed in an

effort to facilitate fast and easy communication between physicists and grid technologies would not have advanced as much as they have without the need to meet the enormous processing power requirements of large particle physics experiments.

In the research presented in this thesis both factors come into play. On one hand, our research investigates how the use of specific state-of-the-art communication technologies can facilitate progress in the field of particle physics. As modern particle physics experiments generate an enormous amount of information, higher data transmission rates essentially mean faster discoveries. Optical fiber is the medium that allows the transmission of information at the highest possible rates, therefore we focus on the use of state-of-the-art optical fiber communication technologies and the benefits these can provide. On the other hand the special requirements of particle physics experiments generate the need to carry out research in areas that would otherwise remain uncharted territories. There is no other application that requires electronic and optoelectronic devices to operate at higher radiation levels than transferring data out of particle physics detectors. This is the reason that led to our study of the radiation hardness of optoelectronic devices at radiation levels never studied before. Much of the research reported in this thesis was carried out while the author was a Marie Curie Fellow at CERN.

1.1 Motivation

Our research is carried out within a specific framework; the upgrade of the largest and most powerful particle accelerator in the world, the Large Hadron Collider (LHC). The LHC will generate $\sim 10^9$ particle collisions/second, at its design luminosity. Particle collisions take place at four points around LHC's 27 km circumference. Each collision point is surrounded by special detectors, called "experiments", designed to detect and reconstruct what happens during the collisions [1]. In-

evitably the magnitude of the collision rate leads to significant technical challenges that need to be addressed. Tens of thousands of optical links are currently installed at the four LHC experiments to meet the data rate requirement that on aggregate is comparable to the global Internet traffic. The optoelectronic components installed on-detector are tested up to very high radiation levels to ensure that they remain operational in the harsh radiation environment close to the collision point. The upgrade of the LHC to High-Luminosity Large Hadron Collider (HL-LHC) that will lead to a luminosity increase by an order of magnitude from the current 10^{34} to 10^{35} $\mathrm{cm}^{-2}\mathrm{s}^{-1}$ [2] is set to increase both the required data rate and the amount of radiation dose that all on-detector components will be exposed to.

The change in the data rate requirement and the radiation levels makes an optical link upgrade necessary. The new, upgraded infrastructure must meet the data rate requirements and the optoelectronic components installed on-detector must be tested up to the - much higher - radiation levels they will need to withstand at the HL-LHC. The optical link upgrade, apart from being a necessity, is also an opportunity. It is an opportunity to move to a network infrastructure allowing more efficient use of network resources through the introduction of new technologies. Most of the major design decisions related to the optical link infrastructure for the LHC were taken in the early 2000s. Since then optical network and optoelectronic technologies have advanced significantly. This progress could now be used to deliver better results, in a more efficient way, to the particle physics community.

1.2 Research Goals

Generating new knowledge regarding the way advances in optical network and optoelectronic technologies can be used to benefit the particle physics community within the framework of the LHC upgrade is the primary goal of this research. Particu-

larly, the focus is on a specific suite of emerging optical fiber technologies - Passive Optical Networks (PONs). PONs promise to deliver the high bandwidth benefits of the fiber to the end users in a cost-efficient manner therefore their use at the HL-LHC could be advantageous in terms of infrastructure efficiency. Their point-to-multipoint structure serves well this purpose since it enables resource sharing. PONs come in many flavors. The aim of this research is to come up with appropriate optical link architectures based on the PON paradigm and evaluate their potential for particle physics applications. The applications of interest are those related to the distribution of specific types of information; namely the Timing, Trigger and Control (TTC), and the data readout signals. Our aim is to utilise a PON (or a PON-like) architecture for the upgrade of the "last-tier" of links that transfer these types of information, i.e. the links residing between the last information-processing stage and the accelerator.

The "last-tier" of links that transfer information face the most demanding data rate and radiation hardness requirements and they will be most affected by the LHC upgrade. The optoelectronic components installed on the detector side operate in a highly radiative environment. Therefore much of the effort in developing the electronics and optoelectronics for the LHC went into irradiation testing and qualification; this will also be true for the HL-LHC. Research on the radiation hardness of optoelectronic components whose radiation resistance limits have not been clearly established is of particular interest to the particle physics community. Such research is of high importance as it has the potential of identifying radiation-immune optoelectronic components - or at the very least it can ensure that the current choice of optoelectronic components is the optimal. Consequently, a second major goal of the research reported in this thesis is to investigate the radiation hardness of any optoelectronic components we propose for use close to the particle collision point.

1.3 Contributions

Throughput the research discussed in this Thesis a number of PON architectures, especially tailored for particle physics applications, were designed and evaluated. The main original contributions of this work are listed below:

- Design and performance assessment of a Time-Division Multiplexing Passive Optical Network (TDM PON) for the distribution of TTC signals at the HL-LHC. The related work is described in Chapter 4 of the thesis.

- Design and performance evaluation of a custom architecture that is based on Wavelength-Division Multiplexing Passive Optical Network (WDM PON) technology. The architecture is intended for transmission of all types of information at the HL-LHC. The related work is reported in Chapter 5 of the thesis.

- Identification of the factors that limit the applicability of WDM PONs at the HL-LHC - also discussed in Chapter 5 of the thesis.

- Design and performance evaluation of a custom, simplified architecture, based on the PON concept and the use of Reflective Electroabsorption Modulators (REAMs) for transmission of all types of information at the HL-LHC. The relevant work is reported in Chapter 6 of the thesis.

- Evaluation of the radiation hardness of the REAMs at unprecedented levels of irradiation. The irradiation tests established, for the first time, the limits of operation of the particular device and shed light into the radiation-induced performance degradation mechanism. The irradiation tests are discussed in Chapter 7 of the thesis.

1.4 Thesis Structure

This Thesis is structured as follows:

Chapter 2, explores the networking and special requirements of the "last-tier" links of the HL-LHC. During this process, the principles of operation of the LHC are briefly described and the different types of information that need to be transmitted from and to the detectors for their smooth operation are identified. The basic links between detector operation and network requirements are provided and the potential impact of an upgrade on them is described. Consequently the technical characteristics of the current links are described and a specific detector is used as a case study to demonstrate how the upgrade is going to affect the network requirements.

In Chapter 3, a literature survey of PON architectures is carried out. The different types of PON technologies are reviewed as well as the main challenges associated to each along with solutions suggested in the literature.

In Chapters 4, 5 and 6 the information presented in Chapters 2 and 3 is utilised to design appropriate network architectures based on PONs that can deliver benefits in a particle physics environment.

Chapter 4 describe work on a new TDM PON architecture that can be used for the distribution of TTC information. Work on physical layer network design, protocol design as well as work that is associated to the special timing requirements of the particular system is described.

Chapter 5 describes the process of designing a PON aiming to transfer all types of information - data, trigger feedback and TTC information - at the upgraded HL-LHC using a single, unified architecture. The reasoning behind the selection of Wavelength-Division Multiplexing (WDM) as the technology of choice is described. The network design process is outlined, while at the same time the limitations of

the architecture are discussed. The chapter is concluded with a critical assessment of the architecture.

Chapter 6 discusses the design of a PON-like custom architecture that could accommodate all types of traffic at the HL-LHC. The design and qualification process is described, demonstrating that the architecture can meet the system requirements as described in Chapter 2.

Chapter 7 describes the irradiation tests carried out on REAMs. The chapter starts with a description of the test setup and moves on to the discussion of results. The impact of radiation both at the component and at the system-level is analyzed.

Chapter 8 concludes this thesis by providing a summary of the work and the main contributions. Suggestions on how the work reported in this thesis can be continued in the future are also made.

1.5 List of Publications

The work presented in this thesis has led to a number of publications. The author of the thesis was the lead author in the following publications (in reverse chronological order):

1. S. Papadopoulos, S. Seif El Nasr-Storey, J. Troska, I.Papakonstantinou, F. Vasey and I. Darwazeh, "Component and System Level Studies of Radiation Damage Impact on Reflective Electroabsorption Modulators for Use in Multi-Gb/s HL-LHC Data Transmission," IEEE Transactions on Nuclear Science, vol. 60, no. 1, pp. 386-393, Feb. 2013.

2. S. Papadopoulos, I. Darwazeh, I. Papakonstantinou, J. Troska and F. Vasey, "An electroabsorption modulator-based network architecture for particle physics applications," Journal of Instrumentation, vol. 6, no. 12, p. C12012, 2011.

3. S. Papadopoulos, I. Papakonstantinou, F. Vasey, J. Troska and I. Darwazeh, "Temperature Variation Effects in a Reflective Electroabsorption Modulator-Based Network Architecture for Particle Physics Applications," London Communications Symposium, September 2011.

4. S. Papadopoulos, I. Papakonstantinou, F. Vasey, J. Troska and I. Darwazeh, "A Network Architecture for Bidirectional Data Transfer in High-Energy Physics Experiments Using Electroabsorption Modulators," in Networks and Optical Communications (NOC), 2011 16th European Conference on, July 2011, pp. 6871.

5. S. Papadopoulos, I. Darwazeh, J. Troska, I. Papakonstantinou, C. Soos, F. Vasey and J. Mitchell, "Passive optical networks for particle physics applications," London Communications Symposium, September 2009.

The author of the Thesis has also co-authored a number of publications, that are related to the work presented in this Thesis. These are the following (in reverse chronological order):

6. I. Papakonstantinou, C. Soos, S. Papadopoulos, S. Detraz, C. Sigaud, P. Stejskal, S. Storey, J. Troska, F. Vasey, and I. Darwazeh, "A Fully Bidirectional Optical Network With Latency Monitoring Capability for the Distribution of Timing-Trigger and Control Signals in High-Energy Physics Experiments," IEEE Transactions on Nuclear Science, vol. 58, no. 4, pp. 1628 1640, Aug. 2011.

7. I. Papakonstantinou, C. Soos, S. Papadopoulos, S. Detraz, C. Sigaud, P. Stejskal, S. Storey, J. Troska, F. Vasey, "Passive Optical Networks for Timing-Trigger and Control Applications in High Energy Physics Experiments," Real-Time Conference, 2010.

8. I. Papakonstantinou, C. Soos, S. Papadopoulos, J. Troska, F. Vasey, S. Baron, L. Santos, S. Silva, P. Stejskal, C. Sigaud, S. Detraz, P. Moreira, and I. Darwazeh, "Passive optical networks for the distribution of timed signals in particle physics experiments," Topical Workshop on Electronics for Particle Physics, pp. 352-356, September 2009.

Chapter 2

Requirements for the Upgraded Optical Links at the HL-LHC

The problem definition phase is typically an integral and critically important part of any problem solving process. This is exactly why the work on identifying how to best use state-of-the-art optical network and optoelectronic technologies to upgrade the LHC optical links, that is the purpose of this thesis, has to start with a requirements definition phase. The discussion of the upgraded optical link requirements is the topic of this chapter. The focus is on the requirements of the links related to the applications of interest, i.e. the transmission of TTC and data readout signals. To capture the requirements of the upgraded links the connection between accelerator and detector operation on one hand and optical link requirements on the other has to be established. Providing background information related to the operation of the LHC is a necessary prerequisite to establish that link. The currently installed optical links and their performance can then be used to demonstrate this relationship at work. After defining the connection between detector attributes and optical link performance parameters, it is meaningful to identify the main accelerator and

detector attributes that are going to be affected during the transition to the HL-LHC. Analysis of how these changes are going to impact the upgraded optical link requirements follows. The upgraded optical links of the Compact Muon Solenoid (CMS) tracker are used as a case study to demonstrate how the LHC luminosity upgrade is going to affect the optical link requirements.

The requirements definition process carried out in this chapter follows a certain methodology. One of its central features is that the requirements are defined with respect to specific network performance metrics that are critical for the operation of the detectors. As the ultimate purpose of our research is to design an architecture that can accommodate the requirements of any detector at any experiment of the HL-LHC, an additional very important feature of the analysis, is the identification of the most "demanding" detector for each metric. Such detector, essentially acts as a bottleneck, therefore it is the one that defines the requirement for the particular metric. These features of the methodology are present throughout the chapter, but they are mostly reflected at the conclusion, where the performance requirements for a unified architecture that could be used to transmit TTC and data readout signals at any of the detectors of the HL-LHC are defined. The conclusion of this chapter is of very high significance for the subsequent work discussed in this thesis, as all the network designs described in the following chapters are based on the requirements set there. It is also important to note that the requirements discussed throughout the chapter are based on the LHC upgrade plans at the end of 2009/beginning of 2010, when the requirements gathering phase was carried out.

2.1 LHC Operation Principles and Required Link Infrastructure

The LHC is the largest particle accelerator in the world as the LHC tunnel has a circumference of 27 km. Inside the LHC two counter-propagating beams of particles, comprised of particle bunches, collide at four points around the LHC (Figure 2.1). At its design luminosity of 10^{34} $\text{cm}^{-2}\text{s}^{-1}$, the LHC will generate $\sim 10^9$ collisions/second [1]. The beam pipe at the collision points is surrounded by special detectors, called "experiments", designed to detect and reconstruct what happens during the collisions [3].

Figure 2.1: The LHC and its experiments [4].

Each of the four LHC experiments uses a number of sub-detectors to detect the different particle species generated during the collisions. As different particle types interact with matter in different ways, each sub-detector utilises a specific type of particle-matter interaction to detect particles. Ultimately all sub-detectors generate electrical signals conveying information about particle properties. To provide an example of this concept, Figure 2.2 shows a transverse slice of the CMS detector, also showing its sub-detectors. The structure of the CMS detector is typical of a modern particle physics experiment and other LHC experiments have a similar structure. As shown in the figure the main sub-detectors of the CMS experiment

are the tracker, the Electromagnetic Calorimeter (ECAL), the Hadronic Calorimeter (HCAL) and the Muon Detector. The tracker deploys ionization to detect charged particles, while other sub-detectors, such as the calorimeters, use different mechanisms. So, the ECAL uses the electromagnetic cascade initiated by photons and electrons and the HCAL identifies hadrons and muons that can initiate a hadronic cascade through interaction with the nucleus of the material [5]. Sub-detectors may also differ in the quantities they measure. For instance, the tracker is placed inside an intense magnetic field and its primary purpose is to reconstruct the trajectory of charged particles. That way the charge and momentum of the charged particles can be determined. The ECAL, on the other hand, measures the energy of photons and electrons by collecting the light generated by the electromagnetic cascade and converting it to electrical signal. From a networking point of view it is important to note that sub-detectors differ in their data generating capacity. This depends on a number of factors, including the detector resolution in terms of the measured quantity and the granularity of the sub-detector; sub-detectors are not monolithic structures, but consist of a large number of small detector elements to locate the detected particles. Design decisions related to the way a detector is read out also have an impact on the required data rate.

Having touched on the operation of a detector and its impact on network requirements, the discussion can move on to higher-level aspects related to the requirements of an experiment from a networking point of view. A system level diagram of a typical detector and the types of data links that are currently being used to facilitate its operation is shown in Figure 2.3. A variety of types of links are currently in use, to support different functionalities. From a system-level perspective the accelerator is merely a particle generator. As the diagram depicts, the particles are input to the next component, the detectors, which generate electrical signals, that depend upon the particle properties. The signal is processed and temporarily

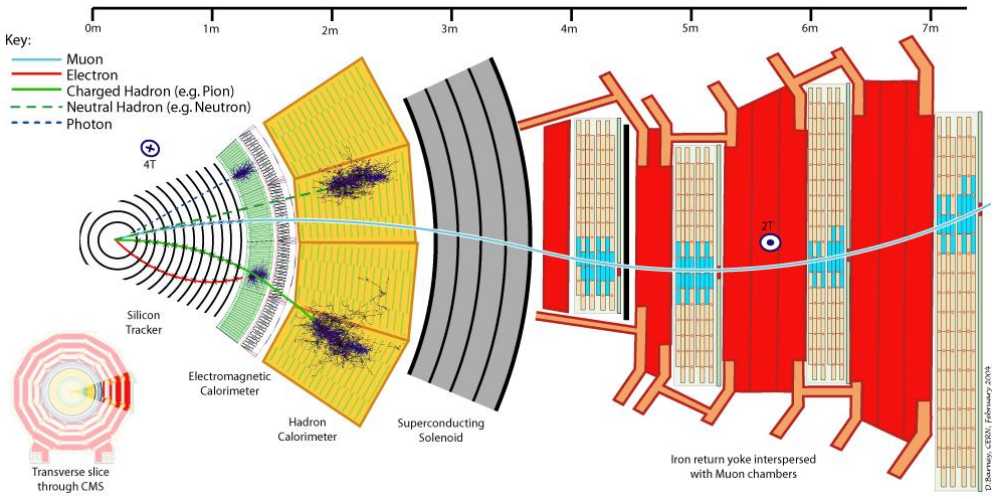

Figure 2.2: Transverse slice of CMS detector [6].

stored by the front-end electronics - the term detector is often used to describe both the particle detector and its associated electronics. Typical operations carried out by the front-end electronics are pre-amplification, i.e. current-to-voltage conversion, further amplification and signal shaping; analog-to-digital conversion is also a task that may be performed by the front-end electronics, depending on whether analog or digital signals are transmitted over the data readout links. The final front-end electronic component is the storage pipeline, which may be analog or digital, depending on the design. Whether to place an analog-to-digital converter at the front-end or not is an excellent example of a design choice that directly affects the obtained data rate.

The required data rate is also greatly affected by the operation of the trigger mechanism. The trigger evaluates whether an interesting event has happened, in order to filter unnecessary information and reduce the data rate requirements. Thus some information will be discarded and only part of it will be transmitted (over the Data Acquisition (DAQ) links of Figure 2.3). As shown in Figure 2.3 the electronics facilitating the trigger decision - Trigger Processor - are located at the counting

room. Information required by the Trigger Processor to take the decision is transmitted from the detector to the Processor over the Trigger Links. The readout decision is sent downstream over the same network that transmits the system clock, comprised of the TTC links. Synchronization is also a function necessary for the operation of a detector. The beams of particles circulating around the accelerator are not continuous; they contain bunches of particles that collide periodically. The two types of synchronization signals - the clock and the trigger - are required to associate the signals with the collision that has generated them and to synchronize data-taking across the experiment. The control network (Experiment Control System (ECS) shown in Figure 2.3) is required in order to facilitate transport of control and configuration commands, [1], [7].

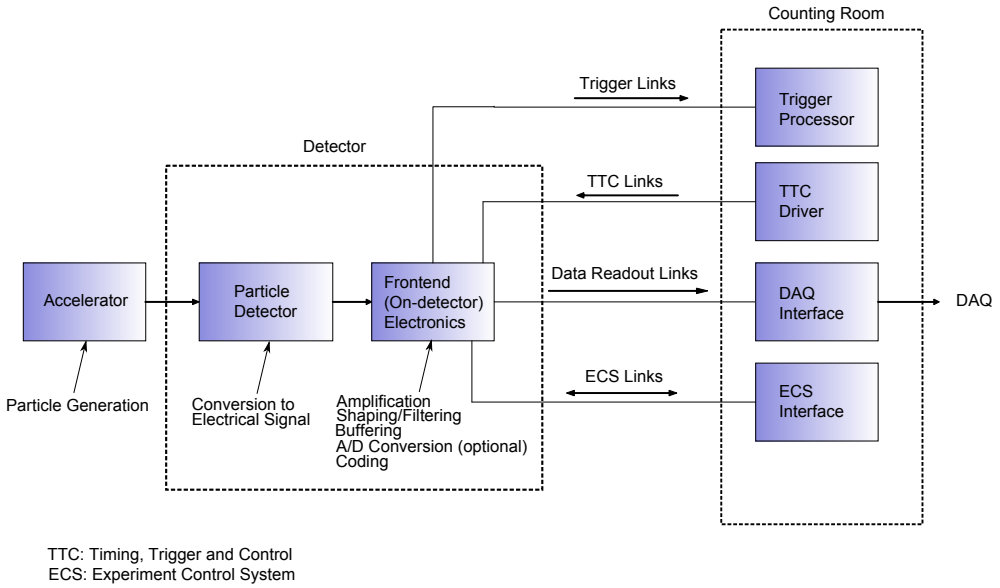

Figure 2.3: High-level view of the detector and its links.

2.2 Discussion of Selected Link Performance Indicators

In order to assess a specific technology and decide on its suitability for use at the LHC experiments, appropriate performance metrics need to be selected. Performance with respect to these metrics should reflect how well a technology covers the operational requirements of the LHC detectors (from now on the term experiment will be used to refer to a collection of sub-detectors, while the sub- before the sub-detector will be dropped and the tracker, the calorimeters etc., will be referred to as simply detectors). Some of the metrics are commonly used in commercial telecommunications networks, while others are important mainly because of the particularities of the application in hand.

Aggregate Data Rate The aggregate supported data rate is a very important metric for the operation of a particle detector, as there is a direct link between the rate of data production by the detector and the particle generation capacity of the accelerator. A high supported aggregate data rate is required to support a high particle generation rate by the accelerator that is always desirable in particle physics. High particle generation rates resulting from a high collision rate lead to faster discoveries, while particle collision at higher energies - that in general results in higher number of particles generated per collision - allow studying particle interactions that do not take place at lower energies.

However, the particle generation capacity of the accelerator is not the only factor determining the required aggregate data rate. The discussion of the detector operating principles showed that the required data rate for data read out depends on a number of factors. Factors that have been identified include the detector resolution in terms of the measured quantity and the granularity of the detector. Design decisions, such as whether to apply any encoding that would result in a reduction

of the transmitted information, any overheads, such as headers, and the trigger rate have significant impact on the resulting required data rate. The overall aggregate required data rate may be derived by considering the set of factors discussed by the equation below:

$$D = CRR * R * N * C * OH * TR \tag{2.1}$$

where:

- D is the overall average data rate requirement.
- CRR is the channel readout ratio, expressing the probability that the smallest data generating unit of the detector - the channel - has data to transmit; this probability depends on both the probability of a detector element being hit by a particle, commonly referred to as "occupancy", but also on the readout strategy. For example if a full readout is carried out the CRR as defined here is 1. However another popular readout strategy is the so-called zero-suppression. In the particle physics community the term zero-suppression is used to refer to the technique where only detector elements with a signal above a certain amplitude are being read out, in analogy to the common use in the telecoms world which means that in a digital word zeros are encoded in such a way that series of zeros can be compressed. If zero-suppression is carried out on-detector, this parameter would be equal to the occupancy of the detector, thus:

$$CRR = \begin{cases} 1 & \text{if a full readout is carried out} \\ Occupancy & \text{if zero suppression is carried out on detector} \end{cases} \tag{2.2}$$

- R is the number of bits required for a single channel readout. It depends on

the required amplitude resolution, but also on the required number of samples. R includes any information per channel transmitted in order to encode the raw data. For example if a time-stamp and an address per channel is being transmitted for a channel to indicate that the associated detector element has been hit by a particle, the corresponding number of bits used to encode these quantities are included in R.

- N is the number of channels of the detector.
- C is the compression ratio, if applicable.
- OH is the overhead; it may include timestamp, header for equalization, as well as any coding overhead, e.g. 8b/10b, depending on the detector. OH commonly refers to information that is added and is not raw data (for example during the framing process).
- TR is the trigger rate. At this stage it can be demonstrated, using an example, why the trigger is required. The maximum trigger rate for the CMS experiment is 100kHz. The collision rate is 40MHz, therefore the trigger reduces the data rate requirement by a factor of 400, in the case of CMS. Even after this data reduction the DAQ network has to carry traffic at rates close of the order of 1 Tbps, [8]. Without use of trigger, the required data rate would rise to a staggering 400 Tbps.

Although there are significant uncertainties related to the values of the above parameters for the HL-LHC, still, the above relationship can be used to provide insight into the impact any future design decisions are going to have on the networking requirements.

An example in order to show the above equation at work and demonstrate the order of magnitude of the aggregate required data rate at the LHC can be drawn

from the CMS strip tracker. The tracker has some 9.3 Million channels (N=$9.3 * 10^6$). The analog data links of the tracker provide 8-bit equivalent resolution (R=8 bits). Although the occupancy of the channels is 1-2% a full readout is carried out, therefore the channel readout ratio used in the calculations is equal to 1 (CRR=1). For CMS the trigger rate is 100 kHz (TR=10^5 1/s). No compression is taking place (C=1), since the data is transported over analog links. The calculation of the equivalent overall data rate required to transmit the information over digital links, without taking into account the overhead of the header (i.e. OH is assumed to be 1) is shown in Table 2.1.

Table 2.1: Aggregate required data rate calculation for CMS strip tracker.

Metric	**Value**
Channel Readout Ratio (CRR)	1
Number of bits/channel readout (R)	8
Number of Channels (N)	$9.3 * 10^6$
Compression Ratio (C)	1
Overhead (OH)	1 (ignored in this example)
Trigger Rate (TR)	10^5 1/s
Aggregate data rate (D)	7.44 Tbps

As the table shows the aggregate average data rate of the CMS strip tracker is equal to 7.44 Tbps. To put this number in perspective, the average US Internet traffic estimate at the end of 2009 was ∼8.3 Tbps [9].

The aggregate data rate requirements are less challenging for links intended for other applications. The required aggregate data rate for the network distributing the trigger and clock of the system, referred to as the TTC network, is determined by the bunch crossing frequency. The information sent over this network is broadcast, so the aggregate data rate requirement is the same as the one per link. Moreover,

the trigger decision is taken once at every bunch crossing. Assuming a binary trigger decision (i.e. determining whether a full readout must be carried out or not) a data rate of twice the bunch crossing rate is enough to transmit the clock of the system and leave the spare extra bit per clock cycle required to transmit the trigger decision. As the bunch crossing rate is currently ∼40 MHz - more precisely 40.0789 MHz - a data rate multiple of the crossing rate can be easily achieved. This data rate is enough to transmit even more complex trigger commands. The aggregate data rate required by the trigger return path, facilitating the trigger decision, is mainly determined by the complexity of the trigger decision algorithm. This data rate, however, is kept to a minimum, as the trigger mechanism is meant to reduce the required aggregate data rate from the detector to the counting room and the trigger decision is always based on a small fraction of the data generated by the detector - more precisely the information used to generate a trigger is a coarse-grain view of data coming from some detectors, typically the calorimeters and the muon chambers [10]. It is important to mention that the data rate, not only of the links used for clock distribution (TTC), but also of the data readout and trigger feedback must be an integer multiple of the clock frequency, since all the links are parts of a larger synchronous system. This restricts the options when it comes to using commercial networking technologies. For example in case a data rate of 1 Gbps is required, Gigabit Ethernet is not an option, as the line rate of the links used at CERN should be either 800 Mbps or 1.6 Gbps to comply with the above mentioned rule, [10].

Data Rate per Link The aggregate data rate is a metric directly related to accelerator and detector performance. However, it is the data rate per link that is usually limited by technology and design choices. The achievable data rate per link in a particle physics experiment is affected by a number of factors. A first,

obvious factor is the maximum data rate supported by the link technology. The data rate is also limited by the availability of high speed, radiation hard electronics, as their construction is a particularly challenging and costly task. Multiplexing a high number of detector channels to transmit the information they generate using one transmitter - from now the term multiplexing ratio will be used to express this quantity, i.e. the number of detector channels multiplexed over a single link - may also be a limiting factor. The multiplexing ratio is limited by the material budget inside the detector and the power consumption. The use of long electrical links that may be required to multiplex a high number of channels over a single link will result in an increase of the material budget and the power consumption inside the detector. Increased material budget inside the detector leads to particle obstruction, thus the particles may either be stopped and remain undetected or converted into other particles that look like signals for other rare processes. Moreover, the use of long electrical links also imposes limitations on the maximum achievable data rate. The available space for a single transceiver is a constraint that must be taken into account, too, as typically the detector design drives the choice of the front-end optoelectronic components and not the other way around. Finally cost and commercial availability have to be taken into account.

It becomes apparent that the value of the data rate per link is the result of a design process that resembles a constraint optimization. In this optimization the power consumption and the material budget inside the detector have to be minimised while the data rate per link has to be maximised. The optimization has to take into account the aggregate data rate requirement, the maximum achievable data rate because of technology and radiation hardness limitations and the physical constraints inside the detector. The relative importance of the parameters to be optimized is not easy to determine. Although inner detectors, such as the tracker, have very high aggregate data rate requirements, minimising the power consumption

and material budget may be more important than maximising the data rate per link in these cases. Thus, it should not be surprising to find out that outer detectors may use higher data rate links than inner detectors.

The above discussion applies to the data readout case. For other applications, setting the data rate per link is more straightforward. For the TTC network the data rate per link has essentially the same value as the aggregate data rate as the TTC is a broadcast network. The trigger feedback links use the same technology as the data readout links, so their supported data rate is the same as the one for data readout links.

Link Length The link length for all types of links is determined by the distance between the front-end and the so called "counting room"; an underground cavern, protected from radiation, where data are aggregated to be sent to the next level of the network hierarchy. The read-out links transfer data over distances of the order of 50-150m [8], [11], [12]. This is also the case for all other types of links.

Latency and Jitter Latency and jitter are important properties of the received signal in telecommunications applications. In a particle physics environment, however, they become of critical importance. More particularly the latency of the trigger feedback loop determines the buffering requirements at the front-end. Large buffer sizes increase the material budget inside the detector, an undesirable outcome. Even more important is for the latency to be fixed and deterministic, so that it can be compensated for. Jitter - that may be interpreted as a random delay component - should therefore be minimised. The primary reason behind the low jitter requirement is the desire to use the low-frequency clock distributed by TTC to drive high speed serial links. This drives the jitter requirement to very low values as the clock multipliers needed to get to Gbps link speeds have stringent jitter

requirements.

Special Requirements All the performance metrics discussed previously appear in most analyses of a typical telecommunications network. However, any links directly attached to the detector have to meet some special "non-conventional" requirements. These include radiation hardness for the front-end components and the links that are placed in a radiation environment, low power consumption and minimisation of the material budget inside the detector.

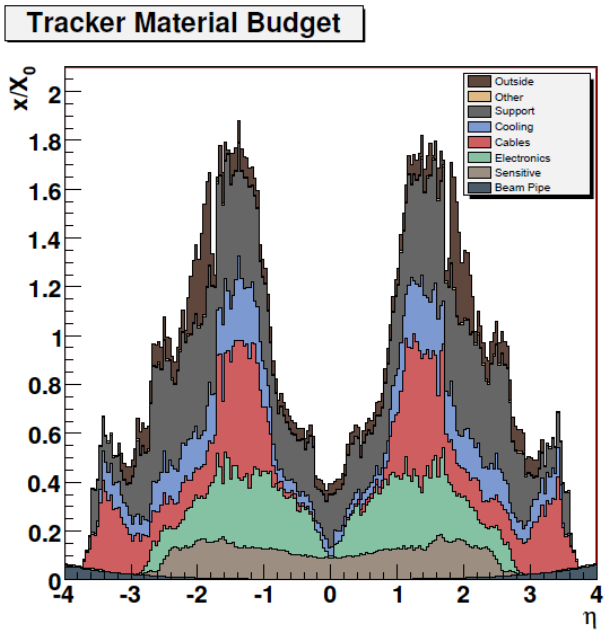

Figure 2.4: Material budget of the CMS tracker (radiation length vs. pseudorapidity) [8].

The radiation flux - i.e. the particles traversing a unit surface per unit time - is proportional to the particle generation rate and inversely related to the distance from the interaction point. The power consumption and the material budget are actually closely related, since a significant amount of material is contributed by

the cabling infrastructure necessary to transfer power to the front end components. The electronics at the front-end should be kept as simple as possible, so that they meet this requirement. Figure 2.4 depicts the different components of the material budget inside the CMS tracker. These are plotted in units of radiation length against pseudorapidity η. The radiation length that is defined as the mean distance a high energy electron can travel though a material before its energy drops to 1/e of its initial energy [13], while the pseudorapidity is a spatial variable defined as η=-ln[tan(θ/2)] , where θ is defined as the angle between the particle and the axis of the beam, [1]. A significant amount of material is attributed to electronics (colored green) and cabling (colored red). Figure 2.5 shows a cross section of the CMS tracker, which offers a visualization of the detector structure.

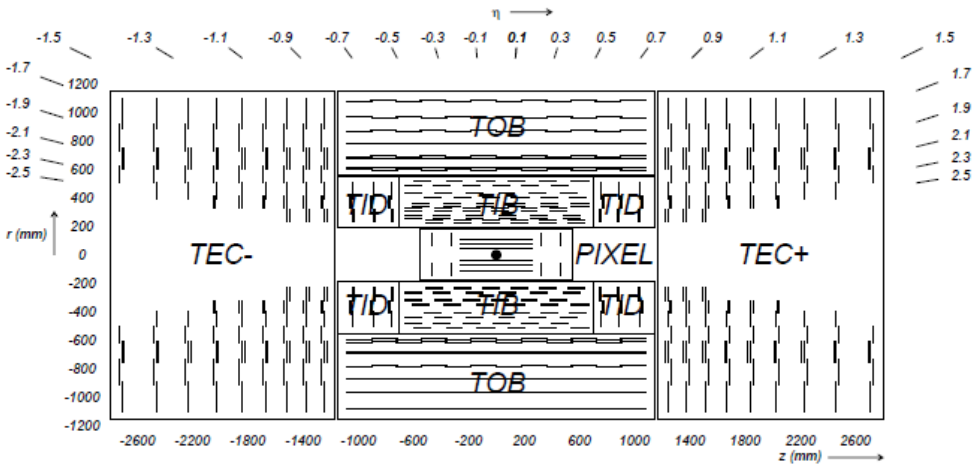

Figure 2.5: Cross section through CMS tracker [8].

Operating temperature range is an important parameter for optoelectronic components installed on-detector. It is a parameter of particular importance for components installed in parts of the experiment that have to withstand significant radiation levels. Since the damage caused by radiation is more severe at higher temperatures, these parts of the experiments are cooled to low temperatures. For

example the CMS tracker volume will need to be operated at temperatures reaching $\sim$-15^{o}C [8].

Table 2.2 summarizes the discussion of the selected performance parameters by outlining both the parameters and the main factors that determine their corresponding requirements.

Table 2.2: Summary of selected metrics and the main parameters affecting their corresponding requirements.

Metric	**Main Dependencies**
Upstream Aggregate Data Rate	Particle generation rate, spatial resolution, amplitude resolution, encoding strategy, overheads, trigger rate, on- or off-detector zero-suppression (Data Readout) Trigger decision algorithm (Trigger links)
Downstream Aggregate Data Rate	Bunch crossing frequency (TTC network)
Upstream Data Rate per Link	Maximum achievable data rate by selected technology, maximum achievable data rate by rad-hard electronics, power consumption constraints, mass/physical constraints, cost, commercial availability
Downstream Data Rate per Link	Bunch crossing frequency
Link Length	Distance between detector and counting room
Latency	Buffering and mass/power consumption constraints, trigger algorithm sophistication, delay compensation mechanism
Jitter	Jitter requirements of clock multipliers necessary to drive high-speed serial links
Radiation Levels	Particle generation rate, distance from collision point
Power Consumption	Physics requirements, distance from interaction point
Temperature Range	Radiation levels, distance from interaction point

2.3 Technical Characteristics of Currently Installed Optical Links

The network performance indicators that have an impact on accelerator and detector operation have been identified above. The accelerator-related parameters that determine the network performance requirements for each indicator have also been analysed in Sections 2.1 and 2.2. The discussion can proceed to demonstrate examples of this analysis in practice. The technical characteristics of the links currently deployed at CERN are discussed. The links are classified in three dimensions; the functionality they support, the type of detector they are connected to and the experiment they are used at. Their technical characteristics are compared according to the category they belong to. The aim of the analysis is to identify the links that would determine the performance requirements of a unified architecture that could support data readout as well as transport of trigger, timing and control information over the same infrastructure. During the analysis the focus is on the links that may be upgraded in the transition to HL-LHC.

2.3.1 Comparison of Link Technical Characteristics According to Functionality

As shown in Figure 2.3 and discussed in Section 2.1, there are a variety of links that are required for the operation of an accelerator. These different types of links are intended to transfer different types of information. Different types of information include [14]:

- Raw data (i.e. data readout).
- Trigger and Clock, as well as information facilitating data flow control.

- Information from the detectors to the Trigger Processor, facilitating the trigger decision.

- Control Information, for example detector configuration commands.

Networks designed to transfer different types of information have different performance requirements. The upstream - from now on the direction from the detector to the counting room will be referred to as upstream and the direction from the counting room to the detector as downstream - aggregate data rate requirement is essentially set by the required data rate for data readout, as other applications require much lower data rate in the upstream direction. The aggregate data rate requirement in the downstream direction is much lower compared to that for the upstream direction, as most of the information is broadcast. The aggregate data rate in the downstream direction is essentially determined by the TTC network. As discussed in Section 2.2 the value of the data rate per link in the upstream direction is essentially the result of a constraint optimization-like design process. The parameters to be minimised are the power consumption and the material budget inside the detector while maximising the data rate per link. During this process a number of constraints have to be taken into account; these include the aggregate data rate requirement, the maximum achievable data rate limitations because of technology and radiation hardness limitations and the physical constraints inside the detector. Determining the relative importance of different parameters is a challenging task that requires collaborative work between teams of scientists designing different parts of the detector.

Determining the downstream data rate requirement per link is less challenging. This is the same as the aggregate data rate required in the downstream direction, as information is broadcast and is determined by the TTC network. The data rate of the TTC network in turn, depends primarily on the bunch crossing frequency.

Latency and jitter are not critical for the data readout and the control network. However they are of high significance for all the components of the trigger feedback loop, i.e. the Trigger Links, the Trigger Processor, the TTC Drivers and the TTC network. The "controllable" component of the delay contributed by the optics is relatively small, leaving little room for optimization. Designers focus on minimising the delay introduced by the electronics facilitating the trigger decision, whose operation is outside the scope of this thesis. However, an important aspect that is relevant to the work discussed here is that the latency of the TTC network is fixed and deterministic. The jitter is also of primary importance for the TTC network and should be kept at very low levels (for CMS the jitter of the recovered clock should be <50 ps).

The length of the links is one of the network performance parameters that does not depend on the application. All links need to transport information from the counting room to the detector that is up to 160 m.

The same is the case for the special requirements - radiation hardness, mass and power constraints - that essentially apply to all components installed on-detector, regardless of the type of information they send to or receive from the counting room. However, the mass and power constraints have a greater impact on the data readout transceivers, due to the higher number of links required by that application [8], [11], [12].

2.3.2 Comparison of Link Characteristics According to Detector Served

The requirements of the optical links are not only affected by the targeted application, but also by the particular detector they are connected to. The required aggregate data rate in the upstream direction - determined primarily by the data

readout requirements - varies widely from detector to detector. Inner detectors - i.e. tracker layers - have very high number of channels as they consist of many elements to facilitate high spatial resolution. For example the CMS pixel tracker numbers $\sim$66x10^6 channels and the strip silicon tracker $\sim$9.3x10^6. On the other hand, the ECAL and HCAL have only $\sim$75000 and $\sim$9000 channels, respectively [8]. Despite the higher resolution of the calorimeters that leads to a high number of bits being generated per channel, the very high number of channels of the tracker detectors results in higher data generating capacity. However, in the case of the pixel tracker, special techniques, such as zero-suppression, are deployed to exploit the low occupancy and reduce the required overall data rate. Moreover, the harsh radiation environment and the stricter material budget requirements because of its proximity to the interaction point, limit both the aggregate and the per link achievable data rate. For these reasons it is typically the tracker layers outside the pixel detector that have the highest aggregate data rate requirements. Still, the radiation environment is quite harsh and the mass and power consumption constraints are stringent, even for these tracker layers. Therefore it is at the calorimeters, where the highest data rate links are currently deployed. In the downstream direction, the aggregate data rate - that is the same as the data rate per link, as information is broadcast - is the same for all detectors. The difference in the link length could be considered negligible, as the experiment dimensions are small relative to the distance between the detectors and the counting room. The mass, power consumption and radiation hardness requirements are more stringent for inner detectors that are closer to the interaction point. The radiation levels increase closer to the interaction point. To reduce radiation damage, detectors close to the interaction point have to operate in low temperatures. For example the tracker operates at temperatures as low as $\sim$-15^oC. It is also important that the inner detectors do not obstruct particles from reaching the outer detectors, therefore the material budget should be minimised [8],

[11], [12].

2.3.3 Comparison of Network Characteristics According to Experiment Served

The optical link requirements are also affected by the experiment they are being used at. The particular networking requirements of different experiments are dictated by their physics requirements that differ between experiments, but also by decisions taken during the experiment design stage. The A Toroidal LHC Apparatus (ATLAS) and CMS experiments are the two general-purpose physics experiments. LHC-beauty (LHCb), on the other hand, explores very rare interactions. LHCb operates at lower luminosity (collision rate), in order to avoid event pile-up - the term event pile-up refers to a situation where several events, happened within the time resolution limits of the detector, mask each other, i.e. they become indistinguishable. The A Large Ion Collider Experiment (ALICE) experiment is quite different to other experiments, as it is dedicated to the investigation of heavy ion collisions. The ALICE experiment is not discussed here, as during the requirements gathering phase at the end of 2009/beginning of 2010, there was no plan to upgrade its networks. Out of the experiments of interest, LHCb has the lowest aggregate data rate requirements owed to its lower operating luminosity. ATLAS and CMS have similarly high aggregate data rate requirements, with the CMS having somewhat more demanding requirements. The overall data rate offered by the currently installed data readout links of the CMS is $\sim$25 Tbps. In all experiments - that actually have similar detector structures - the highest data rate links are those installed at moderate distance from the interaction point. Currently the highest data rate links support a 1.6 Gbps transmission rate. In the downstream direction all experiments have the same aggregate and per link data rate requirements, that are the same

as information is broadcast. This is because of the fact that the TTC network has the same data rate requirements in all experiments, despite the fact that the trigger rate is higher in LHCb; 1 MHz as opposed to 100 kHz for ATLAS and CMS. As ATLAS is the experiment with the largest dimensions it has the longest links (160 m), while the ATLAS trigger feedback loop also has the most stringent delay requirement of 2.5 μs. The harshest radiation environment is encountered at the inner detectors - due to their proximity to the interaction point - of the ATLAS and CMS experiments, as their operating luminosity is higher than that of the LHCb [8], [11], [12].

2.3.4 Network Requirements for a Unified Infrastructure at the LHC

The application that requires the highest aggregate data rate in the upstream direction is that of data readout. The most demanding experiment is CMS and the most demanding detector the strip tracker that generates ∼8 Tbps of traffic. The currently installed optical links for the data readout of the CMS strip tracker have an overall capacity of ∼11 Tbps to accommodate the associated overheads. The aggregate upstream data rate supported by the links installed at the most demanding experiment is ∼25 Tbps. The aggregate data rate is an important metric that can be used to analyze the impact of the upgrade, as it will be directly affected by the luminosity increase. Its magnitude shows that inevitably thousands of links will have to be used to transfer all the data off-detector. Multiplexing all the traffic over one fiber is not a realistic option, not only because of the magnitude of the aggregate data rate, but also because the use of devices necessary for multiplexing, such as Arrayed Waveguide Gratings (AWGs), within the detector space is considered controversial by the particle physics community. Therefore, the data rate per

link is a more important metric as far as the requirements of a unified architecture are concerned. The highest data rate links currently installed offer data rates of 1.6 Gbps. Such links are being used by various detectors in all experiments; typically by calorimeters, such as the CMS HCAL, the ATLAS Liquid Argon (LAr) calorimeter and the LHCb ECAL and HCAL, but also from outer parts of the ATLAS tracker - more precisely the ATLAS Transition Radiation Tracker (TRT). In the downstream direction the highest aggregate data rate - that is the same as the highest data rate per link, since information is being broadcast - is 160 Mbps. The maximum link length of the currently deployed links is $\sim$160 m. The longest links are installed at ATLAS, since this is the largest experiment. The delay of the TTC network should be fixed and deterministic for all experiments and detectors, while the requirement for the root-mean-square value of the random jitter component of the recovered clock is to be <50 ps. The most stringent radiation hardness requirements are those of the detectors closer to the interaction point - i.e. the tracker layers - for the experiments of high luminosity (ATLAS and CMS). The optoelectronic components used to transmit information to and from the CMS strip tracker will need to withstand fluences of $\sim$3.4x10^{14} 1 MeV n/cm^2 and will receive a total dose of 150 kGy over an estimated lifetime of 10 years. Some transceivers serving the pixel detector may have to withstand even higher amounts of radiation, depending on the position where they are installed, however the estimates of the radiation they will be exposed to is subject to greater uncertainty this is why we refer to the corresponding figure for the strip tracker. At the same time the tracker will need to be cooled to temperatures below -10^{o}C to avoid degradation due to irradiation. Currently the power consumption for the CMS tracker stands at 75 mW/link while the corresponding figure for the ATLAS Semiconductor Tracker (SCT) stands at 120 mW/link. These figures give some indication of the power consumption constraints close to the interaction point. A summary of the requirements for a unified archi-

tecture at the LHC is given in Table 2.3. The table also shows the most demanding experiment, detector and application that essentially acts as a "bottleneck" and determines the requirement for the corresponding metric.

Table 2.3: Network requirements for a unified architecture at the LHC.

Metric	**Most demanding experiment, detector and/or application**	**Corresponding performance**
Upstream Aggregate Data Rate	CMS Strip tracker - Data readout	8 Tbps
Downstream Aggregate Data Rate	TTC network	160 Mbps
Upstream Data Rate per Link	CMS HCAL, ATLAS LAr calorimeter, ATLAS TRT, LHCb ECAL, LHCb HCAL - Data readout	1.6 Gbps
Downstream Data Rate per Link	TTC network	160 Mbps
Link Length	ATLAS experiment	160 m
Latency	ATLAS - Trigger feedback loop	2.3 μs
Jitter	TTC network - Clock distribution	Random jitter of recovered clock <50 ps (rms)
Radiation Levels	CMS tracker	Fluence (10 years of operation): 3.4x10^{14} 1 MeV n/cm^2
Power Consumption	CMS tracker	75 mW/link
Temperature Range	CMS tracker	Tracker volume will be operated at temperatures between $\sim$ -15^{o}C and room temperature

2.4 HL-LHC Upgrade and Impact on Optical Link Requirements

Having completed the discussion on the relationship between accelerator operation and network parameters the discussion can now move to predicting the impact of a potential increase of the LHC luminosity on network parameters.

Plans for upgrading the LHC to HL-LHC are already under investigation for many years, since the design phase of LHC. The final goal of the upgrade is a luminosity increase by a factor of 10. There are several accelerator operation parameters that, if modified, would lead to a luminosity increase; these include, for example, the number of particles in a bunch, the frequency at which bunches collide, how much collimated and focused the beam is and the collision angle. Although the range of parameters that could be modified is wide not all of them would have the same impact on network design. A change in the collision frequency would have significant, direct implications on network design, while changing other parameters would affect the network requirements only indirectly, because of the resulting luminosity increase [15].

This makes the bunch crossing frequency along with the number of particles generated by a collision - that is proportional to luminosity - the two main metrics of interest. Although the upgrade plan is subject to modifications, the bunch crossing frequency is unlikely to increase. According to the upgrade scenarios, the bunch crossing frequency will either remain at 40 MHz - the most likely scenario - or be reduced to 20 MHz. The current plan also foresees a two-step increase in luminosity; the first step will result in a luminosity increase by a factor of 3 to 4. The second phase of the upgrade, will lead to an overall luminosity increase by a factor of 10 [15], [16].

Aggregate Data Rate Increasing the particle generating capacity of the accelerator - a parameter directly related to the aggregate data rate requirements - is a primary goal of the upgrade. Simulations show that the increase in the luminosity by a factor of 10 will lead to an increase in the number of particles emerging from the collisions by a factor of ∼5 [17]. Figure 2.6 shows the tracks of high momentum particles ($p_T > 1GeV/c$[1]) emerging from the collision point for different luminosities.

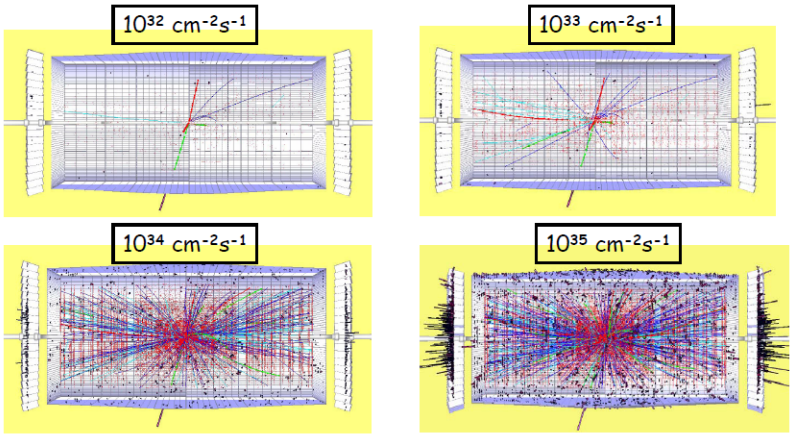

Figure 2.6: Simulation showing the number of emerging high-momentum particles for different luminosities [19].

The increase in the number of generated particles is expected to have a different impact on different detectors. Most of the regions of the calorimeters, for example, are going to perform well at the HL-LHC. In most of the operating range of a calorimeter the term that dominates the energy resolution limit is proportional to $1/sqrt(E)$ [5] - with E being the energy of the incident particle - therefore the energy resolution of the calorimeters can even improve at higher energies. Despite that fact, a full readout of the calorimeter data is under consideration, mainly to simplify the front-end electronics and to achieve higher trigger granularity [20]. In such a case,

[1]The electron volt (eV) is a unit of energy equal to the energy gained by an electron when this is moved across a potential of one Volt. The electron volt is also used as a momentum unit where the division by the speed of light (eV/c) is sometimes dropped and implied [18].

the aggregate data rate requirement is expected to increase by a lower factor than the particle generation capacity of the accelerator, i.e. <5. This is owed to the fact that on-detector zero suppression is under investigation in case a full readout is carried out. If not upgraded, the trackers, contrary to the calorimeters, may not be able to resolve particle tracks since different particles may hit the same detector element. Changing only the number of channels so that all particle tracks can be resolved would result in an increase of the aggregate data rate requirement equal to the particle increase factor, i.e. ∼5. One of the options considered for the CMS strip tracker - currently the most demanding detector in terms of aggregate data rate requirement - is to increase the number of channels to ∼1 Billion to maintain a low occupancy. This is not the dominant upgrade scenario, though, other design options are also considered; the goal of most of these options is to actually reduce the required aggregate data rate. Such an option is the use of a more efficient trigger mechanism. According to this scenario data from the pixel and strip detectors are going to be used in the trigger decision process.

To give an example of the impact of the upgrade on the aggregate data rate requirements, Equation 2.1 will be used, which is repeated here for ease of reference:

$$D = CRR * R * N * C * OH * TR$$

One of the dominant upgrade scenarios for the CMS tracker foresees the increase of the number of channels to ∼19 Million [17]. In other words, the channel count will be increased by a factor of ∼2 compared to the LHC case. According to the same scenario, a full readout without on-detector zero-suppression will be carried out, therefore the occupancy is not going to affect the required data rate. The information is going to be encoded in just one bit representing whether a detector element has been hit or not. The trigger frequency is going to remain 100 kHz.

Ignoring the impact of the compression ratio and any overheads (C=OH=1) the required data rate for the CMS tracker strips is going to be:

$$D = 1 * 1 * 19 * 10^6 * 1 * 1 * 10^5 bits/s = 1.9 Tbps \tag{2.3}$$

The calculations for this scenario show that appropriate design choices may even lead to a reduction in the aggregate data rate requirements of some detectors. However for most detectors this is not the case. Even in the case of the CMS strip tracker considered here, additional layers consisting of ∼116 Million channels are going to be added to provide information to a new Trigger Processor. This will lead to an increase of the aggregate data rate requirement that could even exceed 20 Tbps (the case of the CMS strip tracker is discussed more extensively later in this Chapter as a case study). So, the CMS strip tracker is still likely to be the detector with the highest upstream aggregate data rate requirements, although this will depend on design decisions that have not yet been finalized. An interesting such example is that of the LHCb. Although its current operating luminosity is 2x10^{32} cm^{-2}s^{-1} and it is going to be increased to 10^{33} cm^{-2}s^{-1} , i.e. by a factor of 5 only, a full readout at 40 MHz is under consideration. Such a move has the potential of increasing the data rate requirements by a factor of up to 40.

In the downstream direction, the minimum aggregate data rate required by the TTC network is unlikely to increase. However, the upgrade is seen as an opportunity to increase the data rate to ∼1 Gbps so that advanced trigger commands can be supported. This data rate would also offer ample bandwidth for any other functionalities that may be introduced in the future.

Data Rate per Link As discussed in Section 2.2 the data rate per link is the result of a design process that resembles a constraint optimization. In this opti-

mization several parameters have to be taken into consideration. The outcome may be that the detector with the highest aggregate data rate requirement is served by relatively low data rate links, while the fastest links are deployed at detectors with moderate aggregate data rate requirements. The Gigabit Transceiver (GBT) project foresees a 5 Gbps data rate for the upgraded CMS strip tracker [21]. As far as calorimeters is concerned a full readout is under consideration, in order to simplify the front-end electronics and to achieve higher trigger granularity [20]. This would lead to a data rate of 100 Gbps per front-end board for the ATLAS LAr calorimeter. In such a case multiple optical fiber links per board will be required. The use of links offering data rates as high as 10 Gbps is investigated [22].

In the downstream direction the required data rate per link will be the same as the upstream data rate per link.

Latency and Jitter The latency requirements are expected to be less demanding at the HL-LHC, to allow for the use of more sophisticated trigger decision algorithms that take longer to compute. The maximum allowable latency is expected to be increased by a factor of 2 - increasing the most stringent delay requirement from 2.5 μs to 5 μs. The jitter requirement is expected to remain the same, i.e. the root mean square (rms) component of random jitter of the recovered clock should be $<$50 ps.

Link Length An increase of the link length would be required to remove the counting room that is located underground and transmit data directly to data centers overground. However, such a move is not foreseen by any of the upgrade scenarios.

Special Requirements The luminosity upgrade is going to impact the radiation hardness requirements of the detectors and the associated front-end optoelectronic

components. The increase in the rate of particle generation essentially determines the radiation flux increase. So, the radiation flux will increase by a factor of ∼5. The radiation fluence tolerance levels for the upgraded CMS strip tracker and calorimeter, as set by the Versatile Link project [21] are 6x10^{15} 20 MeV neutrons/cm^2 and 5x10^{14} 20 MeV neutrons/cm^2, respectively. These levels refer to 10 years of operation at the HL-LHC environment. Power dissipation is critical and the requirement for low power consumption is going to be even more challenging to meet with the move to higher data rates. An additional challenge for the tracker is the large increase in the number of channels, which is going to lead to increased power consumption, as each GBT module is expected to consume 2 W of power. Especially for optoelectronic components, uncooled components should be used as cooling would increase the power consumption and the material budget inside the detector. The tracker will operate at low temperatures (reaching temperatures of -15^{o}C) to mitigate the effects of radiation [10]. This essentially means that the optoelectronic components will be required to function at temperatures as low as -30^{o}C [21].

A summary of the metrics discussed in this Section and the way these are going to be affected by the luminosity upgrade is provided in Table 2.4.

2.5 Requirements of the Upgraded Systems - A Case Study

In this section the technical characteristics of a network that could support data readout, transport the information required to take the trigger decision from the detector to the trigger processor, as well as trigger, timing and control information from the counting room to the detector for the upgraded silicon strip tracker of CMS were described.

It is important to note that the purpose of this description is to provide some

Table 2.4: Summary of selected metrics and how these will be affected by the luminosity upgrade.

Metric	**How it will be affected by the luminosity upgrade**
Upstream Aggregate Data Rate	Will increase as a result of the increase in the particle generating capacity of the accelerator or because of design decisions, e.g. in the case of LHCb
Downstream Aggregate Data Rate	Will not be affected as the bunch crossing frequency will remain the same or it will be decreased. However, the upgrade is viewed as an opportunity to increase the downstream data rate.
Upstream Data Rate per Link	Technology allows moving to higher data rates - Upstream aggregate data rate increase also pushes towards this direction, as higher data rate per link would allow reducing the number of links.
Downstream Data Rate per Link	Same comment as for downstream aggregate data rate.
Link Length	Will not be affected by the upgrade.
Latency	Latency requirements are expected to relax to allow the use of more sophisticated trigger algorithms that take longer to compute.
Jitter	Will not be affected by the upgrade.
Radiation Levels	Will increase by a factor equal to that of the particle generation rate.
Power Consumption	Overall power consumption will increase due to the higher data rate. However keeping the power consumption/transmitted bit low will become more challenging.
Temperature Range	Will not be affected by the upgrade.

insight on different aspects of the upgrade process. The particular detector would not determine the characteristics of a unified architecture in the HL-LHC. The selection of the CMS silicon tracker has been made due to the more mature and crystallized status of the upgrade process, which allowed us to provide a more accurate description of the particular detector.

Aggregate Data Rate Simulations have shown that the increase in luminosity by a factor of ∼10 will lead to a corresponding increase in the number of generated particles by a factor of ∼5, [17]. According to the current upgrade plans the strip tracker will consist of two different types of layers. The first type is going to facilitate data readout (data readout layers), while the second type is going to provide input to the trigger processor (trigger layers). Each of the trigger layers will consist of two sub-layers, at approximately 1 mm radial separation. This separation allows discrimination between hits with very low momentum against hits with momentum above 1 GeV - in particle physics the eV is used as a measurement unit for energy, but also for mass and momentum; what is implied though is eV/c for momentum and eV/c^2 for mass measurements. The principle of operation of the trigger layers is shown in Figure 2.7. The reconstructed trajectory of particles with high momentum, shows towards the interaction point, contrary to particles with lower momentum - Figure 2.7(a). Additionally the cluster width of the tracker that is hit by a particle with a low momentum is larger - Figure 2.7(b). The purpose of including information from the tracker in the trigger decision process is to keep the trigger frequency below 100 kHz, [17].

For the readout layers a full readout is going to be performed. The aggregate required data rate was calculated in Section 2.4 (Equation 2.3).

The trigger layers will consist of two layers, a 37.75 Million channel internal layer and a 77.86 Million channel external. The internal layer is going to be served by 2048 links and the external by 4224 links [17]. The address of any channel identifying a high momentum particle will be transmitted. As each link will serve ∼18400 channels in order to encode the address of the channel $\lceil \log_2 18000 \rceil = 15$ bits will be required). The channel readout ratio is estimated to be 0.45% and 0.25% for the inner and outer layers, respectively - expressing the probability of a hit by a high momentum particle. Trigger information must be transported to the trigger

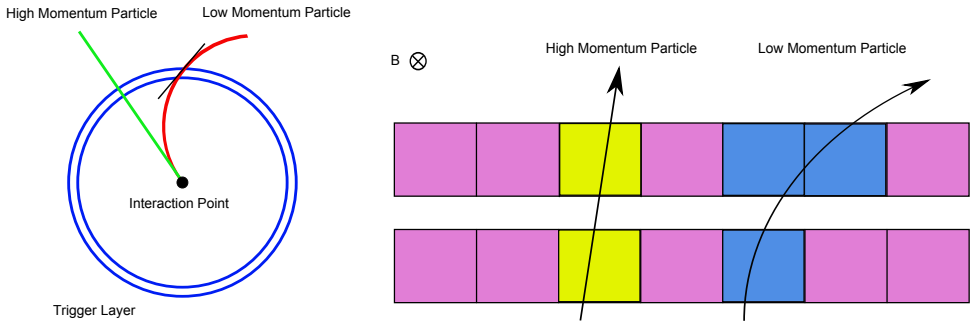

(a) (b)

Figure 2.7: Principle of operation of Trigger Layer: (a) Trajectories of high vs. low momentum particles within magnetic field. (b) Using number of detector elements "hit" by a particle at different detector layers to distinguish between low and high momentum particles [23].

processor at every bunch crossing, at frequency of 40MHz. Ignoring compression and any overheads (C=OH=1), the overall aggregate data rate is going to be:

$$D = [(0.45 * 10^{-3} * 15 * 37.75 * 10^{6}) + (0.25 * 10^{-3} * 15 * 77.86 * 10^{6})] * \\ * 40 * 10^{6} = 21 Tbps \tag{2.4}$$

in the downstream direction the aggregate data rate is expected to be ∼1 Gbps, although the decision has not been finalized.

Data Rate per Link Both tracker and trigger layers are going to be served using GBT links. The GBT maximum supported data rate is 5 Gbps, while it will typically run at a line rate of 4.8 Gbps. The user data rate - i.e. the effective data rate after removing the overheads - is going to be 3.2 Gbps [21], [24], [25]. The downstream data rate per link is the same as the aggregate data rate, i.e. ∼1 Gbps, as information is broadcast.

Latency and Jitter The latency requirement is going to be dictated by the TTC network. The current requirement for CMS is 3.2 μs. As the trigger decision process is going to become more sophisticated, it is expected that the latency requirement is going to relax. An indicative number for the maximum allowable latency that will be used is 6.4 μs, set by the existing ECAL readout pipeline length, although the decision has not been finalized. The requirement for the random jitter component of the recovered clock is most likely to remain unchanged at <50 ps rms [10].

Link Length The current upgrade scenario does not foresee any changes of the link length. The only driving force behind a link length increase is the desire to remove the counting room equipment. However such a move is unlikely, due to the stringent latency requirement [10].

Special Requirements The potential increase of the number of channels combined with the data rate increase make minimisation of power consumption per channel and per transmitted bit very important. It is estimated that the upgraded strip tracker will consume ∼37 kW of power. Out of this ∼21 kW is going to be consumed by the particle detector (0.1 mW per channel for the trigger layers and 0.5 mW per channel for the readout layers) and ∼16 kW by the readout electronics. Each GBT module is expected to consume ∼2 W. The lifetime radiation exposure of the optoelectronic components in the CMS Tracker is expected to reach $6\text{x}10^{15}$ 20 MeV neutrons/cm^2 fluence and 500 kGy ionizing dose [21]. The radiation flux is going to be increased by a factor equal to the increase in the particles traversing the tracker, i.e. a factor of ∼5.

Table 2.5 summarizes the network requirements for the upgraded CMS tracker.

Table 2.5: Network requirements for the upgraded CMS Tracker.

Metric	**Upgraded CMS tracker performance requirement**
Upstream Aggregate Data Rate	21 Tbps
Downstream Aggregate Data Rate	1 Gbps
Upstream Data Rate per Link	5 Gbps
Downstream Data Rate per Link	1 Gbps
Link Length	70 m
Latency	6.4 μs
Jitter	Random jitter of recovered clock <50 ps rms
Radiation Levels	Fluence (10 years of operation): 6x10^{15} 20 MeV neutrons/cm^2
Power Consumption	2 W/GBT module
Temperature Range	Tracker will be operated at temperatures between $\sim$ -15^{o}C and room temperature.

2.6 Conclusions

The analysis in this Chapter has shown that both the aggregate and the per link data rate in upstream and downstream is set to increase at the HL-LHC. This will happen, despite the use of special techniques intended to moderate the data rate increase caused by the luminosity upgrade. The CMS tracker is a good example demonstrating this fact. The special triggering techniques, described in Section 2.5, will still lead to an increase of the overall upstream aggregate data rate, as significant amount of information is required for the trigger decision. Even in cases where a data rate increase is not imposed by the upgrade, as in the case of the TTC network, the transition to the HL-LHC is viewed as an opportunity to upgrade the current links. Radiation hard electronics that can operate at higher data rates the

currently installed can be produced and the particle physics community finds that their use would be beneficial.

Table 2.6: Performance requirements for a unified architecture at the HL-LHC (Constructed taking into account the most demanding experiment, detector and/or application at the HL-LHC - worst-case scenarios are also considered).

Metric	**Performance requirement of most demanding experiment, detector and/or application at the HL-LHC**
Upstream Aggregate Data Rate	21 Tbps
Downstream Aggregate Data Rate	1 Gbps - Broadcast
Upstream Data Rate per Link	10 Gbps
Downstream Data Rate per Link	1 Gbps
Number of "Users" (End-Nodes)	10s of 1000s
Link Length	1 km
Latency	2.3 μs (referring to current max. link length of 160 m)
Jitter	Random jitter of recovered clock <50 ps rms
Radiation Levels	Fluence (10 years of operation): 6x10^{15} 20 MeV neutrons/cm^2
Power Consumption	2 W/transceiver module
Temperature Range	-30^{o}C to 60^{o}C

Table 2.6 that summarizes the performance requirements for a unified architecture at the HL-LHC, demonstrates this trend. As the table shows the upstream and downstream data rates per link are set to increase to 10 Gbps and 1 Gbps, respectively. The upstream aggregate data rate of the probably most demanding detector will reach 21 Tbps. Of course, as the number of "users" is very high (10s

of 1000s) the traffic to all the "users" does not have to be multiplexed over the same same fiber, neither they have to be served by a single monolithic network structure. The same applies to the downstream direction, despite the fact that the information is broadcast, that makes multiplexing easier. The number quoted for the link length is actually higher that the 160 m length of the longer links to take into account the possibility that in the future - after the HL-LHC upgrade - the counting rooms are removed and information is transmitted overground. The latency figure refers to a maximum link length of 160 m (for a link length of 1 km obviously a larger latency has to be accommodated to take into account the longer time required for the signal to travel through the fiber) and takes into account the worst-case scenario, under which the ATLAS trigger algorithm remains as is. The power consumption figure will act just as a benchmark figure and not as a target, as power consumption should be minimum. The temperature range refers to the required operating temperature range of the CMS tracker [21].

The main requirement targets of a unified architecture at the HL-LHC have now been defined. To achieve this we used the most demanding experiments, detectors and applications and considered some of the most pessimistic upgrade scenarios. We can now move on to the definition and exploration of the PON architectural space to identify appropriate network structures that match these requirements, particularly focusing on the aggregate downstream data rate requirement of 1 Gbps and the upstream data rate requirement per link of 10 Gbps.

Chapter 3

An Overview of Passive Optical Network Architectures and Enabling Technologies and their relationship to High-Energy Physics

In this Chapter a systematic literature survey on current trends in the area of PONs is conducted. The survey essentially defines the PON "architectural space" and for the remainder of this Thesis will act as a reference of the "standard" network design options at our disposal. The literature review is a prerequisite to move on to the next step, that of network design. Although the aim of the Chapter is not to conclude on the applicability of PONs for particle physics applications, it does highlight key features of the technologies described that could be of interest to the particle physics community. The chapter is structured as follows; it starts with a short introduction

to the PON concept while it identifies the motivation behind the use of PONs in optical access networks. Consequently, different PON variants are described. A separate Section is dedicating to each of the two key PON technologies; the TDM PON and the WDM PON. After that, optical access alternatives not falling in these two categories (TDM PON, WDM PON) are described. These are technologies that have recently gained considerable attention by the PON research community [26], [27]. Each Section describing a different technology provides an overview of the key features of the technology; it outlines the main challenges that have to be resolved in order to make the technology a viable solution for access networks and in order to enhance its performance characteristics. Finally, the corresponding suggested solutions found in the literature are presented. The conclusion of this chapter provides a short analysis on the possible benefits each technology can offer in a particle physics environment. It also briefly discusses the conditions under which, each of the described technologies can be a viable solution for the upgraded optical links at the HL-LHC.

3.1 Introduction to Passive Optical Networks

PONs is an optical access network technology, whose main feature is the deployment of passive optical components that are configured around a splitter/combiner or a wavelength router. A PON connects one Optical Line Terminal (OLT) to many Optical Network Units (ONUs) in a point-to-multi-point configuration [28] as shown in Figure 3.1.

The development of PONs is primarily driven by an increase in bandwidth demand. To meet this demand the "access bottleneck", i.e. the low-data rate part of the network between the last node and the end users, has to be eliminated. Using the ample bandwidth offered by optical fibers is a straightforward way to achieve

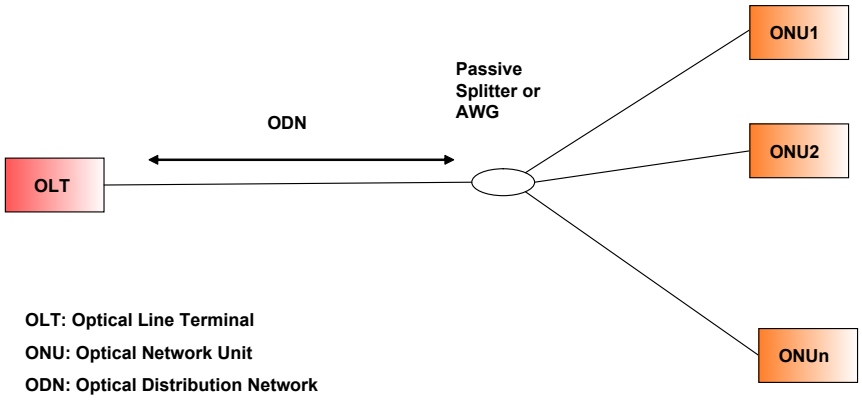

Figure 3.1: Generic PON Architecture.

this goal. The use of optical fiber in the access part of the network is an option that is being researched since the 1980s [29]. The systems utilising fiber in the access part of the network have been termed Fiber-To-The-x (FTTx) systems, where "x" acts as a placeholder for "home", "curb", "premises", etc. depending on where the fiber is terminated. Research on PONs has started as early as the 1980s [29]. As the main obstacle for providing a fiber to each customer's premises is cost, PONs try to reduce the cost per user by sharing the OLT and the distribution fiber - the fiber between the OLT and the remote node. Additional cost savings can be achieved by the removal of all active equipment from the outside plant; thus power installation is not required and overall power consumption can be reduced [29]. In order to ensure interoperability and use economies of scale to lower the PON component cost, standardization of PONs has been attempted since the 1990s [29]. The standardization efforts resulted in a number of PON variants being standardized. These include Asynchronous Transfer Mode (ATM) PON (APON), Broadband PON (BPON)

and the more recent Gigabit PON (GPON) which have been standardized by the International Telecommunications Union (ITU). They also include Ethernet PON (EPON), a standard published by the Institute of Electrical and Electronics Engineers (IEEE) [30]. As resources (distribution fiber, OLT) are shared in a PON, appropriate mechanisms are required to provide access to these resources to different users. Current PON versions use Time-Division Multiplexing (TDM) to multiplex traffic intended for different users in the downstream direction and Time Division Multiple Access (TDMA) to provide multiple access to the common medium in the upstream direction. Although TDM PON is the most widespread deployed PON version - and the only one for which standards exist - PON variants utilising other multiplexing and multiple access mechanisms have gained considerable attention. This shift is primarily caused by the increase in bandwidth demand and the emergence of new traffic patterns caused by the use of video-based services and peer-to-peer traffic. TDM PONs, due to the shared medium mechanism may not be able to provide the necessary bandwidth and Quality of Service (QoS) in the near future, [31]. Instead, PON architectures based on WDM appear to be the most prominent candidates for next-generation optical access networks. A WDM PON uses a dedicated wavelength for each user. Separate wavelengths are used to separate users in the upstream and downstream direction, thus generating two virtual point-to-point dedicated links to each user. Commercial deployments of WDM PONs already exist in Korea [32]. Other PON variants also exist. One such example is the the hybrid WDM/TDM PON, a prominent technology candidate for extending the reach and the splitting ratio of a PON for next-generation PONs. In a hybrid WDM/TDM PON separate groups of users are allocated different wavelengths and traffic from/to different users of the same group is multiplexed in the time domain [33]. A combination of WDM and Sub-Carrier Multiplexing (SCM), has also attracted some attention, especially for Radio-over-Fiber applications [34].

Hybrid WDM/TDM and WDM/SCM PONs are not discussed in this document as they target applications with a quite different set of requirements than ours. The list of PON variants does not end here. Orthogonal Frequency Division Multiplexing (OFDM) [27] and Optical Code Division Multiplexing (OCDM) [26], two schemes that have been extensively used in wireless communications, have attracted considerable research attention over the last few years, due to the potential bandwidth benefits they could offer. Although traditionally intensity modulation and direct detection are the dominant choice in optical communications, a considerable number of systems found in the literature now make use of higher-order modulation schemes along with coherent detection, e.g. [35].

3.2 TDM PONs

The commercialization of the Internet and the advent of the world wide web led to explosive traffic growth in the mid-1990s (in 1996 and 1997 traffic grew by a factor of 100 per year); traffic growth was much higher in the 1990s than in the 1980s [36]. This trend led operators to intensify efforts of developing a cost-efficient way to deliver the benefits of a fiber network to the customers. In 1995 the Full Service Access Network (FSAN) initiative was formed by North American operators with the intention of generating a draft for PON standards. The efforts of FSAN led to the first PON standard. It was the ATM PON (APON) that was issued by the ITU (ITU-T G.983 standard). The standard was further enhanced and the new, improved PON version has been named Broadband PON (BPON), to show that it was not limited to ATM traffic [37], [38]. Among the enhancements was the specification of a separate wavelength band for video transmission, using SCM [37]. ATM PON (APON) and BPON were offering 622 Mbps downstream and 155 Mbps upstream data rates shared between 16 or 32 customers. The maximum network reach offered

by these early PON versions was 20 km. The continuing standardization efforts of the FSAN group resulted in a second standard, also standardized by ITU (ITU-T G.984). The main motivation was to generate a more flexible standard that could accommodate Internet Protocol (IP)/Ethernet bursty traffic with lower overhead, as well as to move to higher data rates. The new version offered 2.488 Gbps in both directions and supported 1:64, as well as 1:128 splitting ratios. Although the maximum physical reach remained 20 km [39] the logical reach - i.e. the maximum reach supported by the protocol - was extended to 60 km [37] [38].

Table 3.1: Parameters of GPON and EPON [39].

	GPON	**EPON**
Standard	ITU-T G.984	IEEE 802.3ah
Max. Downstream Bit Rate	2488Mbps	1250Mbps
Max. Upstream Bit Rate	2488Mbps	1250Mbps
DS/US Wavelength	1490±10nm/1310±50nm	1490±10nm/1310±50nm
RF Overlay	1555±5nm	1555±5nm
Max Split	1:64	1:16/1:32
Max. Reach	10/20km (physical reach) 60km (logical reach)	10/20km (physical)
Max. Budget	15/20/25dB	15/20dB

The ITU has not been the only organization working towards standardization of PONs. As the Internet gained popularity, so did Ethernet, since it has been established as one of the most prominent technologies in computer networks. Ethernet equipment is very cheap due to the high production volume, while commonly each new Ethernet version supports a speed increase by a factor of 10 compared to the previous version [37]. Therefore the Ethernet in the First Mile (EFM) group was established in 2000 to standardize a PON version based on Ethernet. Subsequently,

the EFM Group became part of the IEEE 802.3 standards committee, the IEEE 802.3ah. The IEEE 802.3ah developed a standard referred to as EPON. EPON supports 1.25 Gbps transmission in both directions, although the effective transmission rate is 1 Gbps, as 8b/10b is used. EPON supports 1:16 and 1:32 splitting ratios and its maximum reach is 20 km [39], [37].

A summary of the technical characteristics of the two dominant PON standards are shown in Table 3.1. Although GPON and EPON are the most widely deployed PON variants, the two standardization bodies (IEEE, ITU) have already standardized GPON and EPON versions that support 10 Gbps transmission. 10G EPON has been standardized in September 2009 by IEEE 802.3av, supporting 10 Gbps maximum data rate in both upstream and downstream directions, [40], while at the time of the writing (i.e. end of 2009) the FSAN group is working on the upgraded version of GPON, called XG-PON [41].

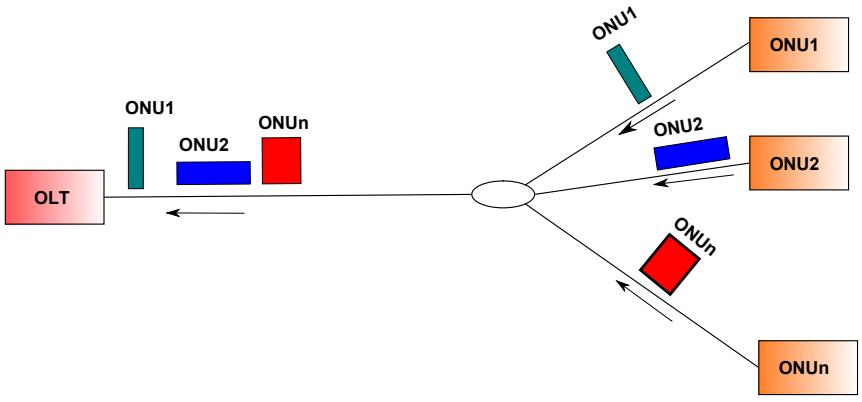

Figure 3.2: Bursty upstream traffic in a TDM PON.

3.2.1 Technical Challenges Related to TDM PONs

Technical challenges related to TDM PONs include [32]:

- The bandwidth sharing mechanism limits the amount of bandwidth per subscriber. Since only one wavelength band is used, subscriber bandwidth for a fixed number of subscribers can not be increased without an increase in the line rate.

- The TDM PON scalability is limited by splitting losses. The more subscribers are added to the network, the higher the splitting ratio and the higher the losses induced by the splitter.

- TDM PON requires a sophisticated timeslot allocation mechanism (Medium Access Control (MAC) protocol). This in turn increases the complexity of the ONU and OLT and their power consumption. Moreover, as different subscribers may be located at different distances from the OLT, the different delay values must be taken into account by the MAC layer to avoid collisions. Therefore a precise ranging mechanism is required to estimate the delay for each of them. Although Dynamic Bandwidth Allocation (DBA) can improve bandwidth utilisation, therefore it can be perceived as an advantage of a TDM PON, it further increases the complexity of the transceiver.

- Traffic burstiness in the upstream direction makes PON transceiver design challenging. As Figure 3.2 demonstrates, packets transmitted in the upstream direction, arrive at the OLT with random phase and amplitude. This complicates the design of the OLT transceiver, which should have high dynamic range and should be able to achieve fast synchronization for successive bursts to reduce guard time.

- Security is an issue for TDM PONs as information is broadcast in the downstream direction. Implementation of encryption algorithms can resolve the problem, but adds to the complexity and cost of the transceivers.

3.2.2 Suggested Solutions

Burst-Mode Operation

One of the most challenging technical aspects of TDM PONs is related to the bursty nature of traffic in the upstream direction. The ONU transmitter and the OLT receiver have to operate in burst mode. At the ONU side this requires a transmitter with high extinction ratio to avoid interference between users, stable and high power during transmission and short switch-on and -off time to minimise overheads. At the OLT side high sensitivity, fast response and high dynamic range are required in order to cope with bursts arriving with an arbitrary amplitude and phase [31].

The generic structure of a burst-mode transceiver is shown in Figure 3.3. As the Figure demonstrates the main components of the receiver are the photodiode that converts the light to current, the transimpendance amplifier that converts the current to voltage and the main amplifier that further amplifies the signal so that it can be processed by the consequent stages. The Clock and Data Recovery (CDR) circuit, although typically not considered part of the receiver, is a critical one to achieve burst mode operation, therefore it is going to be discussed in this analysis. The transmitter consists of the laser driver that generates the necessary current to modulate the laser diode and the laser diode itself. The laser diode converts the current generated by the driver to light that is transmitted over the optical fiber.

The design of a laser driver that meets all the requirements of burst mode operation at a low cost is not a trivial task. Achieving a high extinction ratio

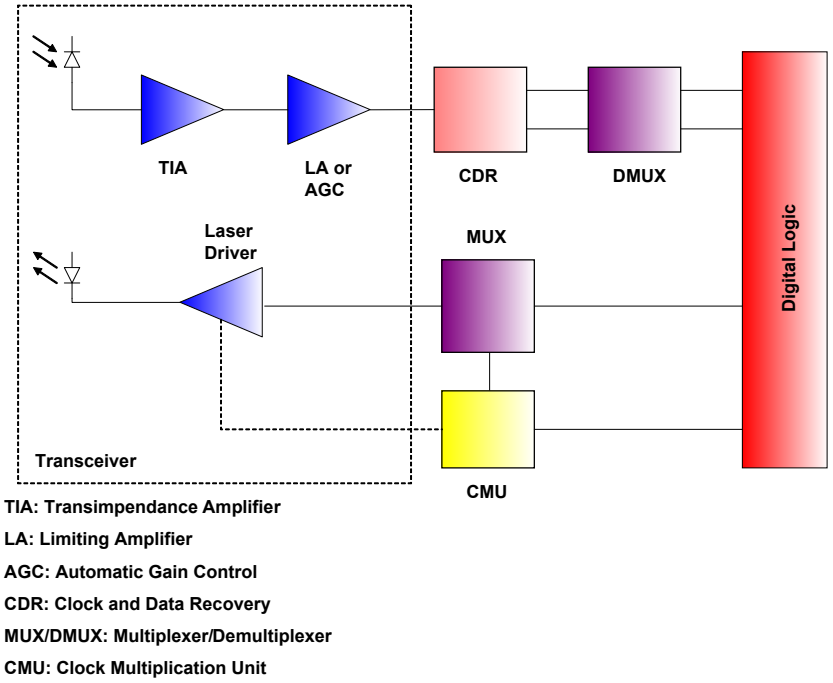

Figure 3.3: Generic structure of burst-mode transceiver [42].

effectively means that the laser should be biased below threshold during periods of inactivity. However, this would prolong the time required for transitions between the on and off states [42]. In [43] a burst mode laser driver with digital circuitry to set up the laser current is presented. The use of a turn-on delay compensation (TODC) circuit is suggested to minimise the effect of turn-on time. The circuit predistorts the signal so that transmitted "1" pulses have sufficient width. A shunt transistor is also used to minimise the switch off time. The transistor is connected in parallel to the laser diodes and drains the carriers from the laser during switch off. In burst mode laser drivers, contrary to continuous mode transmitter case, power control cannot be based on averaging due to long periods of inactivity. Automatic power control based on the peak power is suggested in [44]. Although this approach does allow bit-by-bit threshold adaptation it is very power consuming. Moreover, errors can be introduced at the beginning of each burst because of the drift in the

output voltage of the peak detector. To overcome these issues in [43] a digital power control circuit operating on a burst-by-burst basis is proposed. The circuit is based on an integrate and dump approach and digital storage. A capacitor is charged during a burst, and discharged at the end of it. Charging takes place only during "1"s and the charging current is proportional to the difference between the monitoring photodiode's and the reference current. At the end of the burst the polarity of the capacitor shows whether the bias current should be increased or decreased.

With the move to higher data rates (10 Gbps) the design of burst mode laser drivers becomes more challenging. In 1.25 Gbps systems a single ended Direct Current (DC)-coupled interface to the laser diode is an acceptable approach. However, in 10 Gbps systems its use would induce crosstalk to the receiver implemented in the same optical sub-assembly. Using a differential interface could resolve the problem. There are two ways to implement a differential interface; using DC-coupling or Alternating Current (AC)-coupling. The first approach results in low driving ability, as a constant offset equal to the bias of the laser needs to be applied between the two terminals of the laser driver. Using AC-coupling can alleviate this problem, but the transient response of the coupling capacitor limits the turn-on time of the circuit, [45]. One solution to this problem is suggested in [46]. The authors suggest a technique (baseline wander common-mode rejection) that allows operating the laser driver even before settling down of the capacitor's transients.

At the receiver side two options exist to convert light to current; the use of a PIN or an Avalanche Photodiode (APD). Both burst-mode receivers using PIN [47], [48] and APDs [49] are reported in the literature. The APD has higher cost and requires more complicated electronics since it requires bias and control circuitry [48]. On the other hand it typically provides higher sensitivity compared to the PIN photodiode due to the avalanche gain mechanism. The additional cost of using an

APD is not considered prohibitive, as a burst-mode receiver is required at the OLT side that is shared among many subscribers. The choice of the APD's gain is critical for the overall system performance. Apart from the sensitivity of the receiver, it affects the splitting ratio and the differential reach, as presented in [50], [51]. The findings of this work suggest that when the gain is high and the splitting ratio low the differential reach can be severely limited by the tail after a strong packet.

The main differences between continuous and burst mode receivers can be summarized to the following points [52] and [53]; in burst mode receivers AC-coupling is problematic as the charging and discharging of capacitors prolong the response time of the receiver - although for EPON receivers, AC-coupling using small capacitors is possible due to the more relaxed timing requirements, e.g. [54]. In continuous mode receivers the threshold control - restoration of the logical "1" and "0" levels - can be based on averaging, in burst mode operation fast threshold control circuitry is required. Additionally the clock and phase recovery of a burst mode receiver must be carried out in very short time.

Burst mode transceivers can be classified into two categories depending on the structure of their threshold control circuitry; transceivers using feedback configuration and transceivers using feedforward configuration [52]. In feedback configuration [55] threshold control is carried out at the preamplifier stage. In feedforward configuration [53] the output of the preamplifier is split in two branches one is fed to the input of main amplifier and the other to a peak detection circuit. Therefore threshold control is carried out at the main amplifier stage. The feedback configuration is more stable, but it requires a differential preamplifier [53].

In all types of receivers, the signal output of the amplifying stages should be within the voltage range of the clock and data recovery circuitry. Ideally the amplifying stages output should be such, that the dynamic range of the CDR circuitry is fully exploited. To achieve this for bursts with different amplitude, either a limit-

ing amplifier, either an amplifier with variable gain and an automatic gain control mechanism have to be used [42]. A limiting amplifier is an amplifier with a logarithmic DC transfer function, thus providing high gain when the input is small and low gain when the input is high. Both amplifier types are used in burst mode receiver implementations. In [56], [57] a limiting amplifier has been used at the main amplifier stage of the receiver, while in [58] the use of a preamplifier with automatic gain control functionality is suggested. In [59] an automatic gain control mechanism is used to modify the gain of the preamplifier on a burst-by-burst basis. Our discussion on burst-mode receivers shows that a number of key functionalities such as threshold and gain control need to be performed on a burst-by-burst basis. As any memory would reduce the response speed of the receiver, a fast reset mechanism can be used to enhance receiver performance. In [60] an automatically created reset signal is suggested. The need to transverse different network layers is avoided by exploiting the guard time between packets. By detecting the gaps between packets using special circuitry, communication with the MAC layer is avoided.

The CDR circuit is essential to achieve burst mode operation. With the emergence of 10 Gbps PONs, various schemes have been investigated. The main techniques used for achieving CDR are the use of multi-phase clocks to over-sample the signal and then pick the clock that is closer aligned to the input e.g. [61] and the use of gated Voltage-Controlled Oscillators (VCOs), e.g. [62]. In this technique the oscillator generates pulses in sync with the input signal, [63]. In [63] a hybrid technique is suggested, combining both approaches to construct a 10 Gbps CDR. Other methods have been also reported. One such example is the use of injection-locking and VCOs reported in [64] to construct a 20 Gbps burst-mode CDR.

MAC Layer Efficiency and DBA

In TDM PONs multiple users share the available bandwidth in the upstream direction. Therefore, an efficient MAC mechanism is required whenever there is variation in user data rate and demand. Bandwidth efficiency can be increased using DBA. A DBA algorithm has to support some fundamental functionalities [65]; these include grant sizing, grant scheduling and queue scheduling. Grant sizing determines the duration of transmission for each ONU. Grant scheduling dictates the order of transmission between different ONUs - i.e. it carries out inter-ONU scheduling. Finally, queue scheduling sets the order of transmission for different queues of the same ONU - i.e. it carries out intra-ONU scheduling. DBA mechanisms can be classified from a QoS perspective as shown in Figure 3.4. According to this classification we can distinguish DBA algorithms that perform statistical multiplexing from QoS-oriented algorithms [66], [67]. Statistical multiplexing does not provide any service level guarantees; its main goal is to improve the resource utilisation of the system. On the other hand, QoS-oriented algorithms provide some service level assurances. The assurance may be of absolute or relative nature [67]. Typically Integrated Services (IntServ)-like algorithms are used to provide absolute level guarantees, while Differentiated Services (DiffServ)-like algorithms are utilised when relative service level guarantees are required [66]. IntServ-like algorithms are based on resource reservation and admission control. On the other hand, DiffServ-like algorithms are based on classification of traffic according to QoS requirements and a prioritization mechanism. Both types of algorithms can use either a centralized scheduler to allocate bandwidth to ONU queues implemented at the OLT level, or an hierarchical scheduler; in the last approach typically inter-ONU scheduling is carried out at the OLT while intra-ONU scheduling is carried out at the ONU level [66].

GPON and EPON follow different approaches as far as QoS is concerned, reflect-

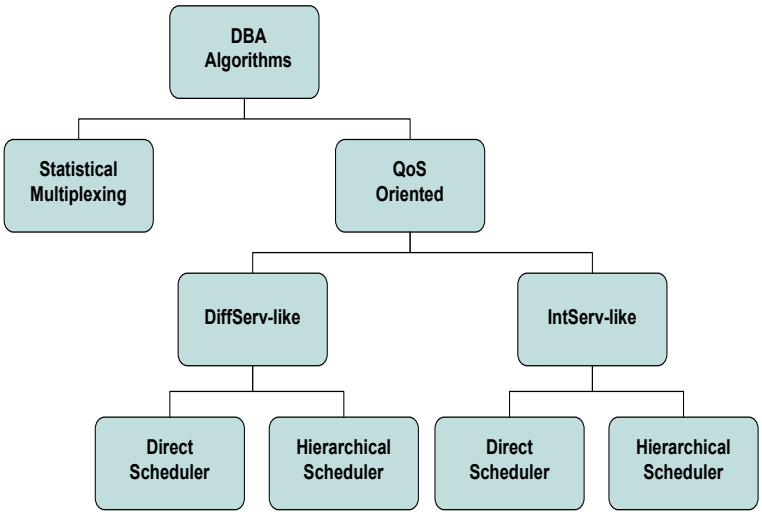

Figure 3.4: Classification of DBA algorithms [66].

ing the different philosophies of the corresponding standardization bodies. EPON is specified within the IEEE 802.3 framework, the same framework that specifies standard Ethernet. As Ethernet mainly targets computer networks, where quality of service traditionally has not been a major concern, EPON is based on a simple standard. On the other hand, GPON is the outcome of ITU's standardization efforts. As a large percentage of the ITU members are operators, GPON is based on a more complex standard that does address QoS [68]. In EPON, bandwidth allocation is carried out by the Multipoint Control Protocol (MPCP) that is also performing ranging and auto-discovery. The part of the protocol related to bandwidth allocation specifies the messages that can be used to transmit the bandwidth allocation information from the OLT to the ONU (GATE message) and the bandwidth request from the ONU to the OLT (REPORT message) [68]. In GPON the part of the standard that is related to bandwidth allocation is the GPON Transmission Convergence (GTC) Layer. Bandwidth allocation is performed regularly - every 125 μs -, as GTC downstream frames are periodically transmitted. Informa-

tion on bandwidth allocation is transmitted using the header of the frame using an upstream bandwidth map. GPON provides support for upstream QoS using Transport Containers (T-CONTs) that can be used to distinguish different queues of the same ONU. Upstream reporting is supported but its use is optional. ONUs can report the bandwidth requirements of each T-CONT using the Dynamic Bandwidth Report upstream (DBRu) field of the upstream frame [68], [29].

The above description of the bandwidth allocation mechanism specified by the EPON standard shows that in EPON there is more freedom for vendors to implement different DBA algorithms. This freedom has led to more research on DBA algorithms that focus on EPON, rather than GPON [68]. In [65] a survey of DBA mechanisms suggested in the literature for EPON is presented. The algorithms are classified according to the approach they follow in order to perform the three main functionalities of a DBA algorithm - grant sizing, grant scheduling and queue scheduling -, also taking into account QoS issues. Several ways to perform grant sizing are quoted. In fixed grant sizing the grant size is fixed for an ONU every polling cycle. In gated grant sizing each ONU is allocated as much bandwidth as it requests. One of the shortfalls of this approach is that it does not ensure fair access to resources among ONUs. In order to overcome this problem, limited grant sizing may be utilised. The ONUs are granted the requested bandwidth up to a specific limit. Above that limit they are assigned the pre-set maximum bandwidth. The value of maximum bandwidth should be carefully selected, as a large value would increase the maximum latency, while a small value would decrease bandwidth efficiency. In order to improve statistical multiplexing the limited grant sizing can be enhanced to accommodate excess distribution. In this approach,the excess bandwidth from ONUs that request less than the maximum bandwidth is allocated to overloaded ONUs. Queue size prediction can be used to calculate the traffic that will be accumulated in buffers during a polling cycle and take it into account during

grant sizing - a technique called exhaustive excess allocation with queue size prediction. The simplest grant scheduling mechanism is round-robin. In this approach the ONUs are polled with the same order during each cycle. Longest queue first and earliest packet first have also been suggested [65], [69]. The analysis in [65] continues with classification of queue scheduling techniques. Intra-ONU scheduling - i.e. queue scheduling - can be either performed at the OLT side using a centralized scheduler, or at the ONU side using an hierarchical scheduler. The first approach has scalability issues, while for the second the complexity of the algorithm is important since the ONU is a cost critical component. Two approaches are quoted; strict priority, where higher priority traffic can preempt (interrupt) low priority traffic transmission and weighted fair queuing. The first approach results in low delay for high priority traffic, but it is unfair, while the second is more fair, but it may degrade the quality of service for high priority traffic.

In [67] a survey of the main algorithms suggested for EPONs to achieve different levels of quality of service is carried out. Interleaved Polling with Adaptive Cycle Time (IPACT) [70] is a DBA mechanism performing statistical multiplexing to improve bandwidth utilisation. This is mainly achieved by means of interleaved polling, a technique where the next ONU that is scheduled to transmit is polled while the previous one is still transmitting, taking into account the round-trip time. Bandwidth Guaranteed Polling (BGP) [71] and Deterministic Effective Bandwidth (DEB) are described as examples of algorithms that can achieve absolute QoS guarantees. In BGP a table containing records of ONUs and their corresponding guaranteed bandwidth is maintained at the OLT. While BGP uses a centralized scheduler, in DEB a hierarchical scheduler is suggested. DEB uses leaky bucket parameters - peak rate, average rate, maximum burst at peak rate - to characterise the traffic of each of its queues and report it to the OLT. The OLT assigns bandwidth according to the effective traffic of an ONU compared to the overall effective traffic and ONUs

allocate resources to queues according to the effective traffic of the queue compared to the overall effective traffic of the ONU. The algorithm uses admission control to guarantee that delay bounds are not violated. DBA for multimedia, [72] is an algorithm following a DiffServ approach applying strict priority queue scheduling using a centralized scheduler to provide relative QoS assurances. In DBA for QoS [73] relative QoS assurances are provided by means of an hierarchical scheduler. At the ONU side strict priority is performed - but only for traffic that has arrived before sending the report to the OLT - while the OLT uses weighted fair scheduling to assign grants to the ONUs. Excess bandwidth is allocated using exhaustive allocation with queue size prediction.

In [68] a comparison of DBA for EPON and GPON is carried out. The results are also extended to next-generation PON (10G PON). IPACT has been considered the selected algorithm for EPON. A simple algorithm is considered for GPON, with reporting from ONUs enabled and the main difference between the algorithm and IPACT being the fixed polling cycle. The authors argue that for EPON the choice for the maximum polling cycle is critical for the performance of the system. The optimum depends on ONU buffer size, transmission delay and DBA processing time at the OLT. Although QoS has not been considered in their analysis, the results show that in EPON a large polling cycle improves performance up to a saturation level. The authors also conclude that fast DBA algorithm response (low processing time) is critical for GPON especially under heavy load, in order to prevent buffer overflow.

Extending the Reach of TDM PONs

Reach extension and the use of higher splitting ratios are fields of intensive research and very much relevant to the move to next-generation optical access networks. Techno-economical studies reveal that these parameters are vital, if PONs are go-

ing to be deployed in a large scale and at reasonable cost [66]. It is obvious that in order to achieve the reach extension/splitting ratio increase a higher power margin is required, which can be achieved using amplifiers. There are several choices of amplifiers that can be used towards this goal. Erbium-Doped Fiber Amplifiers (EDFAs) provide high gain. One issue that needs to be resolved though, is the fact that the window of operation of EDFAs is outside the current PON window of operation. Additionally, in order to cope with the bursty traffic in the upstream direction, adaptive gain control is required [74], as operation of EDFAs in burst mode is more challenging compared to other types of amplifiers [75]. Another option for signal amplification is the use of other dopants, such as thulium and praseodymium. Fiber-doped amplifiers of that kind can achieve amplification within the operating region of PONs. Although this technology is not yet commercially available it may be a viable solution in the future [75]. Semiconductor Optical Amplifiers (SOAs) have also been considered, since they can operate at the wavelength of interest and have a fast gain response, although they cannot achieve the high gain/low noise operation of EDFAs [74]. The use of Raman amplification has also been suggested, e.g. in [76]. In this solution the wavelength of the pumps should be selected carefully in order to avoid depleting the signal traveling towards the other direction while providing sufficient gain. The pump's wavelength for Raman amplification does not fall within the low loss region of the silica, an additional issue to be resolved. In [76], AllWave fiber - with a wide low loss window - has been used to address this problem.

Several alternatives exist as far as the location and the number of amplifiers is concerned. A separate amplifier per ONU can be used, either a SOA or an Erbium-doped waveguide amplifier [74]. However, [77] - a survey of long reach optical access technologies - demonstrates that amplifiers are typically located at the OLT and/or at the mid-span extender. In case the amplifiers are shared between

ONUs, there are two choices; either separate amplifiers can be used for upstream and downstream, or a single - commonly multi-stage - amplifier is used to amplify the signal in both directions. The first approach allows use of different wavelength bands and amplifier technologies for upstream and downstream. It also enables optimization of upstream and downstream amplifier stages separately and avoids problems generated by cross-modulation and reflection [74]. On the other hand, the use of bidirectional amplification results in fewer components and lower cost while burst-mode operation becomes easier [75]. Burst mode operation in a bidirectional configuration can be achieved using a large downstream signal to saturate the amplifier. This solution is suggested in case an EDFA is used as SOAs can operate in burst mode easier. In EDFAs slow input variation can result in large gain transients distorting the output signal [75]. Other methods that have been suggested to achieve burst mode operation of EDFAs include electronic gain compensation, the use of an additional saturating signal [75] and gain-clamping, a technique utilising an optical feedback loop which results in oscillation; the oscillating signal is used to drive the amplifier into saturation [74]. In the case of SOAs, similar techniques are utilised. These include, for example, the use of saturated SOAs, opto-electronic control or all-optical control - achieved in a way similar to gain-clamping [78]. In [78] a technique based on feedforward control of the gain to increase the dynamic range of the amplifier is also presented.

Some noteworthy efforts to extend the reach and increase the splitting ratio of TDM PONs, include the development of SuperPON within the framework of the PLANET project and the development of Long-Reach PON by British Telecomms (BT) [77]. The 20 km maximum reach of PONs has been extended to 100 km, while the splitting ratio has been increased from the 1:32 maximum to 1:2048. SuperPON offered 2.5 Gbps and 311 Mbps in the downstream and upstream directions, respectively. Long-Reach PON delivered 10 Gbps over 100 km, albeit for 1024-way

split. There have been other efforts to increase the reach and splitting ratio of PONs (e.g. the PIEMAN architecture) but include the use of WDM, therefore will not be further analyzed at this point [77].

3.2.3 Current Deployments and Future of TDM PONs

At the time of the writing of this literature review, i.e. at the start of the research at the end of 2009, there are several TDM PON deployments worldwide. The highest number of PON users are located in the Asia-Pacific region [30]. EPON and GPON have dominated in different regions of the world with EPON being the choice of the operators in Asia (e.g. Japan, Korea) while GPON has been mostly deployed in Europe and North America [38]. Although as noted in [30] most Fiber-To-The-Home (FTTH) subscribers are connected to a point-to-point connection, it is predicted that by 2012 the number of PON subscribers will be higher than those served by point-to-point fiber links. According to this paper, the number of FTTx customers is going to surpass the 100 Million mark by 2012, three times more the corresponding number in 2007. In the US companies that have successfully deployed PONs are SBC and Verizon. Both have chosen B/GPON for their networks, [38]. In Asia NTT and Korean Telecoms have chosen EPON [38], [79].

The main trends in optical access technologies include the move to higher data rates (10 Gbps), the use of longer reach and higher splitting ratio and the use of WDM [80]. The main motivation behind the move to higher data rates is the recent shift in user behavior. Users tend to move away from simple web browsing, which generates bursty traffic. Video applications constitute an increasing percentage of the overall Internet traffic. Statistical multiplexing cannot help in this case, therefore a bandwidth upgrade of the network seems necessary. Moreover peer-to-peer traffic is in an increasing trend, leading to higher upstream bandwidth requirements [81]. The enhanced 10 Gbps version of EPON has already been standardized by the

IEEE (IEEE 802.3av standard). The standard has been published in September 2009 [40] and supports 10 Gbps in the downstream and 1 Gbps or 10 Gbps in the upstream direction. The FSAN group is also currently working on upgraded versions of GPON, called XG-PON. XG-PON1 is going to lead to 10 Gbps downstream and 2.5 Gbps upstream, while XG-PON2 will offer 10 Gbps bidirectional transmission [41]. Reach extension and an increase of the splitting ratio is essential since node consolidation and elimination of the metro part of the network could lead to significant cost savings [66]. The main enabling technologies to achieve this aim have been already discussed. WDM is an option and one of the ways to achieve the desirable reach extension, using a hybrid WDM/TDM architecture, which would allow PON overlay. Each PON would then have a decreased splitting ratio, but the overall number of users would be higher. WDM PONs are discussed in the next section.

3.3 WDM PONs

In WDM PONs each ONU utilises a pair of dedicated wavelengths; one for upstream and one for downstream transmission, resulting in a virtual point-to-point connection [80]. Figure 3.5 depicts the generic layout of a WDM PON. At the OLT side one transmitter is used per ONU. Each transmitter emits at a different wavelength. The outputs of all the transmitters are multiplexed using an AWG to be transmitted over the shared part of the fiber. The AWG at the remote node demultiplexes the wavelengths; that way a virtual point-to-point connection is realized. The same mechanism is used for upstream transmission. A WDM PON architecture is best suited for video and peer-to-peer applications, as it can provide high dedicated bandwidth per ONU in both directions [32]. WDM PON is considered mainly an experimental technology as currently it is quite expensive for large-scale

deployment and the bandwidth demand is not evident. Despite that fact, there are already some commercial deployments of WDM PONs, e.g. in Korea [82].

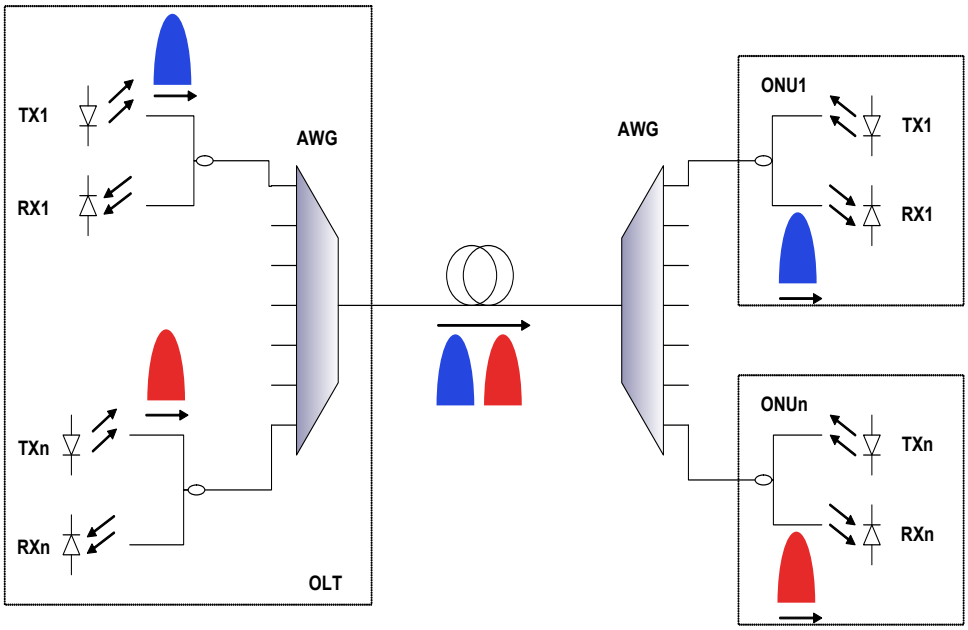

Figure 3.5: Generic WDM PON architecture.

3.3.1 Technical Challenges Related to WDM PONs

The main challenges related to the deployment of WDM PONs are the following [29][31]:

- Components that are used in WDM PONs cost more than their TDM PON counterparts.
- In a WDM PON, at the OLT side, one transmitter is required per ONU, resulting in higher overall number of components.
- Avoiding the use of a wavelength specific source at the ONU side is critical to avoid cost and inventory problems.

- The fact that components' operating wavelength tends to drift with temperature is a challenge, although the use of wavelength agnostic components at the ONU side should, to a certain extend, alleviate this problem.

- Although QoS is guaranteed, as there is a dedicated wavelength per user,this results in low overall bandwidth utilisation.

3.3.2 Suggested Solutions

Athermal Components

One of the advantages of PONs is that they do not require power installation or active electronic components between the Central Office (CO) and the customer premises. In order to maintain this advantage in WDM PONs, the use of athermal AWGs is required, since any wavelength drift with temperature would cause severe performance penalties. One way to achieve this, is the use of materials with temperature dependence of the refractive index opposite to that of silica [83]. That way the wavelength drift because of silica glass is compensated. In [84], use of this method combined with pressure control in order to improve the second-order temperature dependence of the device resulted in an AWG with passband wavelength variation of 0.025 nm in a -40^{o}C to 85^{o}C temperature range. Another suggested solution is the use of mechanical movable parts [85]. Expansion of these parts as temperature rises changes the shape of the waveguides through which the light has to travel within the device. The overall result is that the optical path length remains constant with temperature. In [85], it becomes clear that AWGs produced using this method are commercially available.

Although the development of uncooled transmitters (lasers) is not critical for the commercial success of WDM PONs, it could provide benefits, depending on the evolution path that optical access networks are going to follow. Athermal lasers

could be used mainly in two cases in a WDM PON; in the first case tunable lasers are utilised as ONU transmitters in a Course Wavelength-Division Multiplexing (CWDM)-based PON. In the second case, fast tunable lasers are used at the OLT either as shared transmitters, or to perform Frequency Shift Keying (FSK) modulation by tuning their wavelengths. A Distributed Bragg Reflector (DBR) laser, that can be used as tunable, uncooled transmitter for CWDM applications is reported in [86]. The principle of operation is based on biasing different parts of the multi-section laser with different currents (to generate phase control and gain control regions).

The use of the low-cost, cheap and low-mass Vertical Cavity Surface Emitting Lasers (VCSELs) in PONs may not be feasible in the near future, due to technical issues related to long-wavelength operation of VCSELs. Despite that fact, it worth tracking developments in VCSEL technology, since low-cost, long wavelength VCSELs may be available in the near future. Moreover, for particle physics applications 1.5 μm operation is not mandatory, contrary to commercial networks where due to the longer distances, VCSELs have to operate at the operating window of optical amplifiers. Athermal operation of a tunable VCSEL has been reported for example in [87]. Athermal operation in this case has been based on mechanical movement of a reflective surface (Micro-Electro-Mechanical Systems (MEMS)-based).

In order to achieve fast-switching operation for use at the OLT side Sampled Grating-Distributed Bragg Reflector (SG-DBR) or Grating-assisted Coupler with Sampled Reflector (GCSR) lasers are used. Temperature stability can be achieved using a model based on the time constants of thermal electrical and optical rate equations and an auto-compensating model using distorted pulse current [66].

Architectures to Avoid Using Wavelength Specific Source at the ONU Side

Several architectures have been suggested in order to avoid the use of wavelength-specific ONUs. These include architectures based on tunable lasers, architectures based on broadband spectrum slicing, architectures based on injection-locked lasers and architectures based on sourceless ONUs (light seeding schemes). We proceed by analyzing the advantages and limitations of each technology, as well as suggested solutions to overcome them.

Based on Tunable Lasers In [88] External Cavity Lasers (ECLs) , thermally tuned Distributed Feedback (DFB) and multi-section lasers are quoted as tunable lasers with potential applications in WDM PONs. The ECL can be quite bulky and requires an external modulator for high-speed modulation because of its long cavity length. Thermally-tuned DFB lasers are a potential solution but since they require a thermoelectric cooler have increased power consumption. Another limitation of this solution is their limited tuning range [66]. Multi-section DFB or DBR lasers use multiple sections to achieve gain and phase adjustments which result in wavelength tunability. The wavelength tunability is achieved by adjusting the injected current in different sections of the laser to modify the refractive index [89]. In the same document tunable VCSELs using MEMS are also mentioned as an alternative to achieve laser tunability. The challenges that need to be addressed in order to successfully manufacture long wavelength tunable VCSELs are outlined in [90]. The author favors a MEMS-based approach to achieve VCSEL tunability. Long wavelength VCSEL tunability using MEMS is demonstrated in [91]. A survey of tunable laser technologies [92], does not mention tunable VCSELs as a commercially available option, while in [93], an overview of the VCSEL market, it seems that the long wavelength VCSEL market has not taken up yet. Therefore commercial

availability of tunable VCSELs can be an issue for some time to come.

The use of tunable lasers to manufacture wavelength-agnostic ONUs is still considered too expensive to be a viable solution. Despite that fact the authors in [35] suggest a WDM PON architecture using ECL-based ONUs. In this paper the ECL is used in combination with external modulator for upstream transmission and it also serves as local oscillator for the heterodyne receiver.

Based on Broadband Spectrum slicing This type of architecture tries to exploit the low cost of Broadband Light Sources (BLSs) and use them as wavelength-agnostic light sources at the ONU. The modulated broadband light is spectrally sliced by the AWG at the remote node, resulting in a unique spectrum slice allocated to each subscriber connected to a different AWG port, as shown in Figure 3.6 [31]. One of the main problems related to this approach is the high loss caused by slicing [94] [31]. Moreover, the number of users in a WDM PON based on spectrum-slicing is limited by the spectrum width of the broadband source [31]. Crosstalk is another challenge related to this architecture due to the limited out-of-band rejection level of the AWG. The effect of crosstalk becomes more pronounced when the passbands of the two AWGs - the one located at the remote node and the one positioned at the local office - are not aligned. A study of the effects of loss and crosstalk in spectrum-sliced WDM PONs along with the implications of AWG performance parameters on them is presented in [95]. The presence of beat noise due to the use of an incoherent light source is also a factor limiting the performance of this type of architecture. The effect of beat noise is inversely proportional to the optical-to-electrical bandwidth ratio, m ($m = B_o/B_e$). Thus increasing the optical bandwidth will decrease the effect of beat noise. However, this solution results in low bandwidth efficiency, but more importantly increases the sensitivity of the system to dispersion. Therefore m should be optimized to achieve the maximum possible performance. A study on the

relationship between m and several system parameters - length, bit rate, dispersion coefficients - that can be used as a guide for appropriate choice of m, is carried out in [96].

Several solutions have been suggested in the literature to address the above listed problems. The use of optical pre-amplification, to overcome the high slicing loss is suggested in [97]. The use of Pulse Position Modulation (PPM) instead of On-Off Keying is suggested in [98] to make the signal more resistant to dispersion. A higher value of optical to electrical bandwidth can than be used to alleviate the effect of beat noise. In [99], a method to reduce beat noise based on optoelectronic feedforward compensation is suggested. In this method, the spectrum-sliced signal is subtracted from the data signal before modulation. However, this implies that spectrum slicing is not carried out at the remote node but using a filter at the ONU. Inevitably, that leads to an increase in ONU cost and complexity. Large part of the complexity increase is focused on the ONU electronics.

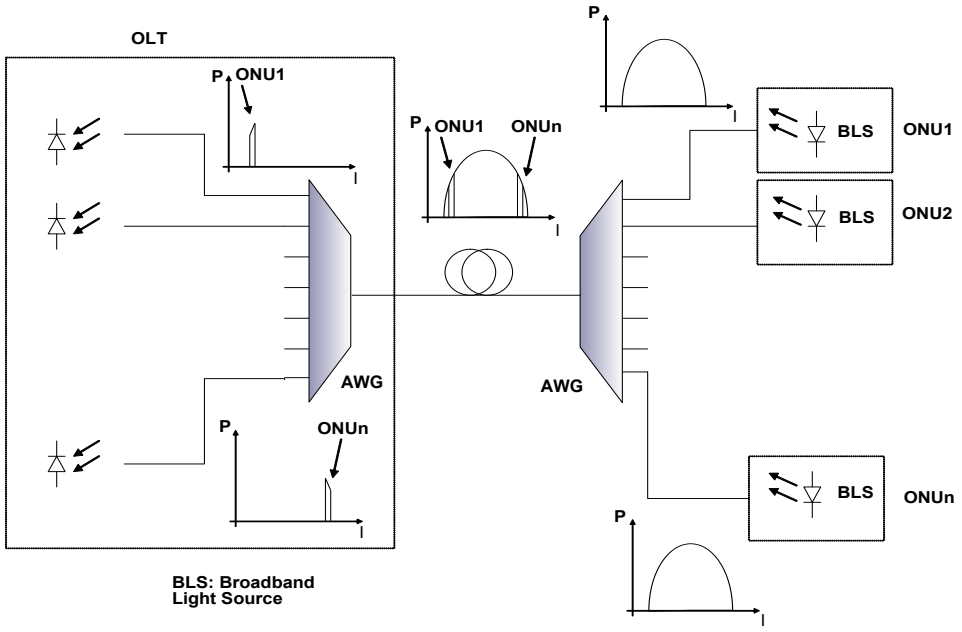

Figure 3.6: WDM PON architecture based on broadband light sources and spectrum slicing [31].

Although the use of Light Emitting Diodes (LEDs) as ONU transmitters is desirable due to cost reasons and has been suggested, for example in [100], other components have also been proposed as BLSs. The use of a LED imposes limitations both on modulation speed - although in [101] a LED with 10 GHz modulation bandwidth is reported -, as well as transmission distance due to its low power. Therefore, the use of Superluminescent Light Emitting Diodes (SLEDs) that can provide higher power has been suggested, for example in [102]. The use of Fabry-Perot Laser Diodes (FP-LDs) has also been suggested [103]. Although FP-LDs offer higher power than LEDs, they have narrower spectrum, therefore the maximum number of channels is limited. Additionally, the performance of the system is limited by mode fluctuations. The use of EDFA as an Amplified Spontaneous Emission (ASE) source is suggested in [104], where spectrum-sliced light from an EDFA is modulated by several modulators, thus providing the light for more than one customers - although this architecture could be classified in another category depending on the precise topology used to deploy this solution.

Based on Injection-Locked Lasers Architectures based on injection-locked lasers typically use multimode FP-LDs as ONU transmitters. As shown in Figure 3.7, Fabry-Perot multimode lasers can excite only one of their modes when a properly adjusted external optical signal is injected into them [88]. As Figure 3.8 depicts, the injected light is typically provided by a centralized source installed at the OLT side. In this architecture the number of users is limited by the number of longitudinal modes of the FP-LD. An additional limitation is imposed by back scattering and reflections of the injected light that cause degradation of the receiver sensitivity in the upstream direction [31]. The modulation index, injected power and bias current are parameters that should be carefully selected in order to achieve efficient locking. The detuning between the injected and the injection-locked wave-

length that can be caused by wavelength drift because of temperature needs to be controlled. A study of the dependencies between these parameters and injection-locking performance is presented in [105]. In [106], a study of the effects of reflection is carried out. The authors suggest the use of incoherent light for injection as its impact on system performance is less destructive when it is reflected. The facet reflectivity of the FP-LD should also be considered during system design. Its impact is analyzed in [107]. In [108] it is calculated that the use of FP-LDs with low front-facet reflectivity (1%) and a relatively long cavity can achieve a compromise between widening the injection-locking wavelength range of the laser, while still achieving better noise performance than Reflective Semiconductor Optical Amplifiers (RSOAs).

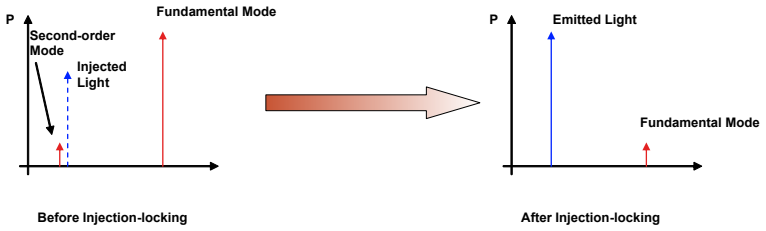

Figure 3.7: Principle of injection-locking [88].

The maximum achievable data rate in the upstream direction is affected by the choice of the light source providing the injected light. The sources that can be used fall into two categories; coherent and incoherent. A large number of proposals utilise incoherent, spectrum sliced ASE sources to provide the injected light. In [109], [110] an EDFA is used as a light source, while in [111] the injected light is provided by spectrum-sliced SLEDs. The main issue encountered in this approach is that the upstream data rate is limited due to the excess intensity noise of the spectrally-sliced incoherent light used to injection-lock the LD. The bandwidth of the injected light needs to be optimized to strike a balance between low excess intensity noise, sufficient optical injected power and side-mode suppression ratio.

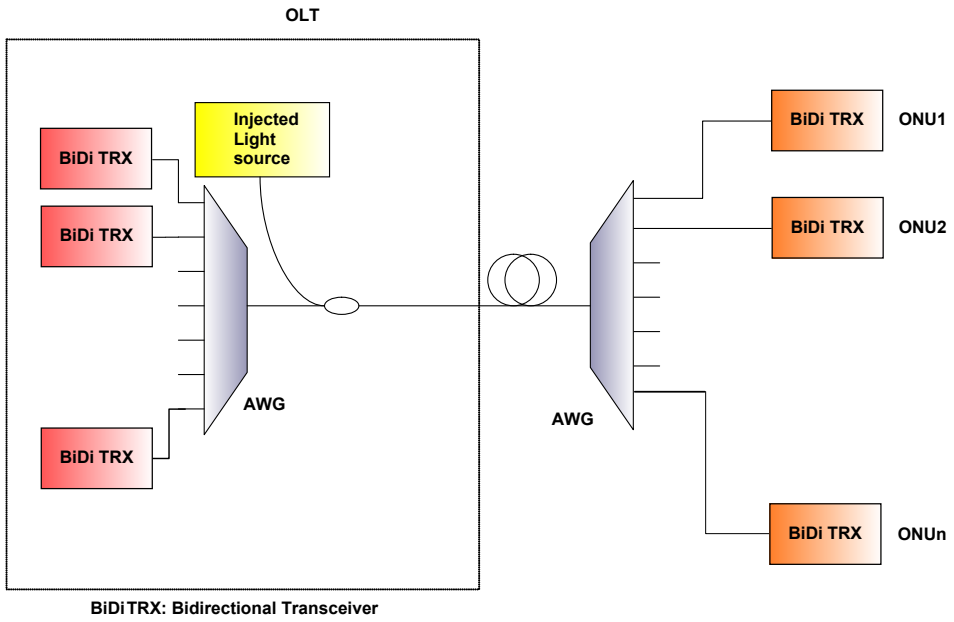

Figure 3.8: Example of WDM PON architecture based on injection-locking [31].

The impact of the filter bandwidth on injection-locking performance is analyzed in [112]. The authors also suggest the use of a SOA to reduce the excess noise. Still, the data rate achieved is 1.25 Gbps - much lower than the required 10 Gbps for data readout at the HL-LHC.

In order to move to higher data rates, the use of coherent light has been suggested. The problem encountered in this approach is the dependence of the performance of the injection-locked FP-LDs on the polarization state of the injected light [113]. In [114] the use of polarization-insensitive supercontinuum pulses is suggested in order to overcome this problem. A 2.5 Gbps data rate is achieved. In [115] a 10 Gbps data rate is achieved using multiple laser diodes and a depolarizer.

As VCSELs provide a cheap alternative to edge emitting lasers, in [116] the use of injection-locked VCSELs is suggested. Another interesting proposal to reduce cost is the use of self-injection locking, where the light emitted from the FP-LDs is spectrally sliced at the AWG and reflected back to the ONUs to injection-lock them

[117]. A delay line is used to remove the coherence between injected and emitted light and code mark inversion is used to avoid data patterning effects.

Injection-locking and its effect on laser performance characteristics has been extensively studied and found to have beneficial effects on the laser's operational characteristics, including its modulation bandwidth [118],[119]. In [120] the authors claim that 80 GHz 3-db bandwidth can be achieved using strong injection-locking.

Based on Sourceless ONUs (Light Seeding Schemes) Architectures based on sourceless ONUs, use modulators as transmitters at the ONU side [31]. The light for upstream transmission is provided by a source installed at the OLT side. An array of devices can be used in this architecture for upstream modulation, such as SOAs [121], Mach-Zehnder modulators (MZMs) [122] and EAMs [123]. The architectures suggested, use either two separate fibers for the injected light traveling downstream and the upstream signal, to avoid reflections, e.g. [124], or a single fiber and a modulator in a loop back configuration [125]. An additional design decision affecting the performance of the architecture concerns the choice of the injected light source; a dedicated light source, typically spectrally sliced by the AWG is one option [121], remodulating the downstream signal with upstream data is the other [126]. An example WDM PON based on SOAs is depicted in Figure 3.9.

One of the technical challenges encountered in the particular architecture is the higher attenuation experienced by the upstream signal. Use of a SOA for upstream modulation can provide benefits due to the fact that amplification and modulation can be carried out using a single device. A single SOA can even be used as a receiver at the same time [66]. As single fiber operation is desirable, it is important to address and solve technical issues encountered when SOA is used in a reflective configuration. In [127], an overview of the technical issues that need to be resolved is given. The light for upstream transmission can be provided by a

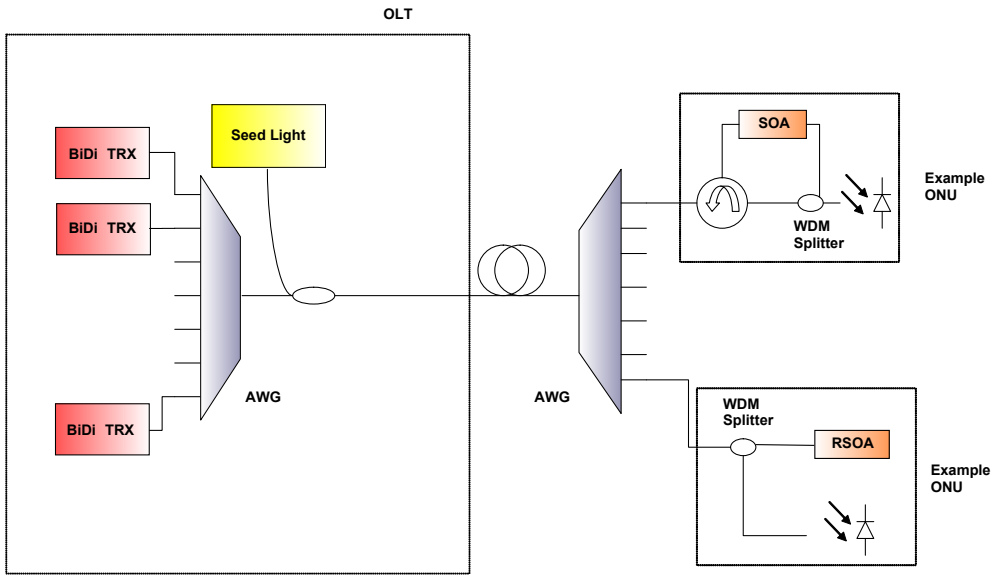

Figure 3.9: Example of WDM PON architecture based on sourceless ONUs [31].

dedicated source at the OLT, which can be either a spectrum sliced ASE source, or Continuous-Wave (CW) light from DFB lasers. However in such a case an additional source, apart from the downstream transmitter, is used. Since it is desirable to eliminate this source, remodulation has been suggested that utilises the light emitted by the downstream transmitter. The main challenge with this approach is the residual component of the downstream modulation on the upstream signal. In order to reduce its effect, a low extinction ratio should be used in the downstream direction that inevitably degrades the quality of the downstream signal. Several solutions have been suggested to address the problem of remodulation noise. Using gain saturation to suppress this component has been suggested in [125]. Use of Manchester coding [128] and SCM [129] have also been proposed as solutions to this problem, since the remodulation noise in these cases is outside the upstream signal's bandwidth [127]. In [126] two additional solution methods are quoted. One relies on filtering to manipulate the extinction ratio of the input signal to the RSOA based on a property of DFB lasers - the method assumes DFB lasers as downstream transmit-

ters. Due to chirp, the "1" and "0" have different spectral characteristics. Thus, appropriate filtering can lead to extinction ratio manipulation before the RSOA. The second method is based on feedforward compensation, as the downstream data is available at the ONU. This in-advance knowledge of the data sequence, can be utilised to modify the modulation current and eliminate the residual component. Reflection tolerance is an additional issue that needs to be treated in light seeding schemes [127]. A detailed study of the effects of reflection is given in [130]. An interesting outcome of this paper is the fact that the allowable reflectivity is very low (-42 dB for the investigated setup offering 1.25 Gbps downstream and 155 Mbps upstream) when a single reflection point for the downstream signal exists close to the OLT. As the reflected signal causes optical beat interference its effect can be alleviated by broadening the spectrum of the signal, so that the spectral content of the interference noise falls outside the receiver bandwidth. In [131] this is achieved by means of bias dithering at the RSOA side or use of phase modulation for the downstream signal. In [132] sub-carrier multiplexing is proposed to address this issue, while in [133] Manchester encoding is utilised to minimise the effect of the reflected signal. An interesting proposal to remove the light seeding source altogether is the use of a self-seeding RSOA, suggested in [134]. In [127] the bandwidth limitations of RSOAs as well as the gain temperature dependence are quoted as challenges related to their operation. The 3-dB bandwidth of the RSOA under discussion in the document was 3 GHz. However, the authors mention that they have managed to achieve 10 Gbps operation using a decision feedback equalizer and forward error correction. Regarding the temperature dependence of the gain it is mentioned that while the gain is quite broadband the actual limitation may be the modulation bandwidth. The operating range of uncooled RSOAs has been studied in [135]. Operation between -20^{o}C and 60^{o}C has been achieved by controlling the bias current.

The limited modulation bandwidth of SOAs is one of the primary reasons why the use of EAMs has been suggested instead. Use of REAMs in combination with a SOA to provide sufficient gain is reported in [123] and [136]. In both schemes 10 Gbps upstream transmission has been achieved. One of the advantages of EAM devices is that they can be monolithically integrated with SOAs. One such device is reported in [137]. A monolithically integrated SOA/REAM is used in [138] to provide a data rate of 40 Gbps in the upstream direction, exploiting the very high modulation bandwidth of the EAM. In [139] an EAM has been modulated up to 50 Gbps with a 2V peak-to-peak driving voltage. In [140] the authors report EAM modulation with 80 Gbps data. Advantages of EAMs, apart from their high modulation bandwidth, include their low power consumption and small size. Still many WDM PON designs use electro-optic modulators, e.g. [124], [141] and [122]. One of the main advantages of electro-optic modulators (Mach-Zehnder interferometers or phase modulators) is that they allow use of advanced modulation formats; currently commercial structures used for such formats are based electro-optic modulator technology; this is illustrated for example in [142] where a survey of technologies for multi-level, multi-dimensional coding is carried out. Their disadvantages include their large size and the high driving voltage required. Despite that fact this requirement becomes more relaxed as technology advances, for example in [143] a 35 GHz Mach-Zehnder driven by 0.3 V peak-to-peak is reported.

3.3.3 Current Deployments and Future of WDM PONs

WDM PONs are currently - at the beginning of the research reported in this thesis at the end of 2009 - considered an expensive option for the access part of the network and the bandwidth demand does not justify such an investment yet. Many of the enabling technologies described in the previous sections are either in experimental status, or considered quite costly to be deployed. Moreover, the current lack of

standards does not encourage high volume production of WDM PON components, which would lead to price reduction. As mentioned in [144], where a comparison between 10G TDM PON and WDM PON is carried out, in the FSAN group (NG-PON) is divided into two groups; NG-PON1, which includes XGPON1 and XGPON2 and NG-PON2, for which the technology is open. It is very likely that this technology is going to be WDM PON. Despite that fact, it seems that it will take a number of years before the first WDM PON standards are published [145]. The expected required bandwidth per subscriber in the downstream direction at the time of publishing of the first WDM PON standards is expected to be around 150-300 Mbps [145]. Thus, although 100 Mbps and 10 Gbps have not been completely ruled out, it should be expected that the first WDM PONs will offer 1 Gbps per wavelength, [144]. This becomes apparent in the few commercial implementations of WDM PON in Korea. In 2007 commercial WDM PONs, based on injection-locked lasers have been deployed [82]. The deployed WDM PON could serve 32 users - 32 wavelengths have been used - over a maximum distance of 10 km and offered 125 Mbps per channel. Also in 2008 a 20 km, 16 user, 1.25 Gbps/channel commercial WDM PON has been deployed [79].

3.4 Other Technologies

This section briefly describes PON technologies not falling under the dominant PON categories - i.e. TDM and WDM PON - that have received considerable research attention recently. The following subsections do not provide an in-depth description of the technologies; the intention is to provide some information regarding the potential benefits and shortfalls of these technologies.

3.4.1 OCDMA PON

The basic operating principle of Code Division Multiple Access (CDMA) systems is the use of codes to distinguish between communication channels. Encoding involves multiplication - more precisely a XOR operation - of each bit to be transmitted by a code in the time domain, the frequency - wavelength - domain or even both. An example of the encoding process in the time domain along with its implications in the frequency domain is illustrated in Figure 3.10. At the receiver side the reverse operation is applied to recover the transmitted information [26].

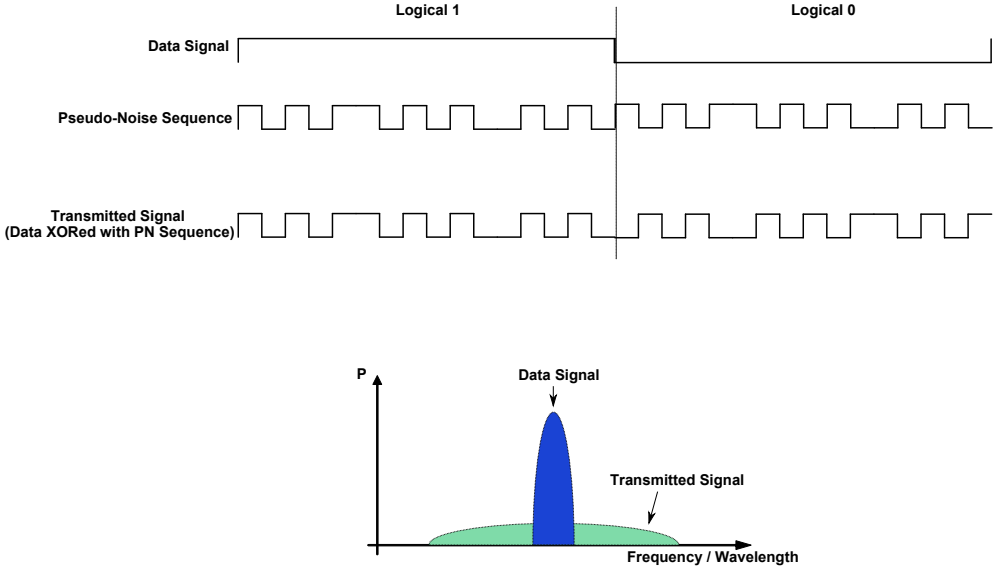

Figure 3.10: CDMA principle of operation.

In [26] an overview of Optical CDMA (OCDMA) technology and its applications is given. This work summarizes the major advantages and disadvantages of the technology.

There are a number of drawbacks hindering the implementation of OCDMA systems. Implementation of OCDMA requires a large array of components, which in their majority are not based on mature technologies. These components are quite complex; an additional factor that increases the cost of the components. In

OCDMA multi-access interference translates to beat and shot noise. In contrast Wavelength Division Multiple Access (WDMA) and TDMA networks are much less affected by these impairments. Dispersion is an issue for OCDMA, since encoding leads to an increase in line rate, which is higher than the bit rate. OCDMA has also lower spectral efficiency than its multiple access counterparts, WDMA and TDMA.

On the other hand OCDMA has some beneficial characteristics, justifying the research interest it attracts. It does not require a complex MAC mechanism like TDMA and it can support more users than both TDMA and WDMA especially when using coding in both time and wavelength domain. OCDMA, like WDMA offers virtual point-to-point connectivity. Its advantage over WDMA though is that it can provide it using a splitter instead of a multiplexer. OCDMA offers high granularity. Many low bit-rate users and users with different data rates can be accommodated easily. OCDMA can support a high number of users transmitting at high speed. It also supports symmetrical operation, i.e. the same bandwidth is offered per ONU in both upstream and downstream directions. In OCDMA security is inherent due to the coding mechanism. It also allows the design of special codes that provide bandwidth and signal quality fairness as well as robustness against wavelength drifts.

3.4.2 OFDM PON

In OFDM multiple user symbols are transmitted in parallel. Each of the symbols is modulating one out of many orthogonal sub-carriers [146]. The same principle can also be used to provide multiple access in which case the multiple access scheme is called Orthogonal Frequency Division Multiple Access (OFDMA). Typically in OFDMA the available sub-carriers are divided into groups called sub-channels, which are then assigned to users. Each user can occupy more than one sub-channels [147].

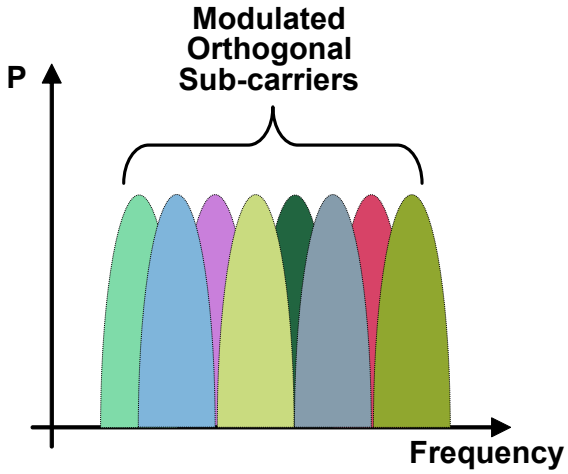

Figure 3.11: OFDM spectrum.

OFDM has several advantages, a fact that becomes apparent by its use in several commercial systems, both in wireless (e.g. WiMAX, WiFi) and wireline (e.g. Digital Subscriber Line (DSL)) communications. One of the fundamental advantages of OFDM is its robustness to dispersion and Inter-Symbol Interference (ISI), due to the longer symbol period [148]. Additionally, OFDM can be efficiently combined with adaptive modulation and coding, a significant attribute for transmission over a varying channel that also increases its spectral efficiency [149] . Equalization becomes easier for OFDM, since it can be performed by means of an one-tap equalizer in the frequency domain [149]. Finally, it has good scalability as dispersion and bit rates increase [27].

OFDM has also several disadvantages, one of them being its high peak-to-average power ratio, requiring a wide dynamic range for some of the transmitter and receiver components. More precisely the transmitter amplifier must be linear over a wide range of signal levels. This increases both the cost and the power consumption of the transmitter. Any non-linearity can result in inter-modulation causing out-of-band emission and in-band distortion of the signal. OFDM is also sensitive to frequency offset, phase noise and I-Q imbalance, which can significantly

degrade the performance of the system. One of the most critical aspects related to OFDM PON deployment is the cost and performance requirements for the Digital-Signal Processing (DSP) analog-to-digital converter (ADC) and digital-to-analog converter (DAC) modules, as the OFDM signal is commonly generated using digital signal processing. Quite fast DSPs are required, while the complexity of the Fast Fourier Transform (FFT)/Inverse Fast Fourier Transform (IFFT) algorithms is not negligible. The DAC should have a quite high resolution and both, the DAC and the ADC should be highly linear and have low jitter and be able to achieve high accuracy [27].

3.5 Passive Optical Networks in High-Energy Physics

The use of a PON-based architecture for high-energy physics applications was first suggested by Ujiie in [150], [151]. The proposed network configuration made use of both TDM and WDM to multiplex traffic from different detector channels. A group of detector channels was assigned a dedicated wavelength and the associated traffic was multiplexed using TDM; traffic from different groups would then be multiplexed using WDM to be transmitted over a single fiber. Multiplexing in the wavelength domain would be achieved using lasers emitting at different wavelengths. The architecture was never implemented, as it was intended for use at the Superconducting Super Collider (SSC), a project that was finally abandoned due to its high cost. At the same time all the LHC experiments implemented point-to-point links to facilitate data transfer to and from their detectors. However, as optical technologies matured, the concept of using multiplexing to increase the efficiency of the optical infrastructure of high-energy physics experiments re-emerged. So, in [152] the possibility of using Dense Wavelength-Division Multiplexing (DWDM) for data acquisition in particle physics experiments is re-evaluated. The primary

focus of [152] is on challenges related to electronics and not optical network design aspects. The suggested architecture makes use of DFB lasers emitting at different wavelengths, although the authors mention that the lasers are also tunable. This renewed interest in the use of WDM led to the first network implementations for particle physics applications based on this technology. More particularly, a WDM PON based on REAMs was the network of choice for neutrino telescope data readout applications [153] [154] [155]. Despite the fact that neutrino telescope detectors have a very different structure than those of the LHC (and HL-LHC), for example they cover a much larger area, the use of WDM PONs for their readout is indicative of the renewed interest in more advanced technologies.

3.6 Conclusions

This Chapter provided an outline of the PON "architectural space". The architectures described here are going to define the tools at our disposal in order to design suitable network structures for the HL-LHC. It is appropriate to close this Chapter with a short evaluation of the described technologies as far as their applicability for use at the HL-LHC is concerned. The purpose of this evaluation is not to design a network at this stage; it is just to highlight interesting features or potential drawbacks of each type of architecture. During this evaluation the requirements for a unified network architecture at the HL-LHC - outlined in Chapter 2 - are taken into account.

TDM PONs are widely deployed and they are expected to remain the choice of the operators for some years to come. Consequently, the particular technology offers advantages in terms of component cost and commercial availability. Despite that the bandwidth sharing mechanism in the upstream direction essentially limits the data rate to levels not compatible to the requirements of a modern particle

physics experiment. Therefore the applicability of TDM seems to be limited to the downstream direction where much of the information is broadcasted.

WDM PONs offer an interesting alternative since they can provide virtual point-to-point connectivity. However, placing an AWG device at the front-end remains controversial, mainly due to reliability concerns. The main arguments against such a move are the fact that it introduces a single point of failure in a harsh environment and that fiber-sharing although a "good to have" feature is not considered to be a very high priority by the particle physics community. Another option would be to place the AWG in the counting room. Although it could be argued that the resulting architecture is essentially one comprised of multiple point-to-point links, the resulting architecture could possibly allow the use a variety of components at the front-end in an efficient manner. Most of these components, require a light source at the OLT side, which can be shared. This could be one of the advantages of using a WDM PON architecture as opposed to multiple point-to-point links. On there are no standards for WDM PONs yet and mass deployment seems may be delayed for some more years. Since there are a number of technology candidates - i.e. spectrum-slicing, injection-locking, tunable lasers, reflective schemes - it is not clear which of the technologies is going to be adopted and therefore will be commercially available at low cost. To take a closer look at the architectures, if tunable lasers win the WDM PON race, they will most probably remain more costly, bulky and complex than simple lasers. In that case it is quite likely that a point-to-point architecture will be a better choice for our environment. Cheap tunable VCSELs, however, could be a promising technology. Possible advantages of a WDM PON based on tunable lasers would be the lower transmitter count for downstream transmission and probably easier maintenance. A spectrum-sliced architecture has the advantage of utilising inexpensive LEDs. On the other hand the current achievable data rate seems to be low compared to our requirements in the upstream direction.

SLEDs - another alternative for spectrum-slicing architectures - are more expensive and typically slower than LEDs, therefore less advantageous. The use of FP-LDs is also a possibility. Again, the main argument for using a spectrum-slicing architecture, in case the AWG is placed in the counting room is the possibility of using lower transmitter count and the ease of maintenance, as the same components could be used in a point-to-point configuration. However, spectrum slicing, possibly in combination with TDM could be used in the downstream direction to decrease the required number of transmitters. Injection-locking appears to be a promising technology. It utilises the same type of components that are already in use in a particle physics environment - i.e. FP-LDs, VCSELs - while it has the potential of significantly enhancing their performance characteristics. However, a thorough study is required to conclude if and how can this be achieved, as a relatively large number of parameters need to be set. Reflective schemes provide a number of options regarding the components that can be used at the ONU side. The particular architecture has attracted considerable research interest over the last years. Using a SOA (or an RSOA) has the advantage of providing gain, that is important considering that light has to travel twice the distance between OLT and ONU. However the particular component is power consuming and offers limited bandwidth. Mach-Zehnder modulators provide high bandwidth, can be used to implement advanced modulation schemes and are already a mature technology. On the other hand they are typically bulky, sensitive to polarization and high voltage levels are required to modulate them. EAMs (or REAMs) provide high bandwidth, they are compact and have low power consumption. However, cost and large-scale commercial availability is a challenge for the particular device, as it is unlikely that the particular device is going to become the choice of manufacturers and operators for next-generation WDM PONs, due to the absence of a gain. Moreover, contrary to the Mach-Zehnder modulators, using EAMs/REAMs to implement complex modulation schemes is

not straightforward. integrated SOA/EAM devices are a promising alternative as they provide both amplification and high modulation bandwidth. However, such a device would probably be quite power consuming for our purposes; also cost and commercial availability is an issue.

Although OCDMA PONs have attracted considerable research interest lately and they can provide high, symmetrical and scalable bandwidth an important feature compatible to our requirements. However, they are in experimental status and they utilise a high number of complex optical components based on immature technologies. OFDMA PONs also provide some performance advantages, such as high bandwidth and high bandwidth efficiency, but require complex, high speed electronics. This is a significant shortfall if they were to be used in our environment.

Having described the main PON variants and having outlined their main benefits and drawbacks we can now move on to the task of network design. The current Chapter can be used from now on as a reference, as a source of information on the main tools that can be used to achieve our goal, that of designing appropriate PON-based network architectures for the HL-LHC.

Chapter 4

Passive Optical Networks for the Distribution of Timing, Trigger and Control Signals at the HL-LHC

4.1 Introduction

In previous Chapters the networking requirements of the upgraded optical links at the HL-LHC have been defined. The PON architectural space has also been explored with the aim of identifying appropriate network structures that can serve as network design templates. The discussion can now move on to the network design process. The discussion will start from the less demanding applications. These are applications that can be served using the simplest and most widely used PON architecture - i.e. TDM PON. It is useful to point out that an application of this kind is one that can be served using a point-to-multi-point architecture.

Chapter 2 shows clearly that TTC applications fall into this category. Traffic in the downstream direction for the particular application is broadcast and the required data rate is moderate. In the upstream direction the required data rate per node ("user") is such that multiplexing traffic from many nodes over a single fiber is possible.

The design and construction of a TDM PON demonstrator proving the feasibility of using TDM PONs for the distribution of TTC signals is the topic of this Chapter. The Chapter starts with a brief description of the current infrastructure also describing the motivation for using a TDM PON architecture for the particular application. Consequently, the rationale behind the particular PON flavor selection is discussed. Next, physical layer design aspects are analyzed. The designed protocol is described. Then, the Field-Programmable Gate Array (FPGA) implementation of the OLT and ONU that were used to construct the demonstrator are described, along with the tests that were carried out to ensure that they can meet the requirements. Finally, aspects related to network performance, such as bandwidth utilisation are discussed.

4.1.1 Motivation

Chapter 2 discussed the different types of information that need to be transmitted to and from the detectors. These include apart from raw data, TTC information that must be transmitted for the smooth operation of the LHC. It is repeated here as a reminder that clock and trigger information is required to associate the signals to the collision that generated them and to synchronize data-taking across the experiment. As shown in Figure 4.1, the so called TTC network is used to transport unidirectionally the clock, trigger and control information from a TTC transmitter (TTCex) to many TTC receivers (TTCrxs) in a point-to-multi-point fashion. Figure 4.1 shows that the TTCrxs currently can be located either in the

counting room or be installed on-detector. An ultimate goal of network design is to be able to serve TTCrxs installed on detector. In the upstream direction, a separate electrical network, variously known as Trigger Throttling System (TTS) or Busy is used to transport low data rate status information from the TTCrxs back to the TTCex.

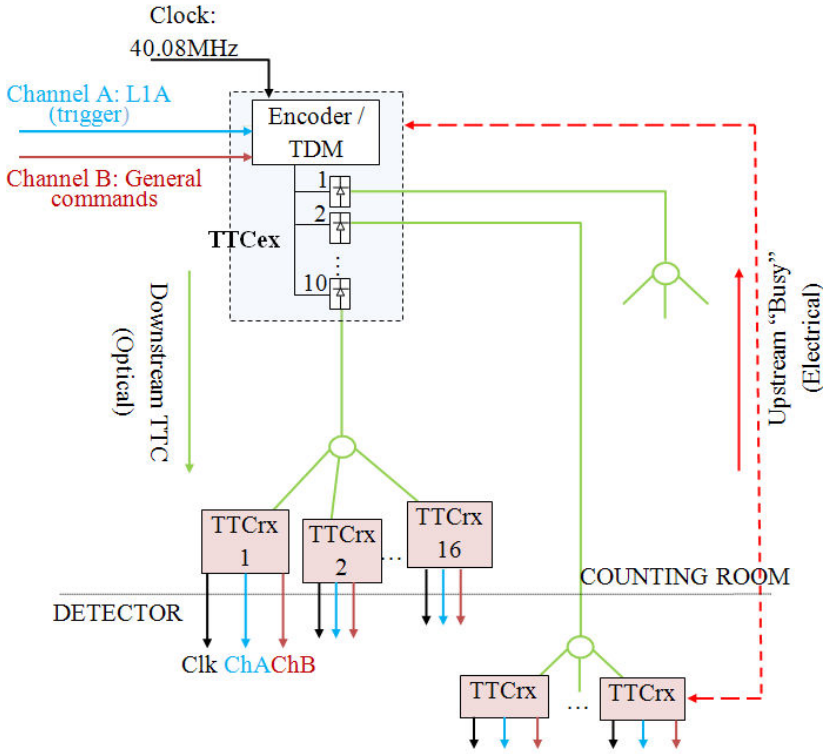

Figure 4.1: LHC TTC and TTS systems.

The forthcoming upgrade is viewed as a good opportunity to upgrade the TTC and TTS networks. One of the main motivation factors for such an upgrade is the construction of a single, consolidated infrastructure that can transmit information bidirectionally. The performance of the current system and the performance requirements for the upgraded system [156] [10] are shown in Table 4.1 - further to the requirements shown in the Table it should be added that the system should provide the flexibility of both individually addressing or broadcasting to ONUs.

One of the key requirements is that of fixed and deterministic latency. The current latency of the system is decomposed to two components in the table; the latency from the Layer 1 Accept (L1A) - the L1A message instructs the system that data should be read out - input socket of a TTCex laser encoder/transmitter module to the L1A output pin of the TTCrx timing receiver ASIC - denoted as Tx and Rx module latency in the table - and the latency introduced by the optical fiber. The reason why there is no number quoted for the latency of the upgraded system is the fact that the actual requirement refers to the overall latency, including the latency of the Trigger Processor and it currently stands at $2.5\mu s$ - ATLAS experiment [11]. Therefore, although a latency requirement for the TTC system per se does not exist, the latency introduced by the TTC network should be kept to a minimum to allow for more sophisticated trigger processing mechanisms that take longer to compute.

Table 4.1: Technical Characteristics of current TTC and TTS systems and requirements of the upgraded system.

Specification	**Current System**	**Target (Upgraded System)**
Downstream Line Rate	80Mbps	>1Gbps
Upstream Line Rate	Very Low (<<1 Mbps)	1Gbps - to represent a symmetric network
Max Link Length	150m	1km
Max Differential Reach	100m	100m
Latency	68ns (Tx and Rx module latency) + 4.9ns/m (optical fiber latency)	Fixed and Deterministic
Jitter of recovered 40MHz clock	50ps(rms)	50ps(rms)
Splitting Ratio	1:16 or 1:32	≥1:32

Figure 4.1 and Table 4.1 show that the current system essentially deploys a point-to-multi-point architecture in the downstream direction while the bandwidth requirements for the upgraded system match closely those of current commercial

TDM PON systems. As discussed in Chapter 3, TDM PON is the most widely deployed PON version, with millions of subscribers worldwide and well-established standards. As a result of the widespread adoption of TDM PONs, low cost transmitters and receivers are commercially available. As such, TDM PON appears to be a prominent candidate for the upgraded version of TTC system. The implementation of the demonstrator discussed in this Chapter was carried out to investigate whether a TDM PON can, indeed, be used to transmit the information currently transmitted by the TTC and TTS systems at the HL-LHC.

4.2 Technology Selection

As discussed in Chapter 3 there are two dominant standardized versions of TDM PON; one is the GPON, standardized by the ITU and the second is EPON, a standard issued by the IEEE [39]. There are several differences between the two standards; as GPON is more focused on QoS, it offers higher performance and a higher power margin. On the other hand, EPON focuses on low cost, therefore EPON transceivers are cheaper. On the downside, EPON does not address QoS, offers lower bandwidth efficiency and a narrower power margin [39]. As for TTC applications a custom protocol needs to be developed to achieve the low delay required for clock transmission - both EPON and GPON make use of long headers that would increase the delay -, the bandwidth efficiency of the commercially used protocol is not of interest. This is also the reason why the QoS offered by GPON cannot be considered an advantage. A GPON feature that could be advantageous is its higher offered data rate in the downstream direction - up to 2.488 Gbps - however, as Table 4.1 shows any data rate above 1 Gbps would suffice for the particular application, a requirement that could be met using EPON. A more important advantage GPON may have over EPON is that GPON transceivers are designed to

meet stricter timing requirements [157]. On the other hand, the higher performance offered by GPON is the reason why GPON transceivers are more expensive [158]. To evaluate the cost associated to each technology and assess which technology is cheaper a methodology similar to the one presented in [158] will be followed. A cost value of $C_{OLT} = US\$2000$ for both EPON and GPON OLTs, and cost values of $C_{ONU,EPON} = US\$200$ and $C_{ONU,GPON} = US\$250$ for an EPON and a GPON ONU, respectively, will be assumed [158] (OLTs are always much more expensive than ONUs which have to be cheap because their cost is not shared between subscribers, as is the case for OLTs). These assumptions will be used to identify the condition under which GPON is cheaper than EPON. At this point we will also define the splitting ratios SR_{GPON} and SR_{EPON} for GPON and EPON, respectively and the number of users N - it will be shown that the value of N is not important, as the interest is on relative and not absolute cost. Using this notation the total ONU and OLT costs can be expressed as:

$$C_{GPON} = N * C_{ONU,GPON} + N * C_{OLT} * SR_{GPON} \tag{4.1}$$

where C_{GPON} is the overall cost for GPON and

$$C_{EPON} = N * C_{ONU,GPON} + N * C_{OLT} * SR_{GPON} \tag{4.2}$$

where C_{EPON} is the overall cost for EPON. Using $C_{GPON} - C_{EPON} > 0$ to identify the condition under which EPON is cheaper and using Equations 4.1 and 4.2 the following equation can be derived:

$$\frac{C_{ONU,GPON} - C_{ONU,EPON}}{C_{OLT}} > SR_{EPON} - SR_{GPON} \tag{4.3}$$

The left hand side of Equation 4.3 is equal to 0.025. In other words, in order for

GPON to be cheaper - and as SR_{GPON} can not be negative - SR_{EPON} needs to be larger than 0.025. Therefore if EPON can serve more than 40 users per OLT, there is no value of splitting ratio for GPON, for which GPON is cheaper. As splitting ratios are typically powers of 2, for splitting ratios greater than 1:32 (i.e. 1:64 or greater), EPON will always be cheaper than GPON. For a 1:32 splitting ratio for EPON, GPON becomes cheaper only for splitting ratios higher than 1:256. It should be noted that the value for the OLT cost used in the calculations is rather at the high end of the cost spectrum, favoring GPON. So, it seems that EPON is almost certainly a cheaper option. This is the reason why EPON has been selected for the construction of the demonstrator.

4.3 Power Budget Calculations and Number of Users

The use of power budget calculations [159] is a valuable tool used by network designers. Power budget calculations can reveal whether the power reaching the receiver is enough for successful signal reception. The system margin M_s can be calculated using the following equation:

$$M_s = \bar{P}_{tr} - \bar{P}_{rec} - C_L - \alpha_{pen} \tag{4.4}$$

where $\bar{P}_{tr}$ expresses the average transmitted power, $\bar{P}_{rec}$ the minimum average received power, also called receiver sensitivity, C_L is the channel loss and α_{pen} is the so-called "power penalty", i.e. the degradation in receiver sensitivity due to departure from the ideal transmission case, for example due to presence of dispersion, a lower extinction ratio value or other signal degradation factors.

For the purposes of the demonstrator, a number of OLT and ONU transceivers were purchased from OESolutions [160]. The OLTs were a 1.25 Gbps EPON OLTs, while the ONUs were 1.25 Gbps EPON ONUs. As in the downstream direction the

data rate used for the purposes of the demonstrator was 1.6 Gbps the associated power penalty was calculated and included in the power budget calculations - more precisely this penalty was calculated to be ∼0.5 dB. Table 4.2 shows the link budget calculations for 1:64 splitting ratio in the downstream direction, using the values provided by the manufacturer and confirmed by measurements. In the calculations the minimum transmitter power provided by the manufacturer was used and a further 3 dB was subtracted from it to take into account the effect of modulation. The minimum sensitivity provided by the manufacturer - reduced by the aforementioned 0.5 dB - is quoted in the table. The calculations show that a power margin of over 4dB can be achieved.

Table 4.2: Link Budget Calculations - Downstream Direction.

Quantity	**Symbol**	**Value**
OLT Transmitter Power	$\bar{P}_{tr,OLT}$	0.5dBm
Overall Fiber Loss @1490nm	$\alpha_f L$	0.2dB
Connector Loss	α_{con}	2dB
Splitter Excess Loss	$\alpha_{excess,spl}$	1dB
Splitting Losses	α_{spl}	18.06dB
ONU Receiver Sensitivity	$\bar{P}_{rec,ONU}$	-25dBm
Power Margin	M_S	4.24dB

Table 4.3 shows the upstream power budget calculations. In this case the interference power penalty from inactive ONUs was also calculated using the approach followed in [159] to calculate the effect of in-band interference in multi-wavelength networks. Its effect was found to be negligible for 64 ONUs. Even for 512 ONUs the power penalty has been calculated to be only 0.2 dB. The calculations reveal that the power margin is even wider than in the downstream direction. This is mainly owed to the use of an APD receiver at the OLT side.

It is worth pointing out that the maximum power penalty reported by the man-

ufacturer after 20 km transmission in the upstream direction including the effects of dispersion, ISI, Relative Intensity Noise (RIN), Mode Partition Noise (MPN), extinction ratio and jitter is only 2.8 dB, lower than the calculated margin of 5.03 dB in Table 4.3. In the downstream direction the corresponding penalty for 20 km transmission is 2.3 dB, also lower than the corresponding margin, which in that case is 4.24 dB - Table 4.2. For TTC applications transmission over only 1 km of fiber is required, therefore the power margin can be expected even more comfortable.

Table 4.3: Link Budget Calculations - Upstream Direction.

Quantity	**Symbol**	**Value**
ONU Transmitter Power	$\bar{P}_{tr,OLT}$	-3.5dBm
ONU Receiver Sensitivity	$\bar{P}_{rec,ONU}$	-30dBm
Overall Fiber Loss @1310nm	$\alpha_f L$	0.4dB
Connector Loss	α_{con}	2dB
Splitter Excess Loss	$\alpha_{excess,spl}$	1dB
Splitting Losses	α_{spl}	18.06dB
Interference Power Penalty (form inactive ONUs)	$P_{interference}$	0.003dB
Power Margin	M_S	5.03dB

Bit-Error Rate (BER) measurements carried out using 1 km of fiber have confirmed that a 1:64 splitting ratio can be achieved and that the margin is more comfortable than the one calculated, allowing a higher splitting ratio to be used. Actually the measurements have shown that splitting ratios of 1:128 in the downstream direction and 1:256 in the upstream direction could be achieved, while maintaining a BER=10^{-12}. Despite that fact, a higher splitting ratio was not pursued, as in a particle physics environment splitters with high splitting ratios are perceived as single points of failure with a potential high impact. A 1:64 splitting ratio was

judged to be a good compromise between reliability and cost efficiency. This choice is also reflected in the protocol implementation, that allows only 64 ONUs per PON. The resulting longer polling cycle length and lower available bandwidth per ONU for high splitting ratios, although not prohibitive, also contributed to the choice of not using a higher splitting ratio.

4.4 Protocol Description

During the survey of PON architectures in Chapter 3, a way of classifying the main functionalities carried out by the MAC Layer was provided. These functionalities include grant sizing, grant scheduling and queue scheduling [65]. For TTC applications, ONUs do not need to maintain different queues, therefore only grant sizing and grant scheduling had to be performed. The main aim of the protocol design was to provide a simple platform that could be used to prove that a TDM PON can meet the application requirements. Simplicity is important for an additional reason; as ultimately, the ONUs would have to be placed at the front-end, minimisation of the size and power consumption of the required electronics is critical. Therefore the designed protocol does not include more advanced features provided by the EPON and GPON protocols, such as autodiscovery and ranging, as they would add significant complexity to the implementation. More particularly the protocol addresses the following requirements:

- Synchronous delivery of a periodic trigger with clock rate 25 ns.
- Auxiliary field to extend or to protect the trigger field.
- Broadcast or individual commands to ONUs.
- Arbitration of upstream channel to avoid collisions due to simultaneous transmissions from multiple ONUs.

4.4.1 Downstream Transmission

In the downstream direction, superframes, consisting of 65 subframes are being transmitted. The downstream transmission line rate is 1.6 Gbps, but the use of 8B/10B encoding limits the effective data rate to values below 1.3 Gbps. The choice of the particular value for the data rate was influenced by the fact that it must be integer multiple of the clock frequency. As shown in Figure 4.2 that depicts the downstream superframe format, a special character - the comma character, <K> - is used at the beginning of each superframe for frame alignment and synchronization. The first two fields of a subframe are dedicated to transmission of trigger-related information. The <T> field, which is 1 byte long, provides the flexibility of assigning different triggers, while the second byte, <F>, is reserved for future use - for example it could be used to extend or to protect the trigger field. The last two bytes of a subframe - <D1> and <D2> - are commands, either individually addressed to a single ONU, either broadcast. Implicit addressing was used, i.e. information to a specific ONU is sent in a specific part of the superframe in order to increase bandwidth efficiency. The duration of a subframe is 25 ns, which is exactly the same as the trigger period. Broadcast and individually addressed commands are distinguished by the most significant bit of the <D1> field; zero indicates broadcast, while one indicates individually addressed command. 64 subframes are sent downstream, corresponding to the maximum number of ONUs served by a single OLT. A 3-byte 65th subframe is used to restore symmetry in the superframe and allow a 25 ns duration between the trigger of the last subframe and the trigger of the first subframe in the next superframe. The <R> character in the last subframe is used by the upstream grant scheduling mechanism and contains the address of the next ONU that is going to occupy the channel.

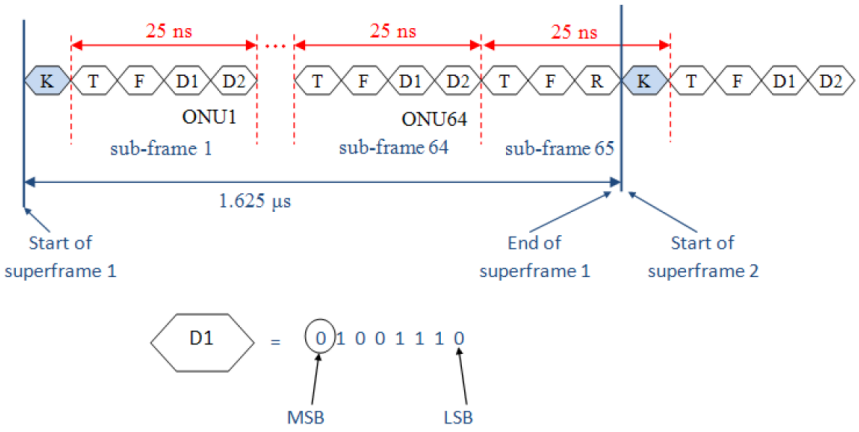

Figure 4.2: Downstream Frame Format.

4.4.2 Upstream Transmission

Once an ONU receives an <R> character containing its address, it switches its laser on and starts transmitting its data. The upstream line rate is 800 Mbps, but as 8B/10B coding is used the effective data rate is lower. The grant size is predefined - it does not change dynamically. The upstream frame is shown in Figure 4.3. It starts with alternating "1"s and "0"s to allow for threshold recovery and CDR locking, necessary for burst-mode reception. It then contains a comma <K> character for frame alignment, followed by the address of the ONU and the transmitted data.

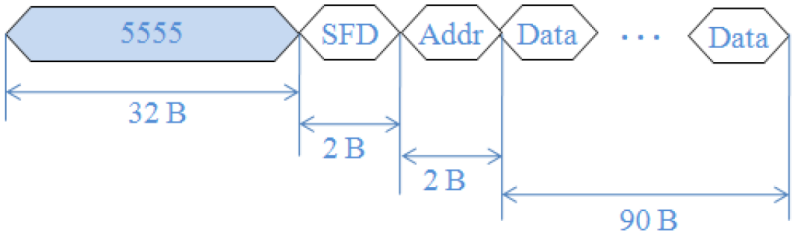

Figure 4.3: Upstream Frame Format.

4.5 Transceiver FPGA Design and Implementation

After discussing physical layer design aspects and describing the structure of the protocol, the discussion can now move on to the description of the OLT and ONU FPGA-based implementations. The focus of the description is on particular measures that have been taken to ensure that the requirement for fixed and deterministic latency can be met.

4.5.1 OLT Transmitter

The transmitter at the OLT side is implemented based on the so-called GTX transmitter of the Virtex 5 FPGA, a more detailed description of which can be found in [161]. The main technical challenge related to the design of the transmitter at the OLT side is that, as shown in Figure 4.4, the Physical Coding Sublayer (PCS) and the Physical Medium Attachment (PMA) sections of the transmitter use different clock references (RXUSRCLK and XCLK in Figure 4.4). These two clock references are not phase aligned and have to be aligned for the correct operation of the serializer (denoted as PISO - Parallel Input to Serial Output (PISO)). The standard solution to this issue is the use of an elastic buffer (referred to as FIFO - First In First Out (FIFO)). However, elastic buffers introduce latency uncertainty, that would violate the requirement for fixed and deterministic latency. To resolve this problem the buffer was bypassed. The Phase-Locked Loop (PLL) of the PMA section was used instead to adjust the phase of the XCLK so that it matches the phase of the RXUSRCLK that was used as a reference. The total latency through the transmitter was measured to be 75 ns. The transmitter was reset a large number of times - 100 - and the latency was measured. The measurements confirmed that the latency remains fixed.

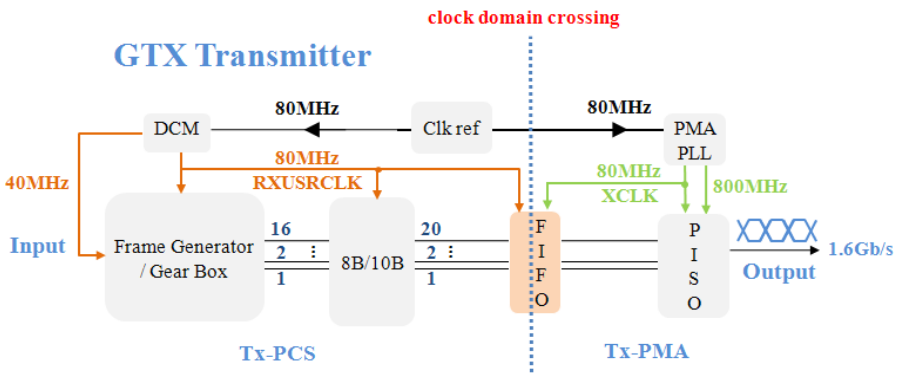

Figure 4.4: OLT transmitter FPGA implementation.

4.5.2 ONU Receiver

The FPGA implementation of the ONU receiver is shown in Figure 4.5. As shown in the figure, the 1.6 Gbps downstream datastream is input to the CDR circuit. After recovering the clock, the retimed data are passed on to the next component in the receiver chain, that is the SIPO block. The operation of the SIPO block requires the use of an 80 MHz frequency-divided clock. The frequency-dividing process - and more particularly the associated phase-alignment process - introduces latency uncertainty. Latency uncertainty arises from the fact that the low-frequency clock may be phase-aligned to any of the edges of the high frequency clock.

In order to resolve the latency issue introduced by the frequency-divider, a barrel shifter - i.e. a "bit-rotating shift register" [162] - was implemented immediately after the SIPO. The relative phase difference of the frequency-divided clock and the first edge of the high-frequency clock can be found using the barrel shifter. In order to determine the phase difference, the fact that the relative phase dictates the order with which the parallel data exit from the parallel lines of the SIPO was utilised, along with the knowledge of the precise position of the <K> character within the frame. To make this point clearer, let us assume that the parallel clock started

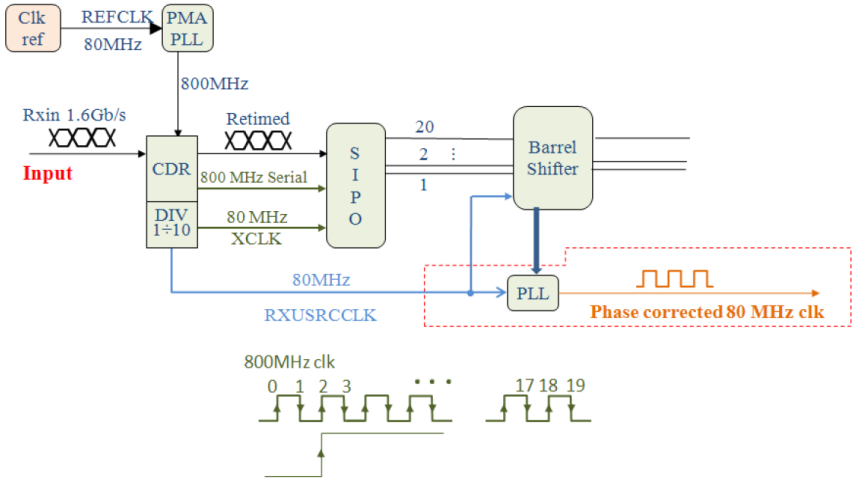

Figure 4.5: ONU receiver FPGA implementation.

from the first edge of the serial clock. Let us also assume that in this case the first bit of the <K> character would come out of the first parallel line of the SIPO, the second bit from the second line and so on. If, on the other hand, the parallel clock was delayed compared to the first edge of the serial clock then the first bit of the <K> character would be transferred to a different output line of the SIPO. Using the barrel shifter the line out of which the first bit of the <K> character came out can be identified. Then this information can be fed to a PLL to perform the phase correction.

Figure 4.6 demonstrates the operation of the barrel shifter concept by comparing the phase of a fixed reference clock to the phase of the recovered clock at the ONU. The comparison was carried out for different barrel shifter values and for both the two different ONUs that were used for the construction of the PON demonstrator. The relative delay between the reference and recovered clock follows a linear trend with the slope of the two lines being 625 ps for both ONU implementations. This value perfectly matches the period between two consecutive edges of the 800 MHz serial clock. The measurement demonstrates that the concept can be used to carry

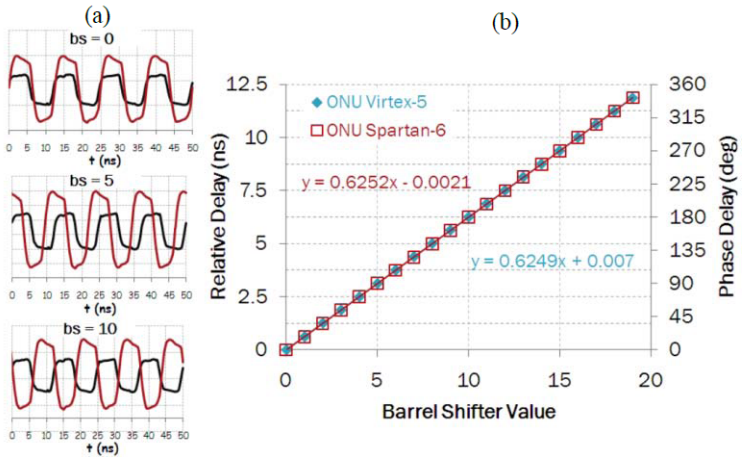

Figure 4.6: (a) Oscilloscope traces of reference clock (red lines - higher amplitude) and recovered clock (black lines - lower amplitude) for various barrel shifter values, and (b) phase difference between reference and recovered clocks as a function of barrel shifter value for both ONUs.

out the required phase correction.

4.5.3 OLT Burst Mode Receiver

The burst mode receiver at the OLT, Figure 4.7, was implemented using a 5x oversampling circuit. Burst mode oversampling works by blindly sampling the incoming datastream at a multiple of the bit rate and making a decision based on the sample that is closest to the center of the bit [163]. This method is preferred over the usual implementations that use PLLs to recover the clock, as PLLs typically have a large time constant and therefore are impractical for high speed serial applications that involve bursts. The oversampling circuit generates 5 samples for each received bit - Figure 4.7 - and then tries to identify the transition region between bits. It is therefore important to provide a sufficient number of transitions in the datastream. In order to achieve this a long <5555> field is transmitted at the beginning of the upstream frame as shown in Figure 4.3. A decision circuit collects all samples from a predefined window of incoming bits and implements a majority voting algorithm

to identify the sample which is most likely to be closest to the center of the bit. If a burst from a second ONU arrives then it will be out of phase with the previous burst - Figure 4.7. In this case, the decision circuit will identify the new transition regions and adjust its decision sample.

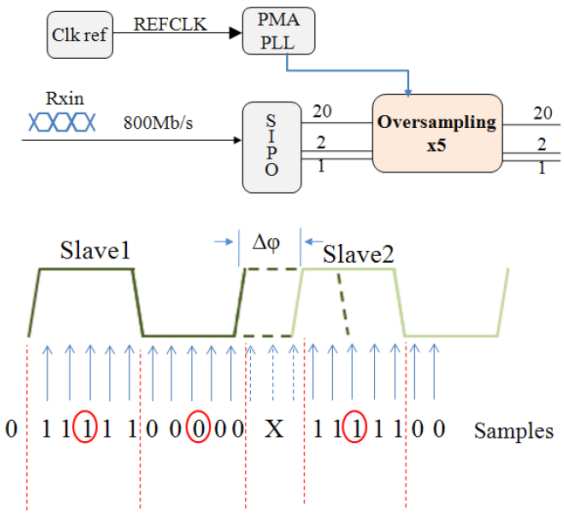

Figure 4.7: Burst Mode OLT receiver FPGA implementation and oversampling concept.

4.6 Upstream Bandwidth Utilisation Aspects

As discussed in Chapter 3 key challenges related to the operation of TDM PONs are the bursty nature of traffic in the upstream direction, their bandwidth efficiency and maximisation of their reach. For the purposes of TTC applications reach extension is not important aspect. Challenges related to the bursty nature of the traffic that in turn can cause latency uncertainty were partially discussed in Section 4.5. On the other hand, while in Section 4.4 the protocol implementation was described, the overall network efficiency was not discussed. In this Section, aspects related to that topic are being touched on. More particularly, one of the key metrics related to

network performance, bandwidth utilisation, is calculated. As in the downstream direction the information is broadcast, analysis of the particular metric is meaningful only in the upstream direction. The analysis of upstream bandwidth utilisation takes into account a number of factors. These include protocol and physical layer related parameters, such as the inter-frame gap, the switch on and off time of the ONUs and the locking time of the CDR. The goal of the analysis is to demonstrate that appropriate safety margins have been applied to guard against effects that can lead to impairments, while at the same time maintaining link utilisation at acceptable levels.

4.6.1 Overhead Decomposition, Dynamic Range and Inter-frame Gap

In order to calculate the upstream bandwidth efficiency, all types of overheads related to upstream transmission need to be listed along with their values. For the shake of the discussion, let us denote as T_{switch} the time elapsing between the start of transmission of data from ONU_i until the start of data transmission from ONU_{i+1}. T_{switch} has a duration equal to that of the polling cycle that in our case is fixed. The duration of the polling cycle is equal to the duration of a superframe, as explained in Section 4.4.1 and shown in Figure 4.2 that is equal to 1625 ns - i.e. T_{switch} =1625 ns. At this point, we will also define $T_{overhead}$ as the amount of time over the duration of T_{switch} during which data transmission is not possible. $T_{overhead}$ includes the overhead due to 8b/10b encoding on user data, $T_{OH,8b/10b}$ protocol overheads, $T_{OH,Protocol}$, including the time required to transmit the address of the ONU and the <K> character for frame alignment and finally, a number of overheads associated to burst mode operation, $T_{OH,BM}$. The last type of overheads includes (Figure 4.8) [157]:

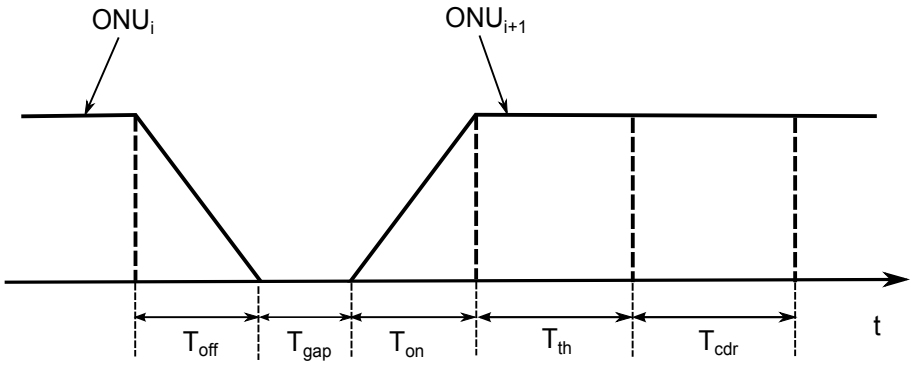

Figure 4.8: Overheads associated to burst-mode transmission.

- The overheads associated to the switch-off and switch-on time of the laser, T_{off} and T_{on}, respectively. As during this time the output power of the laser is not stable, data cannot be transmitted.

- As burst-mode receivers need to adapt the decision threshold on a burst-by-burst basis, T_{th} is required so that the threshold recovery circuitry can adjust the threshold based on the average preamble power level.

- T_{cdr} is the amount of time required for clock recovery by the clock and data recovery circuitry.

- T_{gap} is the additional time required for the receiver sensitivity to recover between two packets. To clarify further why T_{th} is not enough, T_{th} is based on the assumption that the preamble bits can be recovered. However in the absence of T_{gap} this may not be possible. This is due to the fact that in TDM PONs there is transmission before the start of the packet. To make matters worse, adjacent packets may have a large difference in power. In a worst-case scenario a low power packet may be preceded by a high power one. In this case the additional time T_{gap} is required for sensitivity recovery. T_{gap} depends on the required dynamic range [52].

In the case of the demonstrator discussed in this Chapter, the preamble accounts for T_{on} - meaning that transmission of the preamble starts immediately after switching on the laser; this design choice has been made to simplify the ONU circuitry - T_{th} and T_{cdr}. In other words, $T_{preamble} = T_{on} + T_{th} + T_{cdr}$. According to the manufacturer the maximum overall overhead associated to burst-mode transmission - i.e. the maximum suggested value for $T_{preamble}$ - is 420 ns. This value depends on the efficiency of the threshold recovery circuitry and the CDR. Our experiments showed that a value of $T_{preamble}$ ∼250 ns was enough to successfully decode the $< K >$ character, required for frame alignment. However to provide a sufficient margin the preamble value was selected to be $T_{preamble}$ =400 ns.

From the description of the frame structures in the downstream and upstream directions, shown in Figures 4.2 and 4.3, respectively, it can be inferred that the value of the interframe gap T_{IFG}, where $T_{IFG} = T_{off} + T_{gap}$, is 50 ns - under the assumption that upstream transmission is taking place in every superframe. According to the data provided by the manufacturer the switch-off time of the laser is T_{off} =20 ns, while the suggested T_{gap} value is T_{gap} =50 ns, resulting in a suggested T_{IFG} value of $T_{IFG,suggested}$ =70 ns. Despite that fact, a lower value could be used. This is owed to the fact that the values suggested by the manufacturer assume a required dynamic range of 21 dB, while for TTC applications the maximum differential reach is 150 m, therefore even a 5 dB dynamic range would be sufficient. This dynamic range value was derived by adding a 1 dB margin to the maximum peak power variation to take into account manufacturing non-uniformities.

The overall duration to overcome burst-mode induced effects can be calculated to be $T_{OH,BM} = T_{preamble} + T_{IFG}$ =450 ns. To confirm that this margin was enough measurements of the maximum dynamic range as a function of the interframe gap were carried out. The results are shown in Figure 4.9. As shown in the diagram the maximum achievable dynamic range for T_{IFG} =50 ns is 15 dB, showing that there

is a margin of 10 dB against the targeted dynamic range of 5 dB.It should also be noted that the maximum dynamic range measurement for large interframe gap values was limited by the receiver sensitivity. This is the reason for the observed value of the floor being lower than the 21 dB value provided by the manufacturer.

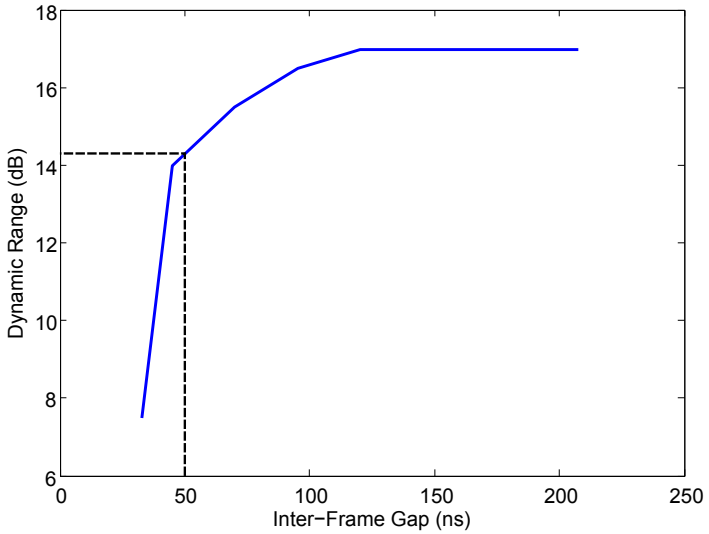

Figure 4.9: Dynamic range as a function of interframe gap.

4.6.2 Overhead and Link Utilisation

Having discussed the main overheads and their associated values all that remains to calculate bandwidth efficiency is an appropriate mathematical framework linking the overheads to bandwidth efficiency. As grant sizing and grant scheduling are carried out statically in the protocol under discussion, it is fairly straightforward to calculate the link utilisation. Taking into account the inherent bandwidth sharing in TDMA the effective data transmission rate per ONU, $R_{ONU,eff}$ becomes:

$$R_{ONU,eff} = \frac{R_{us}}{N}(1 - \frac{T_{overhead}}{T_{switch}}) \tag{4.5}$$

where R_{us} is the overall upstream data rate and N is the number of served

ONUs.

Using Equation 4.5, the effective data rate per ONU as a function of $T_{overhead}$ for different number of users can be plotted. The result for R_{us} =800 Mbps is shown in Figure 4.10. For future TTC applications the targeted number of ONUs is 64, while the overall overhead is $T_{OH} = T_{OH,BM} + T_{OH,protocol} + T_{OH,8b/10b}$ =725 ns. In this calculation a value of 50 ns was used for $T_{OH,protocol}$, to take into account the required time to transmit 2 bytes for $< K >$ character transmission and 2 bytes for ONU address transmission using 8B/10B encoding. The value used for $T_{OH,8b/10b}$ was $T_{OH,8b/10b}$ =225 ns to take into account the additional amount of time required to transmit 90 bytes of user data, compared to the case when 8B/10B was not used. Therefore the effective data rate is ∼7 Mbps, which is much higher than the very low data rate - of the order of kbps - offered by the current electrical links.

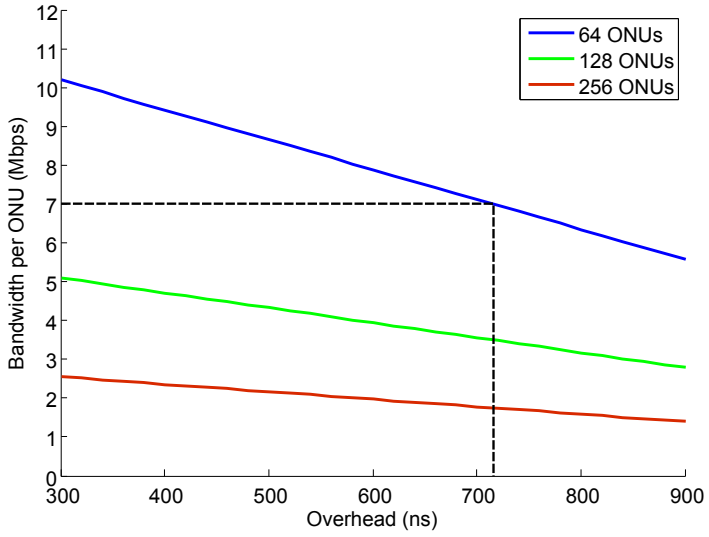

Figure 4.10: Bandwidth per ONU vs. $T_{Overhead}$ for different number of ONUs.

4.7 Conclusions

In this Chapter the first step towards designing PON architectures intended for use in particle physics applications at the HL-LHC was performed. More particularly, the use of a TDM PON architecture for the distribution of timing, trigger and control information was discussed. This type of application is the most obvious candidate for using a PON-based architecture, due to the nature of the traffic requirements that match well the capabilities of commercial TDM PONs. Information in the downstream direction is broadcasted, while the data rate requirement per user in the upstream direction is rather moderate. This calls for the use of a bidirectional point-to-multi-point architecture. A TDM PON matches well the data rate and topological requirements, while its bidirectionality would allow consolidation of the current TTC and TTS networks. As TDM PONs come in different flavors, the most suitable technology was selected based primarily on cost minimisation criteria; the technology of choice was EPON. The maximum number of users to be supported was calculated and an appropriate protocol for the delivery of synchronous trigger and commands continuously was designed, as commercial protocols could not be used for this purpose. The designed protocol provides the flexibility of both individually addressing as well as broadcasting to all ONUs. The protocol was also designed to cope with performance degradation factors associated to burst-mode transmission typical of TDM PONs. FPGAs were used to construct a demonstrator, using an OLT and two ONUs in order to prove the concept. In this implementation the most critical and challenging requirement, that of fixed and deterministic latency in the downstream direction, was taken into account. Special techniques were deployed to address this challenge. The fact that these techniques can guarantee fixed and deterministic latency in the downstream direction was confirmed experimentally. Thus, the concept of using TDM PONs for TTC applications

at the HL-LHC was proved. It should be noted that this Chapter includes only the work where the author of the thesis was directly involved. The work was further extended and perfected by the other members of the team. The use of a TDM PON for TTC applications at the HL-LHC has gained enough support in the particle physics community, so that it appears to be a prominent candidate, likely to be implemented at the HL-LHC.

Chapter 5

WDM PON Architectures for the HL-LHC - Design Alternatives and Challenges

In Chapter 4, a PON architecture for the distribution of timing, trigger and control information at the HL-LHC was described. These types of information, however, form only a subset of the information that will need to be transmitted at the upgraded version of the LHC. Transmitting all types of information, would require the use of an infrastructure meeting the requirements for a unified architecture outlined at the end of Chapter 2. This unified architecture would need to offer much higher bandwidth in the upstream direction. In this Chapter the PON architectures described in Chapter 3 are systematically reviewed, to identify an architecture that could possibly meet these requirements. The analysis shows that the most appropriate solution appears to be that of an architecture based on WDM and reflective modulators. Then the selected architecture is evaluated; the factors that limit its suitability as a unified architecture at the HL-LHC are identified. To the best of

the author's knowledge this is the first such systematic survey of PON technologies for particle physics applications. It is also the first time that a thorough analysis of the applicability of WDM PONs for use at the HL-LHC is conducted.

5.1 Network Architecture - Design Alternatives and Choices

The overview of the requirements for the upgraded links carried out in Chapter 2, revealed that any network infrastructure intended to support data transfer from the detector to the counting room and to the opposite direction will have a number of unique characteristics compared to commercial networks; these include a higher bandwidth requirement in the upstream than in the downstream direction and the fact that formation in the downstream direction is broadcast. Taking these particularities into account, the overview of PON architectures carried out in Chapter 3, can be used to guide us through the selection of the appropriate technology. More particularly:

- TDM PONs can not be utilised to transmit information in the upstream direction due to their multiplexing mechanism. Serving more users in a TDM PON leads to an increase in the overall data rate requirement if the data rate per user is to be maintained at a fixed level. That would lead to prohibitively high aggregate data rate requirement, even for a moderate number of users.

- OCDMA PONs can provide virtual point-to-point connectivity, but are based on relatively immature technologies that are both complex and expensive.

- SCM and OFDMA PONs require complex circuitry, that is best avoided, as it would increase the size and power requirements of the on-detector electronics.

It therefore seems that WDM PONs are the most appropriate solution, as they provide virtual point-to-point connectivity, while at the same time they seem to be the choice of the operators for the next generation of optical access networks (please see Chapter 3). This implies that low-cost solutions may be available by the time of the LHC upgrade - expected to take place during the 2015 and 2020 LHC shutdowns.

One of the key issues hindering WDM PON implementation is the use of wavelength-specific ONUs. The main solutions suggested in the literature to avoid the use of wavelength-specific components were reviewed in Chapter 3. All the solutions, along with the main advantages and disadvantages of each approach with respect to its applicability at the HL-LHC are repeated at this point:

- Use of tunable lasers: The use of tunable lasers is a costly solution; it would also increase component complexity at the front-end, which is not desirable.

- Use of broadband light sources along with spectrum slicing: Although spectrum slicing provides a cheaper alternative to tunable lasers, it cannot meet the high upstream data rate requirement.

- Use of modulators and remote light souces: The advantage of this architecture is that it allows the use of a variety of components at the front-end. These include the SOA, the MZM and the EAM. The SOA is power consuming and has limited speed [164], therefore it does not provide advantages compared to the use of the currently installed lasers. On the other hand, there is interest in modulators in the particle physics community mainly due to their potential radiation hardness [165]. This fact makes the MZM and the EAM good candidates for the next-generation of the optical links as front-end components. The drawbacks of Mach-Zehnder are its high driving voltage requirement and its size. The EAM seems to be a more attractive option. Their use was suggested

and investigated for the LHC [166], but difficulties related to the immaturity of the technology at the time led to the implementation of different types of optical links based on directly modulated lasers [11], [8]. Recently, EAM technology has reached sufficient maturity and devices are now commercially available. The EAM is also easier to use it in a reflective configuration, thus reducing the component footprint and simplifying its use in a single-feeding fiber configuration.

- Use of injection-locked lasers: The use of injection-locked lasers appears to be a viable solution. Despite that fact, this solution will not be investigated in this Chapter. The main reason is related to the fact that the behavior of lasers in a radiation-hard environment, as well as their benefits in terms of cost and mass, have been studied more extensively [167], [168], [10]. Thus there is more interest in exploring the advantages of modulators as front-end components, rather than confirming the benefits of lasers.

The above discussion of the suggested solutions shows that the front-end component is in itself of great importance. The front-end component is a crucial driver for the selection of a particular architecture over other alternatives. Therefore WDM PON architecture based on use of REAMs was selected, as shown in Figure 5.1.

As in WDM PON architectures each user is offered a virtual point-to-point connection, broadcasting of information can be a challenge. Several solutions have been suggested in the literature to overcome this problem. Some of these utilise advanced modulation schemes and relatively complex techniques such as in [169] and [170]. In conventional WDM PONs, complicated and slightly expensive solutions are justified as both unicast and broadcast data need to be transmitted. In the applications of our interest, however, although unicast data are also transmitted, broadcast data transmission is more crucial and therefore it drives the design

process. Moreover, solutions based on advanced modulation schemes would lead to a more complex receiver at the front-end, something that needs to be avoided. This is the reason why such solutions were discarded. A simpler solution, is the use of a single ASE source based on the use of either an EDFA, or a SLED. External modulation of a broadband light source as a means to broadcast information in a WDM PON has already been suggested [171]. An alternative solution would be to use a directly modulated SLED, as high-bandwidth SLEDs are already commercially available [172]. Use of the SLED as a downstream broadcast transmitter has been studied in [173]. A combination of a LED and a SOA has also been suggested in [174]. Use of a FP-LD has been suggested in [175], but this solution will not be investigated here as it is considerably more complex than the rest. An alternative solution in order to broadcast information in the downstream direction would be to use a Broadcast AWG, a device that allows broadcasting of a single wavelength to its all ports, while at the same time it can route wavelengths of another band [176]. Lastly, external modulation of a frequency comb generator or a laser array can also be used to broadcast information, but use of a frequency comb generator would increase the complexity of the system therefore it is not going to be discussed. Use of a laser array would essentially diminish one of the advantages of using a WDM PON architecture, which is the reduction of the number of components, so it is not going to be discussed, neither. In other words, only two solutions appear to be promising; these are the use of a broadcast AWG and the use of a single ASE source, directly or externally modulated.

Using a modulator at the front-end requires an external source to provide the light that is going to be modulated by upstream data. Selection of the appropriate light source represents an additional design choice. Actually any light source that could serve as downstream broadcast transmitter - e.g. EDFA [104], SLED [177], FP-LD [175], frequency comb generator, [178] or laser array, [179] - could also be

used for light seeding. In order to use a single component as a light seeding source, a spectral slicing process needs to take place. This leads to Signal-to-Noise Ratio (SNR) degradation and is one of the topics that are discussed in this Chapter.

5.2 Network Architecture - Description of the Selected Architecture

Figure 5.1 shows the suggested WDM PON architecture, that is studied in this Chapter. At the front-end - on detector - a REAM is used as a transmitter. Different wavelengths are used to separate traffic in the downstream and upstream direction. The downstream transmitter is shared between all users connected to the same WDM PON, as information is broadcast. The light for upstream transmission is provided by the light seeding source, again shared between all WDM PON users. It is important to highlight the fact that the light provided by the seeding source has to travel downstream, be modulated by the REAM and transmitted back upstream, therefore it experiences high losses. The upstream amplifier is shared between users.

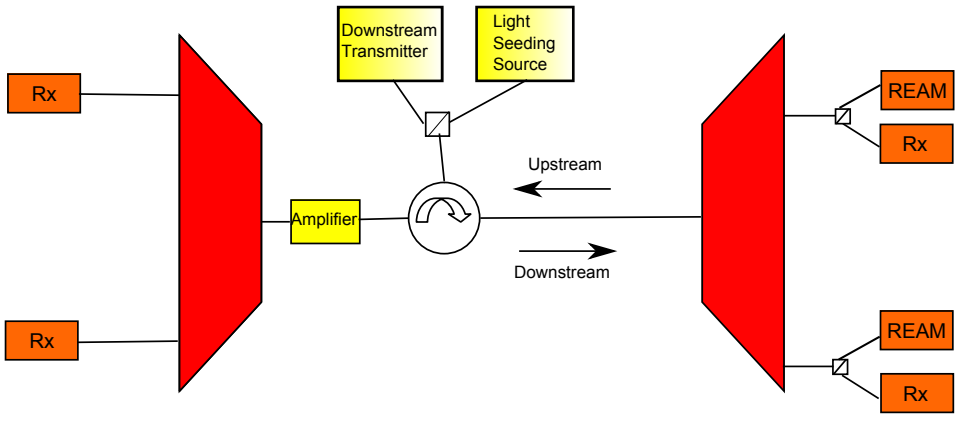

Figure 5.1: Suggested WDM PON architecture.

As mentioned in Chapter 3, although use of WDM has been suggested before

for data readout in particle physics experiments [151], [180], the authors suggest use of expensive tunable or wavelength-specific lasers. This is one of the reasons why WDM was considered too expensive for data readout in physics experiments [181]. Only recently has WDM been considered a viable solution, but only in experiments where the detectors span a large geographical area [182].

On the other hand the use of the EAM as a front-end component for particle physics applications has been suggested in [183] and investigated in [166], but only in a point-to-point configuration. The work presented here is the first proposal of WDM utilisation as a means to design a single infrastructure that can carry both upstream and downstream, but also as an efficient platform that enables the use of a variety of optoelectronic components at the front-end.

5.3 Downstream Power Budget and System Requirements

In this section, the required power per wavelength channel $P_{ch,Tx}$ that should be emitted by the downstream transmitter to meet the data rate requirements is calculated. The required power is evaluated at point 1, as shown in Figure 5.2.

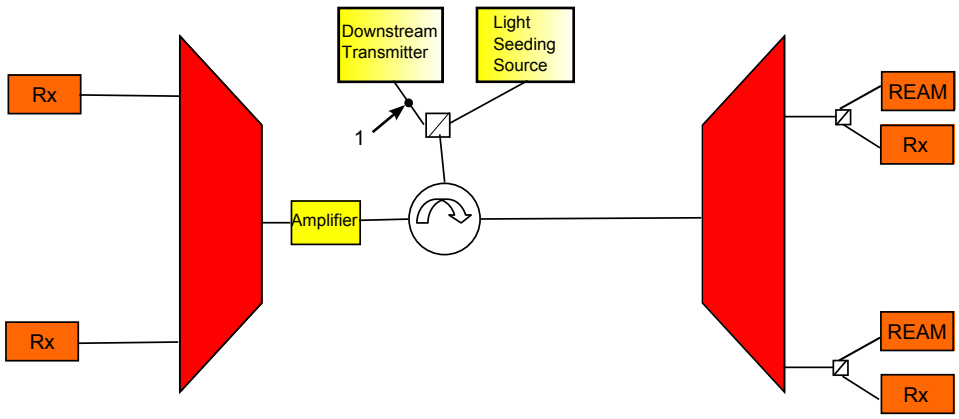

Figure 5.2: Point at which the required power is calculated.

5.3.1 Downstream Power Budget Calculations

An optical receiver can recover the information sent to it only when the average received power is above a certain value. This value, called receiver sensitivity ($\bar{P}_{rec}$), is related to performance requirements and system parameters - for example the required BER and the data rate. The purpose of power budget calculations is to ensure that the received power is at least equal to the receiver sensitivity. The power budget calculations can be carried out using the following simple equation in decibel units [159]:

$$\bar{P}_{tr} = \bar{P}_{rec} + C_L + M_S \tag{5.1}$$

where $\bar{P}_{tr}$ is the average transmitted power, C_L is the channel loss and M_S is the system margin. The system margin allows us to be on the safe side during the calculations and accounts for power penalties that may be overlooked in the initial calculations. The channel loss includes all sources of loss between the transmitter and the receiver. The average transmitter power is typically provided by the manufacturer.

The link budget calculations for the network of Figure 5.2 in the downstream direction are shown in Table 5.1. As in the downstream direction the data rate requirement is at least 1 Gbps, the sensitivity of the receiver was selected to be -27 dBm. This value was used, as in [60] a -26.5 dBm sensitivity has been achieved for a 1.25 Gbps PIN-based burst mode receiver for a reference BER of 10^{-12}. In the case of the discussed network a burst-mode receiver is not required; despite that fact this value was used as a worst-case scenario. The receiver sensitivity value is also in good agreement with measurements of commercial 1.25 Gbps receivers that were carried out. In the link budget calculations a power margin of 6 dB was used, that is higher than the 3-4 dB margin suggested in [159]. This decision was made

to take into account the worst case scenario and due to the fact that there are many factors that could lead to performance degradation for the network under discussion. Typical values for wavelength filter [184], circulator [185] and AWG insertion losses [186] were used for the calculations. These values can be easily found from a survey of commercially available components [187]. The fiber loss quoted was calculated using a value of 0.2 dB/km for fiber losses [188]. As Table 5.1 shows the required minimum power per channel is -12.3 dBm.

Table 5.1: Calculation of Required Transmitted Power per Channel - Downstream direction.

Quantity	**Symbol**	**Value**
Receiver sensitivity	P_{rec}	-27dBm
System margin	M_S	6dB
Filter Loss	α_{filter}	0.75dB
Circulator Loss	$\alpha_{circulator}$	1.5dB
AWG Insertion Loss	α_{AWG}	5.5dB
Filter Loss	α_{filter}	0.75dB
Overall Fiber Loss	$\alpha_f L$	0.2dB
Required Transmitted Power per Channel	$P_{ch,Tx}$	-12.3dBm

5.3.2 Case 1 - Use of a Broadband Light Source and Spectrum Slicing

In case a BLS is used for downstream transmission, the overall power emitted by the BLS is spectrally sliced at the right-hand side AWG of Figures 5.1 and 5.2. Therefore, the overall power emitted by the BLS is shared between users. Let us assume that the elements between the BLS and the input port of the AWG - circulator, wavelength filter - do not have any impact on the shape of the signal spectrum, i.e. they have a flat transfer characteristic in the frequency domain. In order to accurately calculate the power $P_{AWG,Output}$ after the AWG, the following

relationship would need to be used :

$$P_{AWG,Output} = \int_{\infty}^{-\infty} P_{AWG,Input}(f) * |H_{AWG,Port}(f)|^2 \, df \tag{5.2}$$

where $P_{AWG,Output}$ is the power at the output of the AWG port, $P_{AWG,Input}(f)$ is the power spectrum of the light at the input of the AWG and $H_{AWG,Port}(f)$ is the transfer function of the AWG for the specific port. However, to simplify the calculations, let us approximate the losses $L_{slicing}$ due to spectral slicing as $L_{slicing} \approx \frac{B_{BLS,3dB}}{B_{AWG,port}}$, where $B_{BLS,3dB}$ is the 3-dB linewidth of the BLS and $B_{AWG,port}$ is the 3-dB bandwidth of the AWG port. To take into account the fact that the power spectral density decreases toward the edges of the spectrum, the emitted power used in the calculations was reduced by 3-dB - this reduction is more than the worst case scenario, as the difference between the average spectral density and the power spectral density at the 3-dB linewidth point is by definition less than 3-dB. It should also be noted at this point that the methodology used ignores the emitted power outside the 3-dB band. For a Gaussian spectrum, this would incur a penalty of less than 1dB. For now this penalty will be ignored and it will just be assumed that it is included in the 6 dB system margin. At this point, a plot depicting the required power as a function of both $B_{BLS,3dB}$ and $B_{AWG,port}$ can be generated. The result is shown in Figure 5.3. The plot was generated for $B_{AWG,port}$ values ranging from 0.1 to 4 nm. The three curves correspond to $B_{BLS,3dB}$ values of 40, 50 and 60 nm.

The figure shows that the required power at point 1 for an AWG port passband linewidth of 0.8 nm - equivalent to 100 GHz at a wavelength of 1550 nm - is more than 7 dBm for the considered values of source linewidth. It should be noted that the required power refers to the average power after modulating the source, so the required peak power is 3 dB higher. Typical values for commercial SLEDs [189],

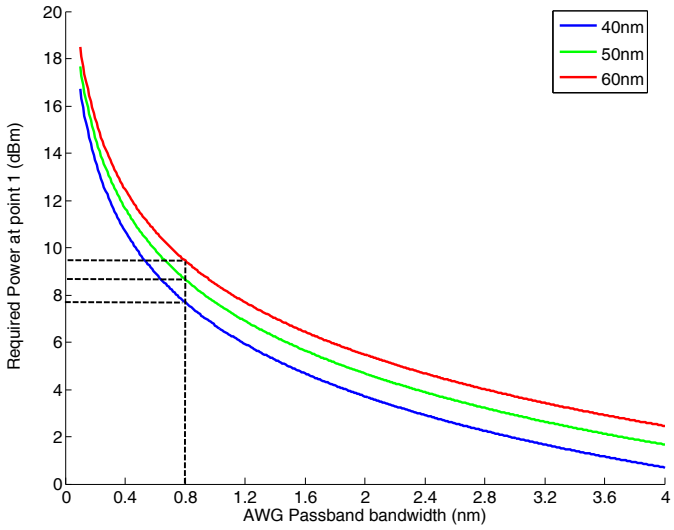

Figure 5.3: Required overall power at point 1 vs. AWG Passband Bandwidth.

Table 5.2: Calculated margin for downstream transmission using different broadband light sources as transmitters.

Solution	**Calculated power margin (dB)**
SLED Directly Modulated	-5.5
SLED Externally Modulated	-10
EDFA Externally Modulated (assuming use of polarization independent modulator)	0.7
Use of LED and SOA	3.5

EDFAs [190], SOAs [191] and modulators [192] were used to compare their peak transmitted power against the required power at point 1. The peak power values were derived from a survey of commercially available components. The margin provided by different solutions was calculated and the results are shown in Table 5.2. A negative margin indicates that the transmitted power is not sufficient, while a positive value means that the power requirement is met. The SLED fails to meet the power budget requirement without external amplification. The combination of an LED and an SOA seems to be the only solution that provides a comfortable

margin out of the solutions discussed. The use of an EDFA along with an external modulator is also possible but the margin is less wide.

5.3.3 Case 2 - Use of a Broadcast AWG

A Broadcast AWG (BAWG) is a device that can simultaneously perform wavelength routing and broadcast a specific wavelength on all its ports. The structure of such a device is shown in Figure 5.4 [176].

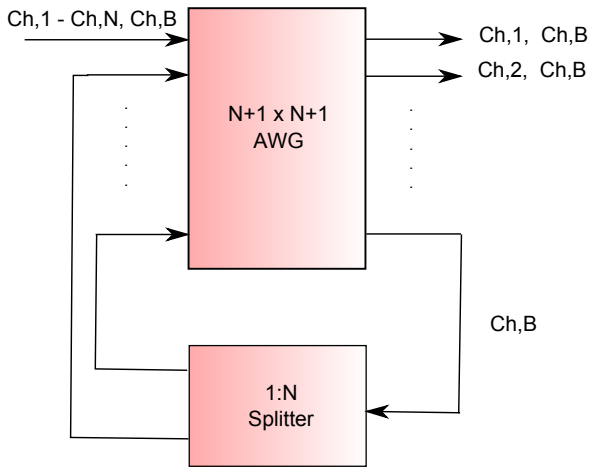

Figure 5.4: Functional structure of Broadcast-AWG.

It is relatively easy to see that although the routed wavelengths (Ch,1 - Ch,n) experience losses equal to the AWG insertion loss $L_{AWG,insertion}$, the broadcast signal experiences a loss of $L_{Ch,B}$:

$$L_{Ch,B} = 2 * L_{AWG,insertion} + 10 * log_{10}N \tag{5.3}$$

In Figure 5.5, the required power at point 1 of Figure 5.2 is plotted against the splitting ratio.

The required average transmitted power for 16 users is higher than 5 dBm, while for 32 users it exceeds 8 dBm. The required peak power is 8 dBm and 11 dBm,

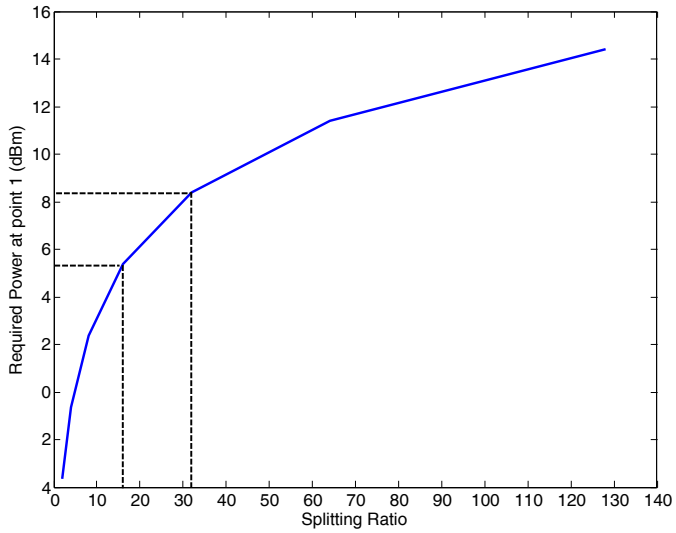

Figure 5.5: Required power at point 1 against splitting ratio.

respectively. It becomes evident that although use of a BAWG is a feasible solution, a high power transmitter is still required. Typically, high-power transmitters are based on DFB lasers; a relatively expensive solution. An amplifier could also be used; in this case, the cost is comparable to that of the previously described BLS-based solutions. A disadvantage of this architecture is the higher number of connections related to the BAWG structure. In a particle physics environment a high number of connections is perceived as more failure-prone, especially in case the AWG is placed inside the detector. Despite that fact the use of a BAWG is a solution that can deliver the required performance.

The conclusion of the analysis of different options for downstream transmission is that there is at least one solution that can meet the networking requirements for a unified architecture at the HL-LHC - that of the BAWG. Additional options exist, at least from a power budget perspective. These include the use of an externally modulated EDFA or the use of a LED along with an SOA. The use of an LED and an SOA may have some important advantages over the rest solutions, as it may be cheaper than the use of a BAWG and large-scale commercial availability should

not be an issue. However, as at least one solution for downstream transmission exists, the discussion will now move on to issues related to the upstream, since it is expected to be the most challenging part of the network to design.

5.4 Upstream Power Budget and System Requirements

In this section, the required power per channel $P_{ch,Seed}$ that has to be emitted by the light source, providing the light for upstream transmission, is calculated. The required power is calculated at point 2, as shown in Figure 5.6. For successful transmission of information in the upstream direction, light has to travel through the right-hand side AWG, be modulated by the REAM and travel back to point 3 of Figure 5.6 and the receiver on the left-hand side.

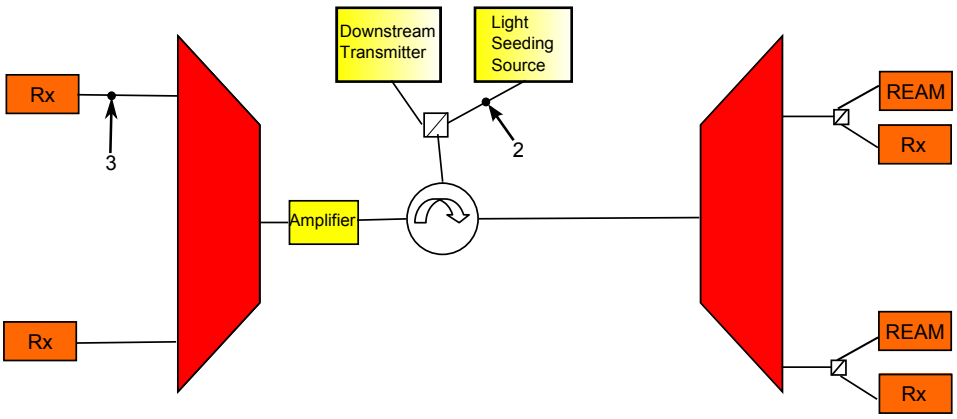

Figure 5.6: Point at which the required power is calculated.

5.4.1 Upstream Power Budget Calculations

The process that was carried out to calculate the required transmitted power in the downstream direction (Section 5.3) will be now repeated to calculate the corresponding required power in the upstream direction. The calculations are shown in Table 5.3. In this case the required power at the receiver input, at point 3 of Figure

5.6 is higher, due to the higher data rate in the upstream direction (10 Gbps). A receiver sensitivity of -19 dBm was assumed, as PIN-based receivers that can provide this sensitivity are commercially available, [193]. A 6 dB margin was used in the calculations. The REAM insertion loss was obtained from [194]. The amplifier gain value that was used is the one quoted in [195]. The rest of the values are identical to those used in the downstream link budget calculations of Section 5.3. The calculations show that an amplifier is required in the upstream direction, as without amplification the required power per channel would be approximately 15 dBm. The only solution to avoid the use of an amplifier is the use of expensive, high-power DFB-based laser arrays, but this essentially would lead to a degeneration of the architecture to an expensive and complex version of a point-to-point architecture.

Table 5.3: Calculation of Required Seeded Power per Channel - Upstream direction.

Quantity	**Symbol**	**Value**
Receiver sensitivity	P_{rec}	-19dBm
System margin	M_S	6dB
Filter Loss	$3\alpha_{filter}$	2.25dB
Circulator Loss	$2\alpha_{circulator}$	3dB
AWG Insertion Loss	$3\alpha_{AWG}$	16.5dB
REAM Insertion Loss	$\alpha_{REAM,ins}$	3.5dB
Overall Fiber Loss	$\alpha_f L$	0.4db
Amplifier Gain	G	25dB
Required Transmitted Power per Channel	$P_{ch,Seed}$	-12.35dBm

5.4.2 Case 1 - Use of an Incoherent Broadband Light Source

Following the approach of Section 5.3, the overall required power at point 2 of Figure 5.6 as a function of the 3-dB passband bandwidth of the AWG port, for different BLS linewidth values, can be calculated. The results are plotted in Figure 5.7.

It is easy to see that for a BLS linewidth of 60 nm and for a typical linewidth

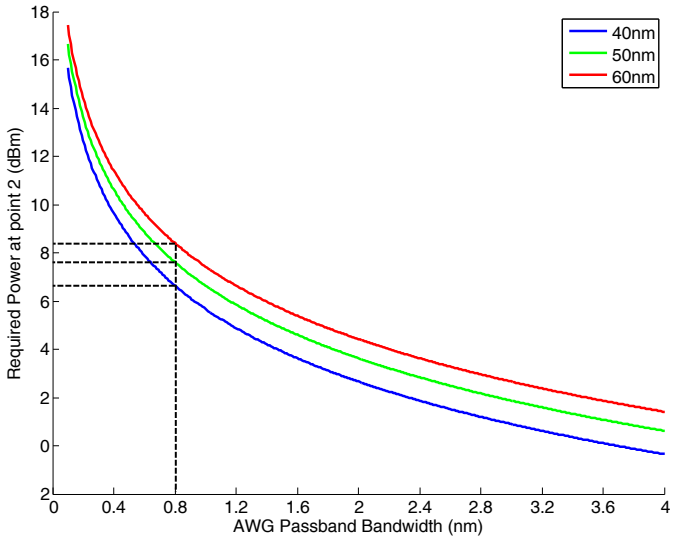

Figure 5.7: Required overall power at point 2 vs. AWG Passband Bandwidth.

value of 0.8 nm per AWG port - corresponding to 100 GHz at 1550 nm center wavelength - the overall required power emitted by the BLS source is 8.5 dBm. Taking into account the fact that the CW optical power should be 3 dB higher - as the calculated power is the average power between "1"s and "0"s - this translates to 11.5 dBm of power. Table 5.4 shows the calculated margin for different BLSs.

Table 5.4: Calculated margin for downstream transmitter using different broadband light sources for downstream transmission.

Solution	**Calculated power margin (dB)**
SLED	-1.9
EDFA	8.3
LED and SOA	3.6

The results show that the SLED fails to meet the power budget requirements, although not by a very wide margin. The EDFA and the LED/SOA combination look reasonable choices from a power budget point of view. At this point it should be noted that the use of a BAWG would not affect the upstream power budget.

5.4.3 Case 2 - Use of a Coherent Light Source

Use of coherent light sources to provide the necessary light for upstream transmission is also an option. These mainly include FP-LDs [196], frequency comb generators [197] and laser arrays [179]. Ideally, the use of frequency comb generators should be avoided, as they are considered an expensive solution. At the same time, using a laser array would result essentially in a point-to-point architecture from a component count viewpoint. Taking into account that in our applications reducing the number of fiber links used is not a very high priority, use of a laser array is not a very reasonable option. A last option is the use of Quantum-Dot (QD) FP-LDs, but we will not discuss this option at this stage as the technology is currently immature. Therefore the discussion of coherent light sources is going to be focused on FP-LDs.

A detailed power budget, as in the case of BLSs is not going to be carried out. Instead, some important points regarding the use of FP-LDs as light seeding sources from a power budget point of view are going to be discussed. As shown in [198] and [103] one of the technical issues that needs to be overcome in order to use FP-LDs along with spectrum slicing is their non-uniform power between modes, as well as the fact that the power is shared between a small number of competing dominant modes - also mentioned in [159]. Therefore even in the case of a high power laser, the side modes away from the gain peak of the cavity may not have enough power to meet the power budget in normal operation. Biasing the laser below threshold would increase uniformity, but would lead to decreased power. The use of a FP-LD would require amplification. Moreover it may require use of MPN reduction techniques.

Therefore, if incoherent light sources can offer satisfactory performance, their use would be preferred. FP-LDs offer an alternative, but there is a large number

of technical issues that need to be resolved. If none of these solutions can meet the requirements, then the advantages of using a WDM PON would be questioned.

5.5 Single-Wavelength Power Penalties

The previous power budget calculations for both the upstream and the downstream directions were based on an important assumption; the assumption that the only factor limiting system performance was the presence of thermal noise at the receiver side. This is not accurate; there is a number of factors that can degrade system performance and lead to an increase in the required received power. The effect of these parameters is going to be analyzed in this section. The purpose of the analysis is to provide an estimate of the impact each of the power penalties can have on the performance of the suggested WDM PON architecture.

The main sources of power penalty in single-wavelength systems that will be discussed are [159]:

- Dispersive Pulse Broadening
- Frequency Chirping
- Extinction Ratio
- Mode Partition Noise
- Intensity Noise

Modal noise, jitter and reflection feedback are also quoted as sources of power penalty. However, modal noise applies only to cases where multimode fiber is used, while jitter is better studied when the electronic parts of the system are complete, as the efficiency of the CDR circuitry plays a vital role. Furthermore jitter and

reflection feedback are better studied using experiments, therefore it would be more appropriate to study their impact during the system implementation phase.

5.5.1 Dispersive Pulse Broadening

In single-mode fibers, dispersion is caused by the variation of group velocity with frequency, causing broadening of pulses propagating along the fiber, as different frequency components travel with different group velocities [159]. Dispersion leads to system performance degradation in two ways; it introduces ISI and it reduces the energy contained within the bit slot, thus worsening the SNR. The analysis in [159] that will be utilised to calculate the effects of dispersion is based on two assumptions. The first is that the pulses transmitted over the fiber have a Gaussian shape. The second is that ISI has negligible impact on system performance, thus the system is designed in such a way that even after pulse broadening the following condition is met: $4B\sigma \leq 1$, where B is the bit rate and σ is the rms width of the Gaussian pulse at the output of the fiber. Under these assumptions, the dispersion-induced power penalty for a source with large spectral width is given by the following expression [159]:

$$\delta_d = -5log_{10}[1 - (4BLD\sigma_\lambda)^2] \tag{5.4}$$

where δ_d is the power penalty, B is the data rate, L is the link length, D is the dispersion parameter and σ_λ is the source linewidth. As the primary quantity of interest is the maximum achievable link length, Equation 5.4 is solved for L:

$$L = \frac{\sqrt{1 - 10^{-\frac{\delta_d}{5}}}}{4BD\sigma_\lambda} \tag{5.5}$$

The maximum distance the signal can propagate before the dispersion power

penalty takes a specific value can now be calculated. The results, highlighting the fact that dispersion is not a concern in the downstream direction, are shown in Figure 5.9. The Figure shows that even using a 4 nm AWG port linewidth, the dispersion penalty becomes 1 dB only after link length of over 2 km.

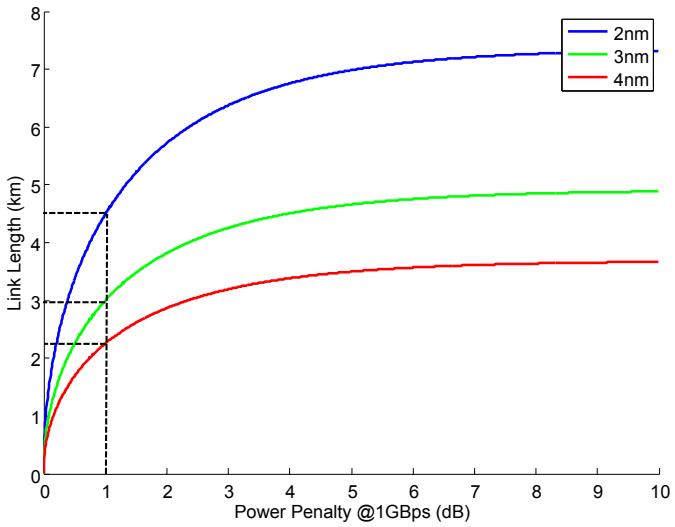

Figure 5.8: Maximum link length vs. power penalty for different AWG passband linewidth values.

In the upstream direction Equation 5.5 is solved for σ_λ to become:

$$\sigma_\lambda = \frac{\sqrt{1 - 10^{-\frac{\delta_d}{5}}}}{4BDL} \tag{5.6}$$

Equation 5.6 is then used to plot the maximum AWG passband linewidth as a function of dispersion penalty. The results, shown in Figure 5.9), show that for 10 Gbps and 150 m link length the penalty reaches 1 dB only for a very large value of bandwidth (above 6 nm). On the other hand, for 1 km there is a limit and this is 0.8 nm, which at 1550 nm center wavelength corresponds to 100 GHz of bandwidth. Although currently it seems that the length of the links is going to be 150 m, care should be taken in case an extension of the links to 1 km is attempted.

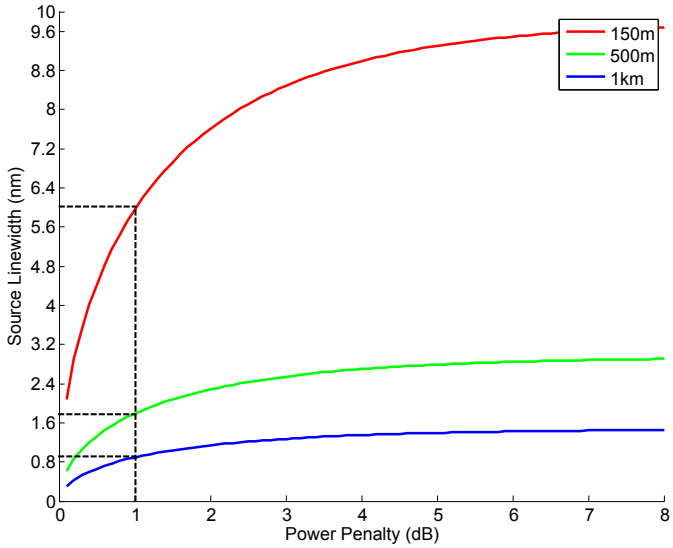

Figure 5.9: Maximum link length vs. power penalty for different AWG passband linewidth values.

5.5.2 Chirping

Chirping can affect system performance in three ways; the first is through its interplay with dispersion. As chirping leads to spectral broadening the chirped signal is more susceptible to dispersion. The second fact that needs to be taken into account is the effect of the combination of chirping and subsequent filtering, which leads to frequency modulation to amplitude modulation (FM-to-AM) conversion, as reported for example in [199] and [200]. Lastly, depending on the amount of chirping and the spacing between channels, spectrum broadening can also lead to an increase in crosstalk, limiting the minimum channel spacing in WDM systems [200].

Chirping is expected to have a more severe impact on upstream rather than on downstream performance due to the higher upstream data rate, therefore the focus of the analysis is going to be the upstream power penalty in this section. In the upstream direction, chirping is introduced by the REAM. According to the analysis

by [201] the power penalty for a chirped Gaussian pulse because of dispersion is given by:

$$P = 10log_{10}(\frac{T_1}{T_0}) \tag{5.7}$$

where T_1 and T_0 are the half-width at the 1/e intensity point after and before transmission, respectively. The relationship between T_1 and T_0 is given by:

$$\frac{T_1}{T_0} = \sqrt{(1 + \frac{C\beta_2 z}{T_0^2})^2 + (\frac{\beta_2 z}{T_0^2})^2} \tag{5.8}$$

where β_2 is the group-velocity dispersion of the fiber, z is the propagation distance and C is the chirp parameter. The relationship $\sqrt{8}BT_0 \leq 1$ will also be used to calculate T_0 from the data rate B and $L_D = \frac{T_0^2}{\beta_2}$, to simplify Equation 5.8. In order to take into account the worst case scenario, the penalty will be evaluated at the 1550nm wavelength window where β_2 is higher - a value of $-21ps^2/km$ for β_2 was used in our calculations.

The only parameter that needs to be determined is the chirp parameter, C. Chirping in EAMs is caused by changes in the refractive index because of absorption changes - absorption and refractive index are connected through the complex refractive index, consequently changing one will lead to changes to the other, described by the Kramers-Kronig relations [201]. Chirp characteristics of modulators are characterised by Henry's parameter α_H, defined as $\alpha_H = \frac{\delta n}{\delta k}$, where n and k are the amplitudes of the real and imaginary part, respectively, of the complex refractive index $n + \jmath k$ of the modulator. Henry's parameter equals $-C$, only if n changes linearly with k, [201]. In general this is not the case. To simplify matters, the effective Henry's parameter, $\bar{\alpha_H}$ can be used [202] that is constant over the range of voltages between V_{ON} and V_{OFF} - therefore a linear relationship between n and k is implied. The most extreme values of $\bar{\alpha_H}$ that have been used in [202] are -1

and 4. A wider range of values can be used to ensure that there is a comfortable margin. The dispersion penalty due to chirping as a function of $\bar{\alpha_H}$ can now be calculated. The result for transmission at 10 Gbps over a distance of 1 km is plotted in Figure 5.10. This analysis shows that the dispersion-induced power penalty due to chirping is not an issue, as the penalty is confined to values lower than 1 dB, even for extreme $\bar{\alpha_H}$ values.

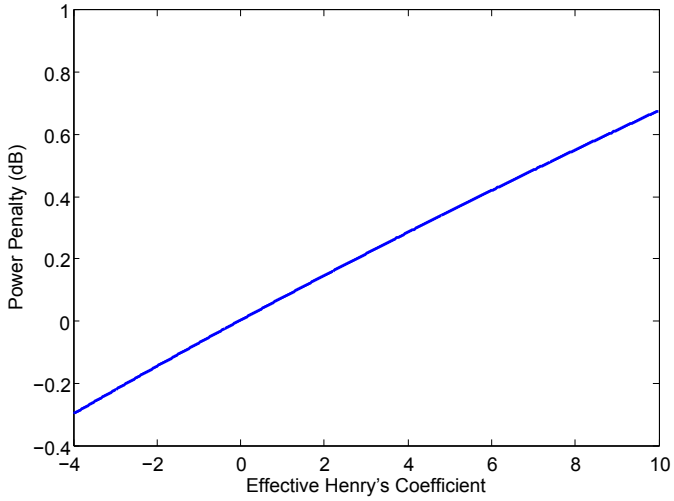

Figure 5.10: Dispersion-induced power penalty due to chirping vs. Effective Henry's Coefficient.

Now let us use the chirping-induced spectrum broadening, B_{br} that is equal to $(1 + C^2)^{1/2}$ [203]. As chirping is associated to the intensity of the envelope of the signal - normally taken as a Gaussian pulse - broadening can be treated as a two step operation; broadening of the Gaussian spectrum and convolution of the Gaussian spectrum by the carrier's spectral content (Typically the carrier is a single tone. However, this term - carrier's spectral content - will be used in the discussion, as in our case spectrally sliced light is one of the alternatives for seeding and it clearly contains more than one tones). As spectrum broadening is relative, the excess required bandwidth, B_{excess}, will be defined as:

$$B_{excess} = \sqrt{\frac{C^2}{T_0^2}} = \sqrt{\frac{\bar{\alpha_H}^2}{T_0^2}} \tag{5.9}$$

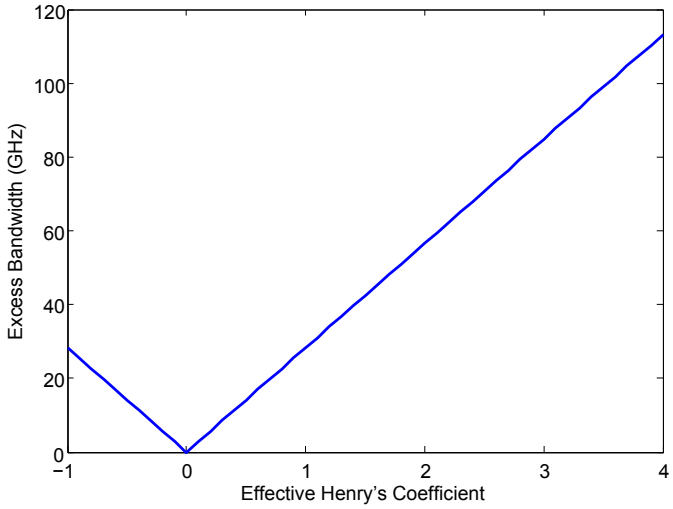

Figure 5.11: Excess bandwidth vs. effective Henry's Parameter.

The excess required bandwidth as a function of $\bar{\alpha_H}$ for a data rate of 10 Gbps is plotted in Figure 5.11. The results show that the excess bandwidth required can be quite large, even of the same same order of magnitude as the original bandwidth of the seeded light - as a reminder, commercial AWGs have a port bandwidth of 50, 100 or 200 GHz. To estimate its impact in terms of power penalty, we assume that the REAM is seeded by light which is spectrally-sliced by the AWG, meaning that at the input of the REAM, the light has a linewidth equal to the passband bandwidth of the corresponding AWG port. This effectively implies that all the excess bandwidth is going to be filtered by the AWG as the signal has to travel through the same port. Therefore, the following relationship can be used to estimate the power penalty:

$$\delta = 10log_{10}(\frac{B_{excess} + B_{AWG}}{B_{AWG}}) \tag{5.10}$$

The estimated power penalty is plotted in Figure 5.12. Figure 5.12 clearly

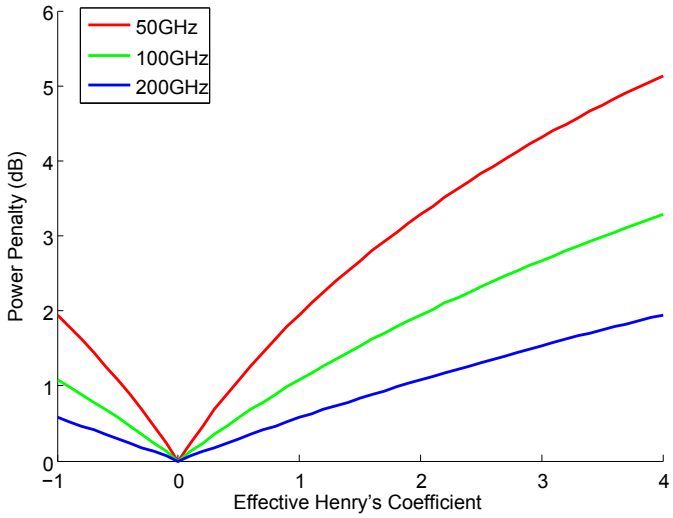

Figure 5.12: Power penalty due to chirping/filtering combination vs. effective Henry's Parameter.

shows that filtering the spectrally broadened signal can have a significant impact on system performance for narrow passband bandwidth and extreme effective Henry's parameter values. On the other hand, for a passband bandwidth of 100 GHz or larger, the power penalty may remain significant, but is confined to values less than 3.5 dB, which is within the system margin limit of 6 dB. The conclusion of the analysis at this stage is that AWGs with passband bandwidth of 100 GHz or more will be used and that the power penalty, although it may be significant, it is within acceptable limits. Optimization of the REAM bias point is recommended. This move could ensure that the penalty is reduced further, to much lower levels. Only after successful optimization AWGs with lower passband bandwidth can be used. The analysis of chirping power penalty in the upstream direction effectively shows that its impact in the downstream direction is going to be negligible.

5.5.3 Extinction Ratio

According to [159] the power penalty induced from a non-perfect extinction ratio can be calculated using the following relationship:

$$\delta_{ex} = 10log_{10}(\frac{1+r_{ex}}{1-r_{ex}}) \tag{5.11}$$

where r_{ex} is the extinction ratio, defined as $r_{ex} = \frac{P_0}{P_1}$. In the previous expression, P_0 is the power emitted when a "0" is transmitted, while P_1 is the power emitted when a "1" is transmitted. A more common way to express the extinction ratio is $r_{ex,dB} = 10 * log_{10}(\frac{P_1}{P_0})$ - please note that the reciprocal of the linear r_{ex} is used. The power penalty as a function of the extinction ratio in dB is plotted in Figure 5.13. It can be seen that an extinction ratio of 9 dB or higher is required to achieve a power penalty of less than 1 dB.

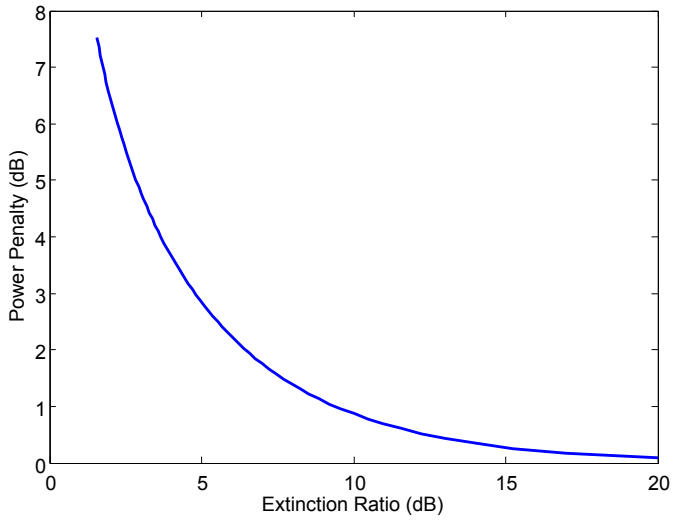

Figure 5.13: Power penalty vs. extinction ratio.

It is important to note that in the previous analysis a thermal noise limited system was assumed. In other words, it was assumed that the standard deviation is the same for the "1" and "0" levels ($\sigma_1 \approx \sigma_0 \approx \sigma_T$). On the other hand, in cases

where a BLS is used along with spectrum slicing, the system may be beat noise limited. In such cases noise is signal dependent. The analysis of [104] - where it was assumed that the Gaussian approximation is valid for the beat noise limited case -, has shown that:

$$\frac{I_1}{\sigma_1} = \sqrt{SNR} = \sqrt{\frac{B_o}{B_e}} \tag{5.12}$$

where I_1 is the average value of the photocurrent for a received 1, σ_1 is the noise standard deviation for the "1" level, SNR is the signal-to-noise ratio and B_o and B_e are the optical and electrical bandwidth, respectively. Assuming that beat noise is limiting the SNR of the "0" level as well, and using $I = RP$, where R is the responsivity of the receiver and $r_{ex} = \frac{P_0}{P_1}$, the following relationships can be derived:

$$\sigma_1 = \sqrt{\frac{B_e}{B_o}} R P_1 \tag{5.13}$$

$$\sigma_0 = \sqrt{\frac{B_e}{B_o}} R P_0 = \sqrt{\frac{B_e}{B_o}} R r_{ex} P_1 = r_{ex}\sigma_1 \tag{5.14}$$

Taking into account that

$$Q = \frac{I_1 - I_0}{\sigma_1 + \sigma_0} \tag{5.15}$$

and after some simple calculations, we derive:

$$Q = \frac{1 - r_{ex}}{1 + r_{ex}} \sqrt{\frac{B_o}{B_e}} \tag{5.16}$$

It is important to note that in Equation 5.16, Q is not power-dependent, which shows that there is no trade off between power and extinction ratio, as in the thermal noise-limited case. The SNR reduction as a function of the extinction ratio can now

be plotted in case the system is beat-noise limited.

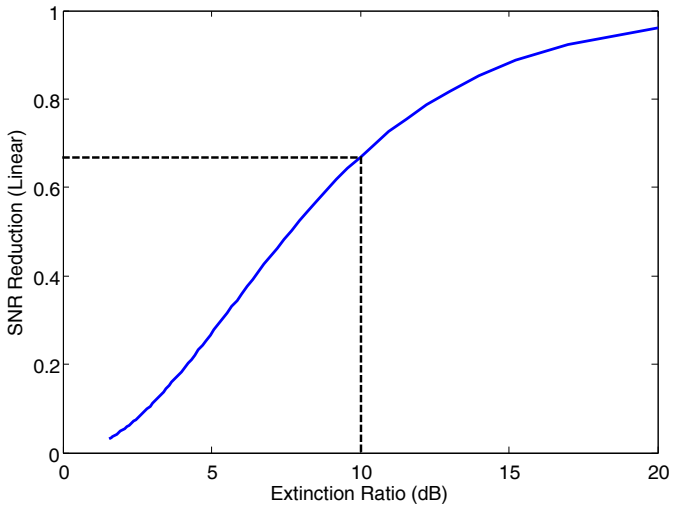

Figure 5.14: SNR reduction vs. extinction ratio.

Figure 5.14 shows that for an extinction ratio value of 10 dB - a relatively high value for commercial transmitters - the SNR degrades to 0.65 of its value for perfect extinction. This is a significant SNR reduction and it should be taken into account during system design, in case spectrum slicing is chosen to either broadcast information in the downstream direction, or to inject light into the modulators. The extinction ratio requirements are expected to be more demanding in the upstream direction, where margins are less comfortable.

5.5.4 Relative Intensity Noise and Mode Partition Noise

According to [159] the output of semiconductor lasers exhibits noisy behavior even when the bias current remains constant. This noise can be attributed to spontaneous emission and shot noise generated by electron-hole recombination. RIN, typically reported in dB/Hz, refers to optical power fluctuations of the laser output relative to the average power. MPN on the other hand refers to the phenomenon where although the total optical output power remains constant, the power of each

individual mode fluctuates. Typically, MPN on its own is not considered a factor that degrades system performance. As mentioned in [159] for example, the interplay of MPN and dispersion and not MPN itself, is what leads to SNR reduction.

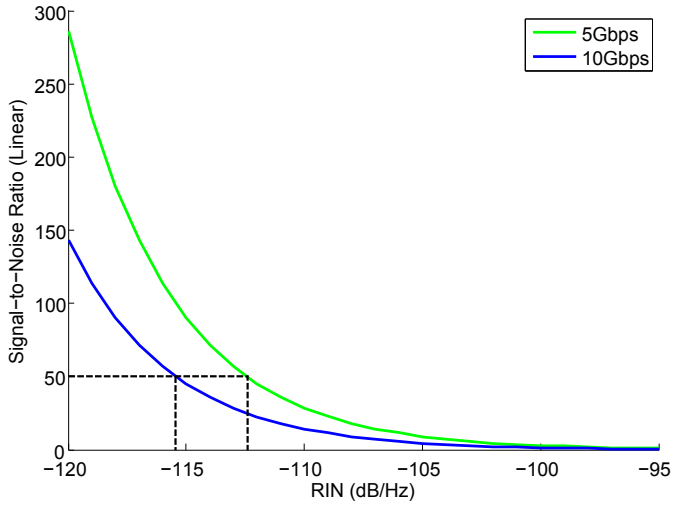

Figure 5.15: SNR vs. RIN.

Since RIN and MPN refer to the operation of semiconductor lasers, we are interested in these quantities mainly due to the possibility of using a laser as a CW light source to inject light into the modulators. The reason why RIN and MPN are being discussed together, is that in the architecture of interest, MPN would be converted to intensity noise after spectrum slicing. As ensuring that the upstream SNR is sufficient for 10 Gbps transmission is critical, at this stage providing an indication of the RIN requirement for the spectrally sliced light is important.

As RIN for commercial lasers is typically reported in dB/Hz its impact will be evaluated using the following simple relationship:

$$SNR = \frac{1}{RIN_{dB/Hz} B_{el}} \tag{5.17}$$

The SNR as a function of the RIN in dB/Hz is plotted in Figure 5.15. The Figure shows that the required values to achieve an SNR of 49 - corresponding to a BER

value of 10^{-12} - are -112 dB/Hz and -115 dB/Hz for 5 and 10 Gbps transmission, respectively. These values are considered high - i.e. easily achievable - as typically commercial devices have lower RIN levels. However, these are quite challenging values to achieve when it comes to the MPN of a spectrally sliced multi-mode FP-LD. This is evident by the fact that 10 Gbps transmission using this technique has not been achieved. Moreover, meeting the power budget requirement using a FP-LD is not an easy task, while the number of users are limited by the number of modes. Therefore use of a FP-LD as a CW light source does not appear to be an attractive option.

5.6 Multi-wavelength Power Penalties

Multi-wavelength system implementation poses a number of additional challenges, which have to be addressed. The effect of a number of power penalties that are not an issue for single-wavelength systems have to be taken into account. This is the topic of this Section. More particularly the effect of the following power penalties is discussed [159]:

- Heterowavelength Linear Crosstalk
- Homowavelength Linear Crosstalk
- Nonlinear Raman Crosstalk
- Stimulated Brillouin Scattering

5.6.1 Heterowavelength Linear Crosstalk

Heterowavelength or out-of-band crosstalk is caused by the non-perfect transfer characteristic of wavelength filtering devices - such as AWGs - in a WDM network.

The issue arises when the transmittivity of the filter is non-zero outside the wavelength region of interest. In that case out-of-band power can reach the detector. Assuming that the photodetector responsivity does not vary across channels and that the peak power is the same for all channels the power penalty δ_X can be expressed as [159]:

$$\delta_X = 10log_{10}(1 + X) \tag{5.18}$$

where $X = \sum_{n \neq m}^{N} T_{mn}$ is the integrated transmittivity of the filter across all channels, apart from the channel of interest - assuming that m is the channel of interest and n is the channel to be filtered, T_{mn} is the transmittivity of the filter at channel n, i.e. the ratio of the output optical power over the incident optical power for the undesired channel n. It is important to note that the above power penalty expression is calculated based on eye closure and not on BER. In our case heterowavelength crosstalk could be an issue only in the upstream direction, as in the downstream direction information is broadcast. Using typical crosstalk level values of -25 dBm for adjacent and -30 dBm for non-adjacent channels [204] power penalty can be plotted as a function of the number of channels.

Figure 5.16 shows that heterowavelength crosstalk is not a source of concern as the penalty remains low even for 250 channels. The number of users in the case of the WDM PON architecture under discussion is expected to be limited by the wavelength region of operation of the REAMs. Typically these devices have a wavelength region of operation of $\sim$20 nm. In case channels are spaced $\sim$1 nm apart the number of users will be limited to $\sim$20. Although this is not a thorough calculation of the number of the number of users it is sufficient to provide an initial estimate of the users supported and show that this number is much lower than 250.

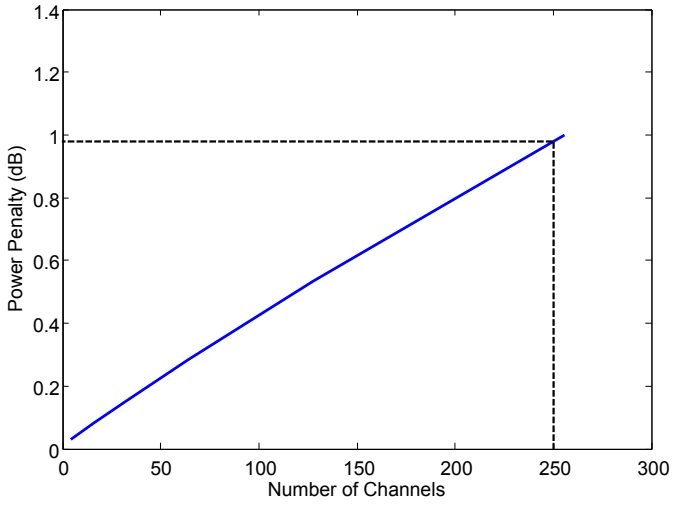

Figure 5.16: Heterowavelength linear crosstalk power penalty vs. number of channels.

5.6.2 Homowavelength Linear Crosstalk

Homowavelength or in-band crosstalk can have a more severe impact on system performance than heterowavelength crosstalk, as the interfering signal has the same wavelength as the signal of interest. The cause of homowavelength crosstalk is out-of-band transmission from other channels, in the same wavelength range as the wavelength of interest.

In the case of the network architecture under discussion, homowavelength crosstalk could be an issue only in the upstream direction. Imperfect filtering of the CW light source at the right-hand side AWG of Figure 5.6 could result in homowavelength crosstalk. According to [159], the homowavelength crosstalk-induced penalty is given by:

$$\delta_X = -10log_{10}(1 - r_X^2 Q^2) \tag{5.19}$$

where r_X can be defined as a function of the average crosstalk level X as $r_X^2 = X(N-1)$, where N is the number of channels. In our case, the average

crosstalk level in the upstream direction can be calculated from the adjacent and non-adjacent crosstalk level values of the right-hand side AWG of Figure 5.6. Assuming a broadband light seeding source with a uniform spectrum the crosstalk power of channel n, P_n relative to the power of the channel of interest m, P_m is:

$$P_m = 2 * L_{AWG} * P_n \tag{5.20}$$

where L_{AWG} is the adjacent and non-adjacent crosstalk value of the AWG, for adjacent and non-adjacent channels, respectively. Multiplication by a factor of 2 is necessary to take into account the fact that the signal has to go through the AWG twice. It should be noted that the left-hand side AWG can not further reduce crosstalk, as the interference is in-band. The power penalty can be calculated and plotted as a function of the number of channels. The results are shown in Figure 5.17.

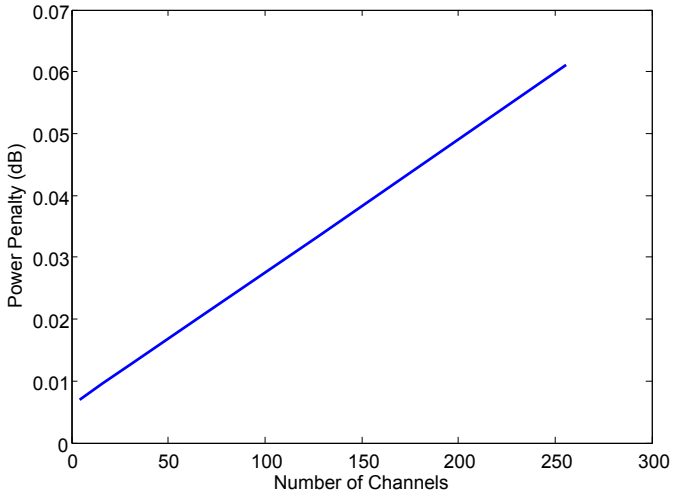

Figure 5.17: Homowavelength linear crosstalk power penalty vs. number of channels.

The Figure shows that the penalty is negligible, even for a very high number of channels, such as 250 where it takes a value of <0.07 dB. One of the main reasons for

this outcome is the fact that the upstream signal is filtered twice by the right-hand side AWG of Figure 5.6.

5.6.3 Stimulated Raman and Brillouin Scattering-Induced Crosstalk

Both Raman and Brillouin scattering are inelastic types of light scattering, meaning that during these processes light changes its frequency in the process. Both are caused by interactions of light with phonons - vibrations of the atoms in a crystal lattice [205] - with the only difference between the two being that in Raman scattering light interacts with optical phonons, while Brillouin scattering is caused by light interactions with acoustic phonons [205].

What is important in our case is that the effect of both types of scattering becomes significant at high power levels, therefore imposing limitations on the highest amount of power that can be launched to the fiber. According to [159] the stimulated Raman scattering induced power penalty δ_R can be estimated using the following relationship:

$$\delta_R = -10log_{10}(1 - D_R) \tag{5.21}$$

where D_R is the fractional power loss which is taking its maximum value for the shortest wavelength channel and can be calculated by, [159]:

$$D_R = \frac{1}{2}M(M-1)C_R P_{ch} L_{eff} \tag{5.22}$$

where M is the number of channels, P_{ch} is the power per channel and L_{eff} is the effective interaction length given by the relationship $L_{eff} = [1 - exp(-\alpha L)]/\alpha$, while C_R is given by, [159]:

$$C_R = \frac{S_R \Delta v_{ch}}{2A_{eff}} \tag{5.23}$$

S_R is the Raman gain slope, Δv_{ch} is the channel spacing, and A_{eff} is the effective core area of the optical fiber. Using the above relationships, we can easily find that for 1 km of link length, even using extreme values, for example launching an overall power of 80 dBm, for 128 channels and 600 GHz channel spacing - the particular combination of numbers was arbitrarily chosen just to illustrate the point - the power penalty is only 0.68 dB. Therefore Raman scattering is not an issue in our case.

Brillouin scattering on the other hand leads to limitation of the overall, instead of the per channel power launched to the fiber. The power threshold limit P_{th} can be calculated using the relationship, [159]:

$$P_{th} \approx \frac{21 A_{eff}}{g_B P_{th}} \tag{5.24}$$

Therefore the power threshold for 1 km of fiber is 21 dBm, which is higher than the saturation power of low-cost SOAs and EDFAs that we intend to use.

5.7 Beat Noise, Signal-to-Noise Ratio and System Requirements

The analysis conducted using link budget calculations is based on the assumption that noise, with the exemption of RIN, is generated at the receiver and therefore is implicitly taken into account using the receiver sensitivity [159]. This approach fails to take into account other sources of optical signal fluctuation. Typical factors that can lead to such fluctuations include, apart from RIN, noise caused by beating between the signal and spontaneous emission and between spontaneous emission

and itself. Beat noise is a typical source of SNR degradation in amplified systems. It is also a major performance limiting factor in spectrally sliced systems, thus, very much relevant to the performance assessment of the the network under discussion.

5.7.1 Downstream Beat Noise and Signal-to-Noise Ratio Calculations

The SNR of spectrally-sliced incoherent light sources including effects caused by modulation has been thoroughly investigated in [206]. The results of this analysis, although very useful, depend on the electrical filter and the pulse shape. However the results of [206] can be used to derive a simplified expression for CW light. This expression has also been used to calculate the potential capacity of a system based on a spectrally-sliced EDFA in [104]. According to this approach the SNR can be calculated using the following relationship:

$$SNR = \frac{mB_o}{2B_e} \tag{5.25}$$

where B_o and B_e are the optical and electrical bandwidth respectively while m takes a value of $m = 1$ for polarized and $m = 2$ for unpolarized light, respectively, [99]. Assuming that B_e is 0.7 times the required transmission rate - which in the downstream direction is 1 Gbps - and taking into account the fact that a $BER = 10^{-12}$ corresponds to an optical SNR of 49 [104], SNR can be plotted as a function of B_o; B_o is equal to the passband bandwidth of the AWG. The results are shown in Figure 5.18.

The figure shows that the required SNR of 49 (approximately 17 dB) can be achieved even for optical bandwidth lower than 50 GHz. Typically, standard commercial AWGs come at 50, 100 or 200 GHz channel spacing. In other words, a value of 50 GHz for optical bandwidth represents the worst-case scenario (inefficiencies

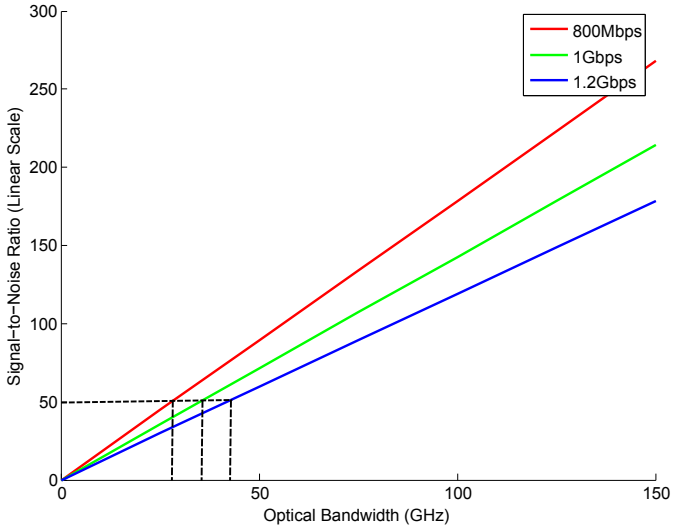

Figure 5.18: SNR vs. Optical Bandwidth for different data rates.

introduced by guard bands can be ignored, as flat-top AWGs with very low guard band are available). The analysis shows that network performance in the downstream direction, in case a spectrally sliced BLS is used, is thermal noise and not beat noise limited.

5.7.2 Upstream Signal-to-Noise Ratio Calculations

The same methodology as above can be utilised to derive an estimate of the limitations imposed by excess intensity noise on upstream data rate. Again the results are valid in case an incoherent BLS is used to inject light into the REAMs. The maximum data rate as a function of the optical bandwidth is plotted in Figure 5.19.

The results show that a 5 Gbps data rate - i.e. a data rate equal to the one of the upgraded CMS tracker, please see Chapter 2 - can be theoretically achieved using less than 200 GHz of bandwidth. However, the conclusion of Section 5.5.3 has to be taken into account. According to that, the imperfect extinction ratio has an impact on the achievable SNR in beat noise limited systems. Referring back to Figure 5.14 and taking into account that the extinction ratio of commercially available 10

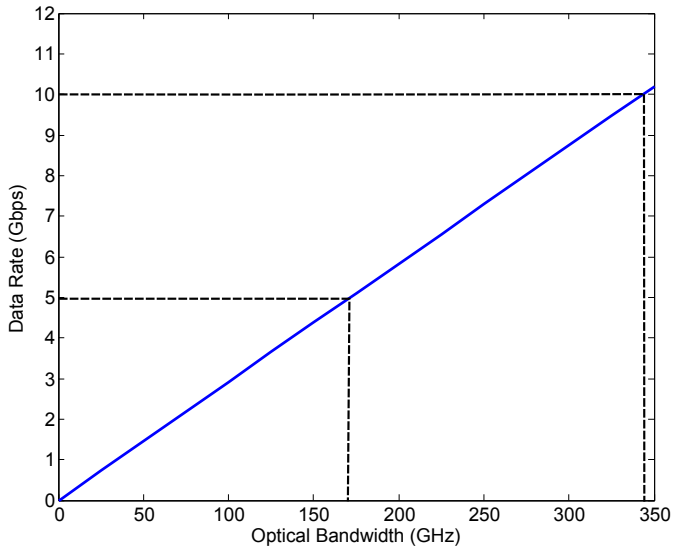

Figure 5.19: Achievable data rate vs. optical bandwidth.

Gbps REAMs can be as low as 8 dB [207], the SNR reduction factor is going to be ∼0.52. This translates to a corresponding increase in the required optical bandwidth by a factor of ∼1/0.52. Thus, the required bandwidth for 5 Gbps transmission now becomes ∼384 GHz. This bandwidth value is unacceptable, as commercial AWGs having a passband bandwidth of >200 GHz are not available. Moreover the corresponding linewidth value at 1550 nm is ∼3 nm, so assuming a wavelength region of operation of 20 nm for the REAMs, the number of users reduces to only 6. Thus, the costs of implementing a WDM PON architecture and the associated complexity, outweigh the benefits due to reduction in component count. It is obvious that the initial performance goal of achieving 10 Gbps transmission in the upstream direction is not possible. Therefore, using a spectrally sliced incoherent BLS to inject light into the modulators is not a good option to meet the performance goals of a unified architecture at the HL-LHC.

5.8 Conclusions

In this chapter the PON architectural space was explored to identify the most suitable candidate for a unified architecture at the HL-LHC. An architecture based on WDM PON was proposed, mainly due to the fact that the virtual point-to-point connections it offers could be used to meet the very high upstream bandwidth requirements using a single fiber. Moreover, a number of components related to this PON variant are based on mature technologies. Different options to achieve broadcasting of information in the downstream direction were also outlined. One advantage of this type of architecture - WDM PON - is that it offers several options as far as the front-end components (ONUs) is concerned. Different options were briefly discussed. An architecture based on the use of REAMs appeared to be the most appealing option. The particular optoelectronic device has interesting properties that have attracted the interest of the particle physics community in the past. This interest informed our decision. However as modulators do not emit light, a remote light source, providing the light for upstream transmission is required. The different options were outlined. The reasons for preferring some particular solutions over others were also discussed.

Having selected most of the features of the architecture - e.g. the fact that it was based on a WDM, reflective scheme using REAMs - the discussion could move on to the evaluation of the architecture and the detailed assessment of different architectural alternatives. The performance assessment was carried out in two stages. The first stage involved calculating the link budgets and evaluating the single-wavelength and multi-wavelength power penalties. According to these calculations meeting the specifications for a unified architecture at the HL-LHC appeared to be feasible. However, the second stage of the assessment, showed that the system is beat noise limited and that the limitations imposed by this type of noise

are severe. Using a BLS and spectrum slicing to inject light into the modulators is not an architectural option that can meet the upstream data rate requirements. Other options to inject light into the modulators exist, but they do not appear very attractive in terms of cost and complexity. In other words, the WDM PON architecture presented and analysed would be limited if it were to be used for the application of interest. There is one promising way to resolve the problems related to beat noise and use a single, high power source to inject light into the modulators; this is the use of Quantum-Dot Laser Diodes (QD-LDs) [208]. However currently this is an immature technology and large scale commercial availability, as well as cost, are issues. As there is interest in the use of REAMs as front-end devices in the particle physics community, this idea will not be dropped at this stage. In the next chapters, this idea will be taken forward and other, simpler architectures will be explored to facilitate the use of REAMs in a unified architecture at the HL-LHC.

Chapter 6

A Custom Passive Optical Network Architecture for Bidirectional Global Information Transmission at the HL-LHC based on Reflective Electroabsorption Modulators

In Chapters 4 and 5 two different PON architectures were described targeting different applications at the HL-LHC. The first was a TDM PON architecture aimed at transmitting timing, trigger and control data, while the second was intended for transmission of all types of LHC information. Although the analysis in Chapter 4 showed that the TDM PON can meet the requirements of the targeted application,

the discussion of the WDM PON architecture in Chapter 5 showed that applying the PON concept to transmit all types of information at the HL-LHC is challenging. Although using an architecture based on standard PON technologies, such as those described in Chapter 3, may be possible, the resulting architecture would be too costly for the advantages it could offer. Despite the outcome of the discussion in Chapter 5 there are aspects of the WDM PON architecture that are desirable. These include the bidirectionality of the architecture, the efficiency it offers through resource sharing - as in the case of the downstream transmitter and the CW light source - and the use of a potentially radiation-hard REAM device at the front-end. In this Chapter a simpler alternative architecture is proposed and discussed. The architecture is essentially based on the PON paradigm, as it does not feature any active devices between the front- and the back-end. It is also especially designed to retain the main advantages of the WDM PON of Chapter 5, albeit using a simplified network structure.

The present Chapter starts with a description of the suggested architecture. As one of the key features of the architecture is the use of REAMs at the front-end, a discussion of the operating principles of REAMs, along with key metrics commonly used to characterise them, follows. The discussion then moves on to the performance evaluation of the architecture. This is carried out in a number of stages; firstly, preliminary power budget calculations are carried out and the impact - and importance - of relevant penalties is estimated. Then, the effect of uncontrolled - e.g. temperature - and controlled - e.g. operating wavelength - environmental parameters on the operation of the REAM is measured. Finally measurements directly related to network performance are carried out. The purpose of the work presented in this Chapter is to prove the concept of using the discussed architecture as a unified architecture at the HL-LHC.

6.1 Network Architecture - Description and Dimensioning

In Chapter 2 the requirements for a unified architecture at the HL-LHC were discussed and defined. A subset of the requirements is repeated in Table 6.1. The values of the Table highlight one of the key difference between commercial network applications and data transmission at the HL-LHC; the fact that higher bandwidth is required in the downstream direction. As discussed in Chapters 4 and 5 in the downstream direction most information can be broadcast and hence resources - fiber and transceivers - can be shared. In the upstream direction, however, the high data rate requirement per user makes multiplexing much more challenging. As mentioned in Chapter 5, the selection of front-end components is a major driver of the network design process. The architecture of Chapter 5 made use of a particular optoelectronic component, the REAM. As explained the reason for that choice was the interest of the particle physics community on EAMs, due to their potential radiation hardness, as well as their low mass and power consumption [165].

Table 6.1: Selected Requirements for the Upgraded Optical Links - Reminder.

Quantity	**Value**
Upstream Data Rate	10 Gbps (per user)
Downstream Data Rate	<1 Gbps (broadcast)
Link Length	<1 km

This combination of factors led to the design of the architecture depicted in Figure 6.1. The designed architecture matches well the highly asymmetric, upstream-intensive nature of traffic, while it enables use of REAMs at the front-end in an efficient way. The downstream transmitter as well as the CW optical source, which provides the light to be modulated by the REAMs for upstream transmission, are shared. These two components are located in the “counting room”, which is an

environment set away from the high radiation environment of the detector and is shielded from radiation. An upstream/downstream pair use the same fiber with information being separated using different wavelengths as illustrated in Figure 6.1. The wavelength used for upstream transmission will be in the 1520-1560 nm window where REAMs, optical transmitters and receivers are commercially available. The downstream wavelength is chosen to be 1490 nm mainly to the possibility of extending the work presented in Chapter 4, where commercial TDM PON transceivers were used to transmit information in the downstream direction.

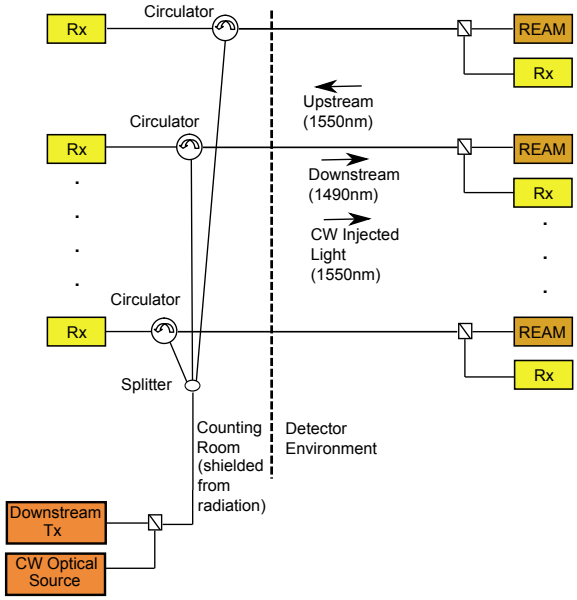

Figure 6.1: Suggested Network architecture.

To form the basis for the subsequent evaluation of the network performance carried out in this chapter, power budget calculations were carried out for both upstream and downstream directions. Typical commercially available component parameter values [187] were used for the calculations. For the upstream, parameter values and the link budget calculations are presented in Table 6.2. The final power margin, depends on the splitting ratio $1 : N$, the REAM insertion loss $\alpha_{REAM,ins}$

and other power penalties $\alpha_{pen,us}$ caused by the non-ideal behavior of optoelectronic devices thereby resulting in deviations from the ideal model assumed in power budget calculations [159]. The impact of the power penalty, particularly that of the penalty caused by the imperfect extinction ratio of the REAM, is a topic discussed later in this chapter in more detail.

Table 6.2: Link Budget Calculations - Upstream Direction.

Quantity	**Value**
Seeding Source Power	7dBm
Receiver Sensitivity	-19dBm
Overall Fiber Loss	0.4dB
Connector Loss	2dB
Splitting Loss	$1 + 10log(N)$
Filter Loss	1.5dB
Circulator Losses	1.5dB
REAM Insertion Loss	$\alpha_{REAM,ins}$
Power Penalties - Upstream	$\alpha_{pen,us}$
Power Margin	$19.6 - 10log(N) - \alpha_{REAM,ins} - \alpha_{pen,us}$

For the downstream, parameter values and the link budget calculations are presented in Table 6.3. Comparing the power margins in the upstream, $M_{S,us}$, and downstream directions, $M_{S,ds}$ reveals that the number of users that can be served is limited by upstream and not by downstream performance. This is due to two factors; the first is the insertion loss of the REAM, that for typical REAM devices [207] is between 3.5 and 5 dB. The second is the value of the downstream power penalty that for commercial 1 Gbps transceivers and for a link length of 1 km is <2 dB. Moreover, any bit rate dependent penalties would have a higher value in the upstream direction, where the data rate is higher. This is the reason why the discussion in this Chapter focuses on the upstream and not the downstream

direction.

Table 6.3: Link Budget Calculations - Downstream Direction.

Quantity	**Value**
Transmitter Power	0dBm
Receiver Sensitivity	-25dBm
Overall Fiber Loss	0.2dB
Connector Loss	2dB
Splitting Loss	$1 + 10log(N)$
Filter Loss	1dB
Circulator Loss	0.75dB
Power Penalties - Downstream	$\alpha_{pen,ds}$
Power Margin	$20.05 - 10log(N) - \alpha_{pen,ds}$

At this stage it is useful to use the power margin expression to calculate the maximum number of users the system can serve. Since the system is upstream-limited the condition under which the system has reached its limitations is given by:

$$19.6 - 10log(N_{max}) - \alpha_{REAM,ins} - \alpha_{pen,us} \geq 3 \tag{6.1}$$

where, as suggested in [159], a value of 3 dB was used for system margin. Solving Equation 6.1 for N_{max}, we derive:

$$N_{max} = 10^{\frac{16.6 - \alpha_{REAM,ins} - \alpha_{pen,us}}{10}} \tag{6.2}$$

Equation 6.2 gives the maximum number of users the system can serve.

6.2 Electroabsorption Modulators - Operating Principle and Performance Indicators

The use of REAMs is a key element of the architecture of Figure 6.1. In order to evaluate the impact of REAM operation on upstream performance, a description of its operating principles is required. EAMs are devices that modulate light based on the variation of the absorption of semiconductor material with the application of an external electric field [209]. The main physical mechanisms utilised to achieve this are the FKE and the QCSE [209], [201]. The EAM discussed in this chapter is a REAM from CIP [207] based on QCSE.

QCSE is observed in semiconductor Quantum Well (QW) structures. QW structures exhibit a staircase absorption profile, as electron and hole energies are quantized and form discrete energy levels [201]. The confined electrons and holes are bound to form excitons, resulting in discrete absorption peaks. The application of an external electric field affects the absorption profile of the material through various mechanisms. As shown in Figure 6.2 the application of an external electric field leads to a simultaneous red-shift, broadening and lowering of the exciton absorption peak.

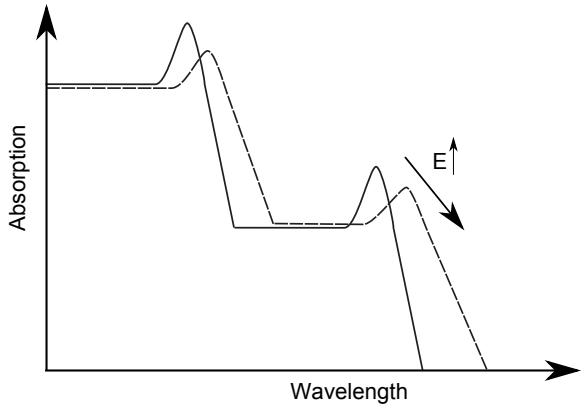

Figure 6.2: Quantum well absorption profile changes with the application of an external electric field.

Typically, EAMs are utilised to modulate monochromatic light. The wavelength of the light source is selected to be longer than the exciton absorption peak wavelength. Hence, the application of an electric field leads initially to an increase in the material absorption at this wavelength, as the exciton absorption peak is red-shifted. However, as the absorption peak keeps moving to longer wavelengths, broadens and its amplitude decreases, the absorption at the source wavelength is reduced [201].

One of the main metrics that can be used to illustrate better the absorption profile of an EAM and characterise it, is its static response. The static or electro-optic response $T(V)$ - also known as transmission characteristics, switching curve [209] or transfer function [201] - is defined as the ratio of the output light intensity $P_{out}(V)$ over the input light intensity P_{in} as a function of voltage for static conditions - i.e. at DC - [209]:

$$T(V) = \frac{P_{out}(V)}{P_{in}} \tag{6.3}$$

The generic shape of static response of a QSCE-based EAM is depicted in Figure 6.3. The static response is essentially the inverse of the induced attenuation. Figure 6.3 demonstrates graphically that the static response of QCSE-based EAMs typically decreases with increasing reverse bias voltage until reaching a minimum and then starts increasing. The shape of the static response and its minimum transmission point depend on the structure of the particular device, as well as external variables. These variables include temperature, wavelength, polarization and optical power [209].

The shape of the static response is very important as it determines the value of one of the primary parameters leading to performance degradation; the extinction ratio. The extinction ratio value at DC is given by $ER|_{dB} = T(V_L)|_{dB} - T(V_H)|_{dB}$.

Therefore the extinction ratio is determined by the shape of the static response and the choice of the operating voltages V_H and V_L as depicted in Fig. 6.3. The static response is therefore a very useful characterisation tool that will be used in this Chapter.

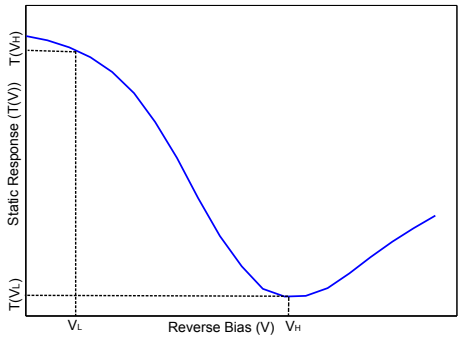

Figure 6.3: EAM static response and selection of operating voltage (based on measurements).

Other metrics commonly used to characterise EAMs are their small-signal frequency response and their chirping characteristics. The small-signal frequency response is the frequency response of the modulator, under the assumption that the input modulating voltage is so small that the transfer characteristic can be considered linear [209]. Chirp, on the other hand, as discussed in Chapter 5, is the spurious frequency modulation Δf of the intensity modulated output light with respect to the input light [209]. The small-signal frequency response will not be discussed in this Chapter for two reasons; firstly, the small-signal frequency response for the REAM device discussed in this Chapter is determined by the associated electronics and not the device itself - QCSE is a very fast process. The associated electronics are, anyway, going to be substituted by radiation-hard electronics that could have a very different frequency response. The second and probably more important reason, is that the small-signal frequency response proved to be a poor predictor of the large signal frequency response, something that could be expected. The large-signal

frequency response is essentially the response of a dynamic, non-linear system [209]. On the contrary, the definition of small-signal frequency response assumes a linear, memoryless system. This is the reason why the static response was used for an initial, quick performance evaluation, but dynamic measurements were carried out to verify that REAMs can, indeed, be used as front-end components and inform the decision on whether to go ahead with radiation tests or not.

6.3 Power Penalties and Static Performance Measurements

Equation 6.2 reveals that to calculate the number of users that can be served by the network architecture of Figure 6.1 the upstream power penalty needs to be calculated. This Section starts with a decomposition of the power penalty to the different factors causing it. It then focuses on REAM operation and characterisation. The static response is used to this end; external parameters that can be controlled and their impact on static response is discussed, with a view of optimizing them. Consequently, the impact of environmental parameters that can not be controlled is discussed in order to estimate their impact on network performance.

6.3.1 Power Penalty Components

The power penalties affecting single-wavelength and multi-wavelength networks were outlined and discussed in the framework of the analysis of the WDM PON architecture presented in Chapter 5. For the network architecture discussed in this Chapter only the single-wavelength penalties are of interest. The relevant penalties that could affect the operation of the network are the following:

- Dispersive Pulse Broadening

- Chirping
- Relative Intensity Noise
- Extinction Ratio

Other penalties that affect single-wavelength networks include modal noise and mode partition noise, but are irrelevant to the architecture discussed in this Chapter. Jitter also leads to performance degradation but depends mainly on the electronic parts of the system. As custom electronics are typically developed for the optical links of the LHC - and the same will be the case for the HL-LHC - jitter measurement is not possible at this stage.

Dispersive Pulse Broadening As discussed in Section 5.5.1, in single-mode fibers, dispersion is caused by the variation of group velocity with frequency. This causes pulse broadening, as different frequency components travel with different group velocities [159]. Dispersion is one of the primary performance-limiting factors of optical communication systems. However, for systems utilising optical sources with narrow linewidth, such as the architecture of Figure 6.1, the dispersion-associated power penalty remains negligible for values of μ <0.05, where μ is defined by the relationship [159]:

$$\mu = |\beta_2| \, BL \tag{6.4}$$

In the above relationship, $|\beta_2|$ is the second-order dispersion parameter, B is the data rate and L is the transmission length. For the network architecture under discussion B=10 Gbps and L=1 km, while for $|\beta_2|$ a value of 20 ps^2/km can be used - a typical value for standard single-mode fibers [159]. The value of μ can be calculated to be μ =0.002, therefore dispersion is not an issue for the architecture

discussed in this Chapter.

Chirping As discussed in Section 5.5.2 REAMs introduce chirping that can affect system performance. The part of the analysis of Section 5.5.2 describing the effect of chirping through its interplay with dispersion is valid for the network architecture discussed in this Chapter. In Section 5.5.2 the power penalty for a data rate of 10 Gbps and transmission distance of 1 km was calculated as a function of the effective Henry's coefficient, a parameter expressing the amount of chirping introduced by the REAM. The results are plotted in Figure 5.11 and show that the dispersion-induced power penalty due to chirping is negligible, even for extreme effective Henry's coefficient values [202].

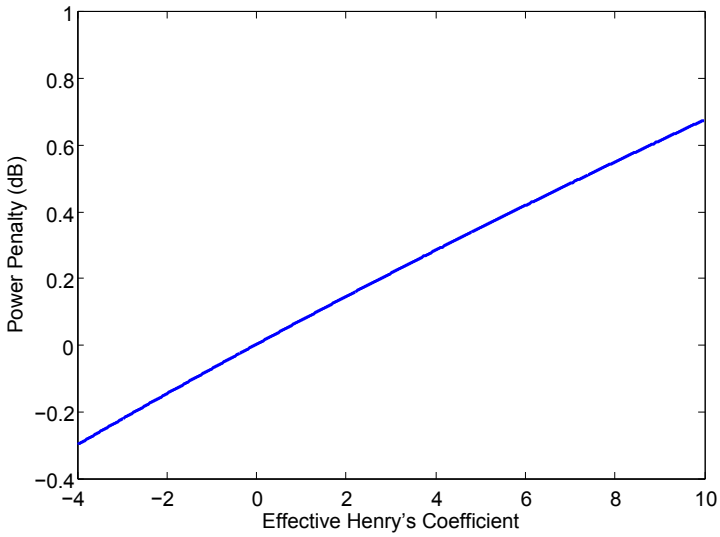

Figure 6.4: Dispersion-induced power penalty due to chirping vs. Effective Henry's Coefficient.

Relative Intensity Noise The analysis in Section 5.5.4 concluded that the required RIN value to achieve a BER value of 10^{-12} for 10 Gbps transmission is -115 dB/Hz. The suggested CW source for the architecture discussed in this Chapter is a DFB laser. Typically DFB lasers - especially high-power DFB lasers - provide

a much higher quality optical signal with RIN values around -145 dB/Hz [210], therefore the RIN requirement is expected to be easily met.

Extinction Ratio The extinction ratio is one of the primary metrics used to characterise EAMs. At the same time a low extinction ratio is one of the main performance limiting factors in networks utilising modulators. The relationship defining the power penalty related to a non-perfect extinction ratio δ_{ex} was discussed in Section 5.5.3 but due to its significance it will be repeated here [159]:

$$\delta_{ex} = 10log_{10}(\frac{1+r_{ex}}{1-r_{ex}}) \tag{6.5}$$

In the above Equation r_{ex} is the extinction ratio defined as $r_{ex} = \frac{P_0}{P_1}$. As a more common way to express the extinction ratio is $r_{ex,dB} = 10 * log_{10}(\frac{P_1}{P_0})$- please note that the reciprocal of the linear r_{ex} is used -, the power penalty can be plotted as a function of the extinction ratio in dB. The result is shown in Figure 6.5.

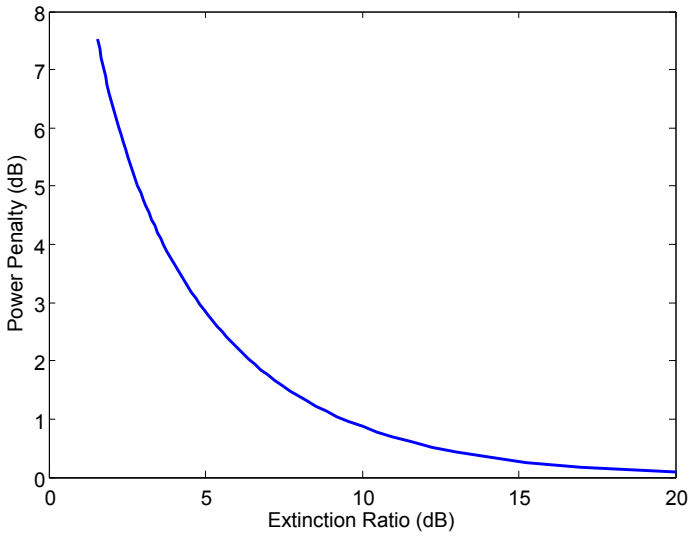

Figure 6.5: Power penalty vs. extinction ratio.

It can be seen that an extinction ratio of 9 dB or higher is required to achieve a

power penalty of less than 1 dB, while an extinction ratio of 5 dB leads to a power penalty only marginally lower than 3 dB - which is the margin we have used in out calculations. For extinction ratio values below 4 dB the power penalty increases rapidly, therefore the minimum extinction ratio requirement will be set to 4 dB.

6.3.2 Reflective Electroabsorption Modulator Performance and Operating Parameters

The previous discussion of the various power penalties essentially shows that the operation of the REAM can have a significant impact on network performance. More precisely, the extinction ratio, a quantity that is determined by the operation of the REAM, is the primary channel through which the operational characteristics of the REAM affect the power budget calculations. The achievable extinction ratio in static conditions, in turn, is determined by the REAM static response - and the choice of the operating voltage levels. It is therefore important to discuss the environmental parameters that affect static response, quantify their impact and examine possible measures that need to be taken to guarantee that the network requirements are met.

The primary factors that affect the static response of EAMs and will be further discussed are [209]:

- Optical Power
- Wavelength
- Polarization
- Temperature

It can be observed that out of these parameters, the first two - optical power and wavelength - are determined by the network designer, while the last two -

polarization and temperature - can vary. Polarization control would require the use of polarization controllers and polarization-maintaining fibers a complicated and expensive solution to be avoided in a particle physics environment, where simplicity is important. Moreover, in a particle physics environment - more particular for components installed on-detector - both the bulk and power consumption must be limited, therefore the usual approach of using a thermoelectric element to stabilize the REAM temperature can not be utilised. Therefore, the sensitivity of the static response of commercial REAMs with respect to the above parameters is measured, in order to optimize the first two parameters and to estimate the impact of the variation of the last two. The REAM device used for all the measurements discussed in the rest of the Chapter was a 10 Gbps InP-, QCSE-based, REAM of type R-EAM-1550-LS made available by CIP photonics [207].

The setup that was used to measure the REAM static response at different operating conditions is shown in figure 6.6. A tunable laser diode was used to inject light into the modulator. As the output optical power of the laser could be varied between 6 dBm and 9 dBm, while the interest was in the performance of the system at lower power levels, the output power of the laser was arbitrarily set to 7 dBm and a variable optical attenuator was connected to the output of the laser, to set the optical power of the light injected to the system. The light was then routed to the REAM via a circulator. After being absorbed and reflected by the REAM, the light was subsequently routed to an optical power meter.

Impact of Optical Power The increase of optical power injected into the REAM leads to a decrease in the REAM-induced attenuation due to saturation [209]. As the main mechanism causing saturation is related to the induced photocurrent [209], that is maximised at high absorption levels, to investigate the impact of optical power on REAM-induced attenuation, the latter was measured at the attenuation

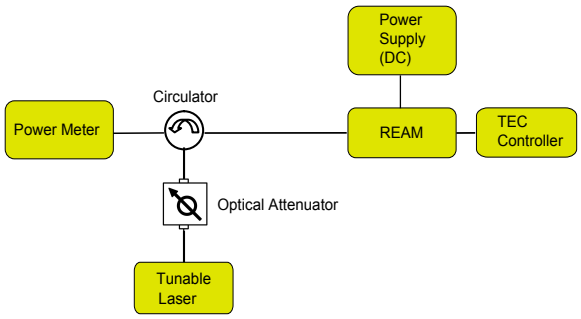

Figure 6.6: Measurement Setup.

maximum of the static response. The measurement was carried out by setting the wavelength of the tunable laser diode to 1545 nm, the temperature of the REAM to 25^{o}C and the bias voltage to 2 V, which was identified to be the bias voltage at which the attenuation maximum took place. Then the attenuator of Figure 6.6 was used to adjust the optical power injected into the modulator. The REAM-induced attenuation was deduced using the optical power measured and the attenuation of all components used in the measurement setup. The results of the measurement are shown in Figure 6.7. The results show that the induced attenuation varies by $<$1 dB for an optical power range of 10 dB. Moreover, at the low end of the range - that is closer to the optical power levels that would be injected into the REAM for realistic splitting ratios - the attenuation variation exhibits a decreasing trend. Therefore the impact of the injected optical power on REAM performance may be considered negligible.

Impact of Wavelength In order to measure the impact of the injected light wavelength on REAM static response, the output wavelength of the tunable laser was varied between 1510 nm and 1640 nm. The REAM bias voltage was varied between 0 V and 3.8 V and the static response was calculated at each wavelength from the power measured at the output of the circulator by taking into account the connector- and circulator-induced losses at the particular wavelength. The results of

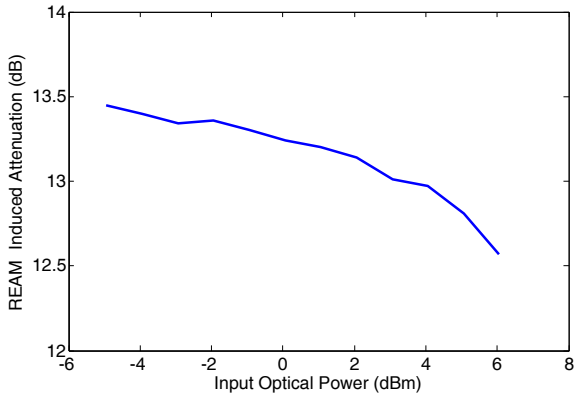

Figure 6.7: Input Optical Power Vs. Maximum REAM-Induced Attenuation.

the measurements are shown in figure 6.8 and clearly show that care is needed when choosing a bias voltage-wavelength combination to achieve optimum performance in terms of minimising the insertion loss of a device and maximising its extinction ratio. To determine the optimum operating wavelength range, the required voltage swing to achieve the maximum extinction ratio was calculated and is shown in Figure 6.9, right axis. The overall power penalty associated to the extinction ratio and the insertion loss was calculated, also as a function of wavelength - Figure 6.9, left axis. Both the required voltage swing and the overall penalty should be minimised, therefore, the selected the operating wavelength range should be in the 1550 nm region. It is also interesting to note that both the values of the overall penalty and the voltage swing remain within a reasonable range for wavelengths between 1540 nm and 1560 nm; the overall power penalty remains close to its minimum, while the operating voltage is below 3 V. Thus the REAM discussed has an operating wavelength range of $\sim$20 nm.

Impact of Polarization In order to assess the polarization dependence of the REAM static response, the setup of Figure 6.6 was modified as shown in Figure 6.10. A polarization controller was inserted before the REAM and was used to

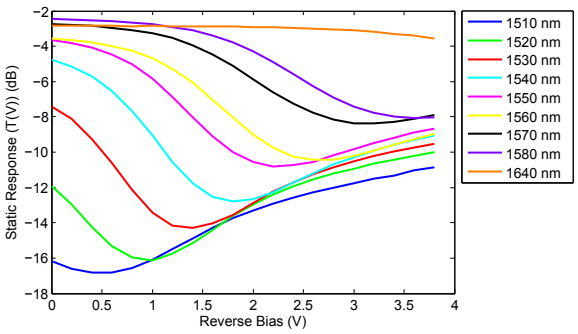

Figure 6.8: Static response as a function of wavelength.

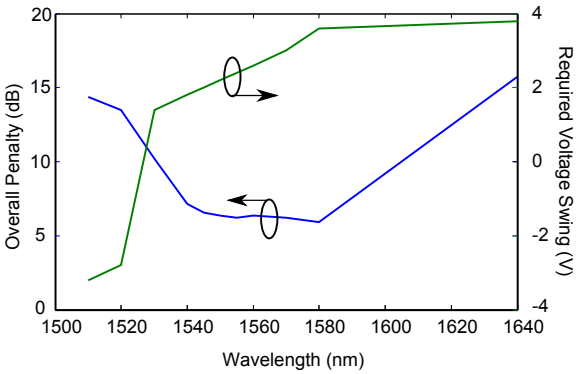

Figure 6.9: Overall induced penalty due to insertion loss and imperfect extinction ratio vs. wavelength (left axis) and required voltage swing vs. wavelength (right axis).

adjust the input light polarization.

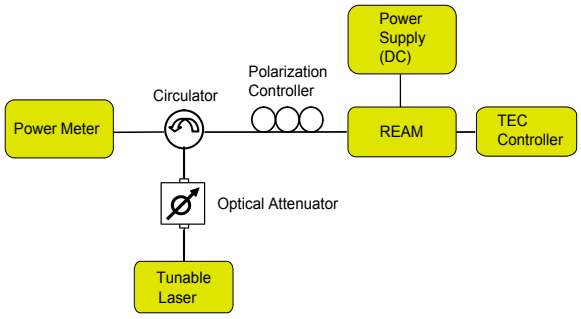

Figure 6.10: Measurement setup for static response polarization dependence measurement.

The worst- and best-case input light polarizations, resulting in the minimum

and maximum extinction ratios, respectively, were identified. The corresponding static response curves are shown in Figure 6.11. As the Figure shows the extinction ratio difference between the worst- and the best-case scenarios is <1 dB, therefore the impact of polarization can be considered negligible.

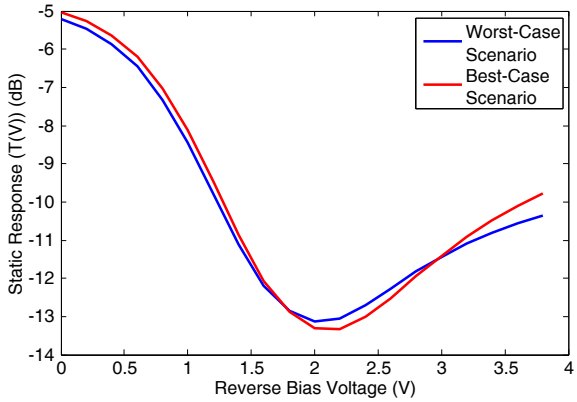

Figure 6.11: Static response polarization dependence.

Impact of Temperature The same measurement methodology that was used to investigate the impact of wavelength on static response was also utilised to investigate the impact of temperature variation. The static response at 1550 nm was measured at three different temperatures (10 °C, 30 °C and 50 °C) and the results are shown in figure 6.12. The temperature range of 40 °C was close to the maximum temperature range that could be achieved using the thermo-electric cooler of the device. Thus, the temperature range used was the closest achievable to the maximum temperature difference inside the detector discussed in Chapter 2. Figure 6.12 reveals a number of important trends with increasing temperature, namely increase of the insertion loss, decrease of the reverse bias voltage level at which the static response minimum occurs and a slight increase of the maximum extinction ratio.

To assess the impact of temperature and evaluate whether a compensating mechanism is required, it was assumed that the modulation voltage levels are determined

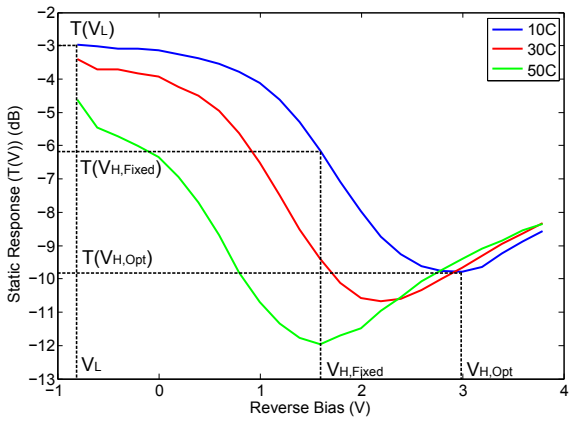

Figure 6.12: Temperature Dependence of Static Response.

by the static response at the highest operating temperature. The reason is that the static response minimum occurs at low voltage levels when the operating temperature is high. Operation at higher voltages would require the use of both the decreasing and the increasing parts of the static response, leading to significant non-linear effects. The modulation voltage levels were thus set to $V_L = -0.8$ V and $V_{H,Fixed}$ =1.6 V to maximise the extinction ratio at the highest temperature, as shown in figure 6.12. The obvious problem encountered in this case is the sub-optimum choice of voltage levels at lower temperatures - the optimum at 10 °C, $V_{H,Opt}$ =3 V is also shown in figure 6.12 - leading to a decrease of the extinction ratio. Figure 6.13 shows the calculated extinction ratio power penalty for different temperatures, both when the modulation voltage levels are fixed and when optimum voltage levels are used. Referring back to the architecture shown in figure 6.1, the additional power penalty results in a decrease in the number of users that can share a single downstream transmitter/CW source combination by a factor of ~ 1.8. Considering that the temperature range variation at the HL-LHC may be even larger, the conclusion is that a voltage adaptation mechanism is required to avoid significant performance degradation.

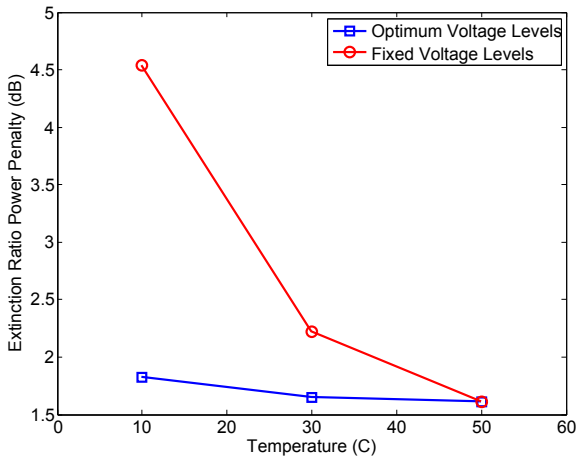

Figure 6.13: Extinction Ratio Power Penalty Vs. Temperature, for λ=1550 nm.

6.4 Dynamic Measurements

Although static measurements provide valuable information allowing us to select optimum values of operating parameters with reasonably good accuracy, dynamic measurements are required to validate the feasibility of the system. As explained in Section 6.1 the focus is on upstream performance, as the maximum number of users that can be served using the architecture of figure 6.1 is determined by the upstream performance constraints. Figure 6.14 shows the setup used for the measurements. The setup is similar to the one used for the static response measurements, but with a Pseudo-Random Binary Sequence (PRBS) source and a wideband amplifier being used to generate a $2^7 - 1$, 10 Gbps PRBS data stream and modulate the voltage applied to the REAM. The power of the laser was set to -6.6 dBm, its wavelength to 1545 nm, while the temperature of the REAM was set to 25^{o}C. A 10 Gbps PIN photodiode receiver with a pre-amplifier was used instead of a power meter to receive the modulated light. The output of the receiver was connected to a Digital Communications Analyzer (DCA) to view and further analyze the received waveform.

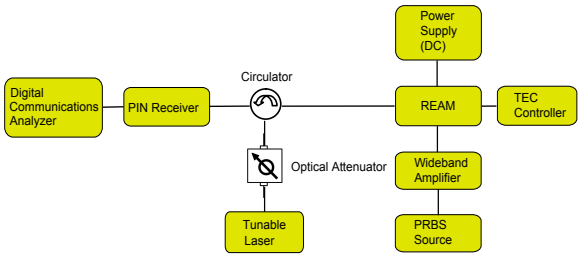

Figure 6.14: Dynamic measurement setup.

The average optical power at the input of the receiver was modified by changing the optical attenuation at the output of the tunable laser. The quality of the signal was measured using the value of Q, a commonly used indicator for the quality of a modulated signal. Q is defined as the ratio of the optical power difference between the mark (I_1) and space (I_0) levels to the summation of the standard deviation - rms values - of noise at the mark (σ_1)and space (σ_0) levels [159]:

$$Q = \frac{I_1 - I_0}{\sigma_1 + \sigma_0} \tag{6.6}$$

For noise-limited systems, such as the one discussed in this Section, Q determines the BER, equation 6.7 [159]:

$$BER = \frac{1}{2} erfc(\frac{Q}{\sqrt{2}}) \approx \frac{exp(-\frac{Q^2}{2})}{Q\sqrt{2\pi}} \tag{6.7}$$

where $erfc$ is the complementary error function.

The plot in figure 6.15 shows the value of Q - left axis - and the corresponding estimated BER - right axis - as a function of the average received optical power. The recorded eye diagrams for Q=7 ($BER = 10^{-12}$) and Q=9 ($BER = 10^{-19}$, that is error-free) are also shown in the inset of the figure. As the diagram shows, the required average power to achieve a BER of 10^{-12} is -16.4 dBm.

The maximum number of users that can be served by the architecture of Figure

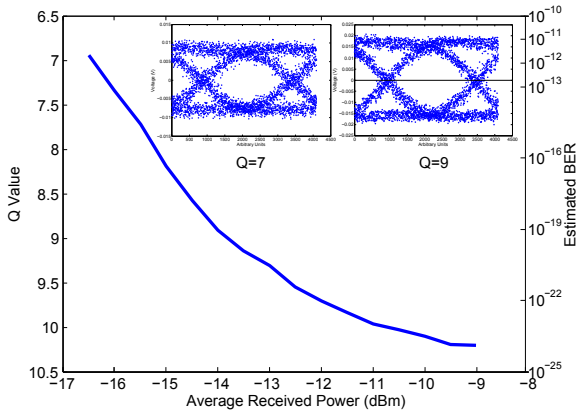

Figure 6.15: Q-Value and corresponding BER Vs. average received power - eye diagrams for Q=7 and Q=9 (inset).

6.1 can now be calculated. The link budget calculation for the experimental setup of Figure 6.14 is shown in Table 6.4. Obviously the power margin in this case is equal to 0, therefore, it is easy to conclude that $\alpha_{REAM,ins} + \alpha_{pen,us} = 3.3$. Substituting in Equation 6.2 we derive $N_{max} = 10^{1.33} \approx 21.3$. Thus, taking into account that the splitting ratio has to be a power of 2, the results suggest that a 10 dBm DFB laser can serve 16 users. Use of a 20 dBm DFB laser can also be considered to increase the number of users and explore the possibility of achieving higher cost savings. Additional cost reduction compared to a point-to-point architecture is achieved due to the downstream transmitter sharing. Increasing the power of the downstream transmitter could also lead to cost savings in a similar way to upstream. However, it is important that even without these improvements the architecture appears to meet the performance requirements and at the same time be cost-efficient in comparison to a point-to-point configuration using REAMs where one cheap low power laser is used as a CW optical source per REAM.

Table 6.4: Link Budget Calculations - Experimental Setup of Figure 6.14.

Quantity	**Value**
Seeding Source Power	-9.6dBm
Receiver Sensitivity	-16.4dBm
Connector Loss	2dB
Circulator Losses	1.5dB
REAM Insertion Loss	$\alpha_{REAM,ins}$
Power Penalties - Upstream	$\alpha_{pen,us}$
Power Margin	$3.3-\alpha_{REAM,ins}-\alpha_{pen,us}$

6.5 Conclusions

In this Chapter a new, simplified architecture was suggested as a unified architecture at the HL-LHC. The architecture is based on the PON paradigm and utilises REAMs as front-end devices for upstream transmission. It matches well the highly asymmetric, upstream-intensive nature of traffic generated by particle physics experiments. It enables resource sharing in the downstream direction, while at the same time provides the required point-to-point connectivity in the upstream direction. The limitations of the architecture were discussed, with a focus on the maximum number of users it can serve. To achieve this, link budget calculations were carried out. The power penalties affecting network performance were discussed in detail. The operational characteristics of REAMs, their dependencies and the impact they can have on system performance were also discussed. Finally, dynamic measurements were carried out to prove the concept. The measurements showed that although temperature variation may call for a compensation mechanism to limit its impact on the number of users that can be served, the architecture appears to be cost-effective, while at the same time it meets the bandwidth requirements for a unified architecture at the HL-LHC. In other words, the work presented in this chapter, sets a solid basis for the next step to be carried out; that of radiation hardness tests of REAMs at HL-LHC radiation levels.

Chapter 7

Radiation Tests of Reflective Electroabsorption Modulators - Component and System-Level Studies

In Chapter 6 the use of a passive optical architecture for the distribution of all types of information at the HL-LHC was suggested . In the same Chapter experimental demonstration of this architecture showed that it can meet the bandwidth requirements of the upgraded optical links. However, one of the key features of the suggested network design was the use of REAMs at the front-end. As this is an optoelectronic component untested at HL-LHC radiation levels, it is necessary to carry out a study of its radiation hardness. This is the topic of this Chapter.

The Chapter starts with a more detailed description of the main purposes of our test and a short overview of the literature on REAM irradiation testing. Consequently, a description of the test setup is given. More information is provided

on the performance parameters monitored during the test and environmental parameters, like radiation levels. The evolution of the device performance metrics during irradiation is then discussed. The possible mechanisms behind the observed radiation-induced performance degradation are also briefly discussed. After the component-level study, the discussion moves on to system-level aspects. Ultimately, the decision on the applicability of the suggested architecture in Chapter 6 is based on this analysis. The Chapter ends with a summary of the main contributions of the test and a conclusion on the feasibility of using REAMs at the HL-LHC.

7.1 REAMs; radiation resistance and their potential for use in particle physics applications

EAMs have attracted the interest of the particle physics community in the past. Their use for particle physics applications was first suggested and investigated in the 90s for the LHC [166, 211, 212]. The key attribute of interest was their potential radiation hardness, while their potential low mass and low power consumption was also considered an advantage [165]. However, difficulties related to the immaturity of the technology and to the complexity of the system implementation at the time led to the implementation of different types of optical links based on directly modulated lasers [11] [8].

The EAM technology has since matured and devices are now commercially available. The feasibility of the use of EAMs in particle physics applications from a network perspective was demonstrated in Chapter 6. Still, there is a lack of studies on the behavior of EAMs at HL-LHC radiation levels. Although the behavior of lasers and photodiodes in such conditions has been recently studied [168] there is no similar research on EAMs. Previous studies of the radiation hardness of EAMs related to particle physics applications were targeting lower radiation levels as their

focus was the use of EAMs at the LHC. In [166] a fluence - i.e. overall number of particles incident to the device per unit surface - of $\sim$1.3x10^{14} 1 MeV neutrons/cm^2 was used, while in [212] and [211] the tests quoted were using fluences of $\sim$5x10^{14} 1 MeV neutrons/cm^2 and $\sim$6x10^{13} 24 GeV protons/cm^2. These fluence levels are more than an order of magnitude lower than the HL-LHC tracker qualification fluence levels, discussed in Chapter 2. Apart from particle physics, radiation tests of EAMs were also carried out to assess the feasibility of their use in another area; this of space applications. However, these tests, too, targeted targeted lower fluence levels, as the space environment is less hostile. According to the authors in [213] a fluence of only $\sim$4x10^{14} 1 MeV protons/cm^2, that was used to test the radiation hardness of EAMs for space applications, is equivalent to $\sim$14000 years in orbit. The quoted fluence level is again very low compared to the HL-LHC qualification levels. The primary goal of our test is to address this research gap and investigate whether EAMs remain operational at HL-LHC fluence levels.

An additional, less obvious goal is to establish the radiation resistance limits of EAMs, as device failure was not observed in any of the previous studies. Radiation tests can be costly and require a considerable investment of manpower. It would therefore be ideal if our test identified, once and for all, the operation limits of the devices. To achieve this aim, the fluence levels used during the test should be as high as possible.

The use of fluence levels causing device failure has a beneficial side effect; it allows gaining significant insight into the radiation-induced performance degradation mechanism. Monitoring the evolution of appropriate device parameters during irradiation can also help to this end. Previous tests - [166], [212], [211] - were primarily focusing on the evolution of the static response with increasing fluence, as this is the main metric determining whether the device remains operational or not. However, the operation of EAMs is fundamentally based on the change of the absorption spec-

trum with voltage. The static response is, essentially a "snapshot" of this change at a specific wavelength. Therefore, online absorption spectrum measurements, could yield significant information as far as the degradation mechanism is concerned. To our knowledge only [213] reported on the impact of irradiation on absorption spectra. However, the authors identified only small changes of the absorption spectrum with radiation, owed to the relatively low fluence levels used. Moreover pre- and post-irradiation absorption spectrum changes were examined and reported only for the same and not across bias voltages. As one of the primary purposes of our test is to gain insight into the radiation-induced performance degradation mechanisms, online absorption spectrum measurements were carried out during the irradiation process.

Exploring the impact of absorption spectra changes with increasing fluence on significant aspects of modulator performance from a system-level perspective, like the extinction ratio and optimum wavelength of operation is of critical importance. Previous studies, such as [166], [213], did not investigate that link. In this Chapter the significant insight gained through the online absorption spectrum measurements is utilised to carry out a system-level analysis. The maximum operating fluence levels of the EAM-based network architecture described in Chapter 6 can then be established taking into account the optimum operating wavelength. This allows for a more accurate assessment with respect to the feasibility of using REAMs as front-end devices at the HL-LHC.

7.2 Experimental Setup and Methodology

The test was carried out using two unpackaged, bare-chip 10 Gb/s REAM devices, of type R-EAM-1550-LS purchased from CIP photonics [207]. The two devices were measured to have an insertion loss, defined by the manufacturer as the modulator-

induced attenuation for a reverse bias voltage of -0.6 V, of 6.6 dB and 5.4 dB, respectively. Their extinction ratio or modulation depth, that is defined by the manufacturer as the maximum difference in modulator-induced attenuation for reverse bias voltage between 0 and 3 V, was measured to be 9.5 dB and 10.9 dB, respectively. Both the insertion loss and the extinction ratio were measured at the nominal operating wavelength of the device, that was 1550 nm. The operating reverse bias voltage range of the devices was between -0.6 and 4 V.

The two devices were irradiated at the IRRAD3 irradiation zone of the CERN-PS (Proton Synchrotron) east hall irradiation facility [214]. The IRRAD3 irradiation zone uses the so-called PS-T7 proton beam-line; a beam-line that provides 24 GeV/c protons with a beam spot of 2 cm^2. The beam can provide a proton flux in the region of 2-9x10^9 p cm^{-2} s^{-1}. The flux homogeneity within the beam spot area is better than $\pm$10%. The flux depends on the beam profile and on the number of spills delivered that can be between 1 and 3 per PS supercycle of 14.4-19.2 s. Each spill of duration $\sim$400 ms can deliver up to 2x10^{11} protons [215]. The REAM samples were positioned on a remotely controlled "table" that could move the samples in and out of beam. The beam intensity is monitored during irradiation by a secondary emission chamber while the beam position and profile is measured by an instrument based on proton-induced Secondary Electron Emission (SEE) from thin aluminium foil [216]. The measurements provide a $\pm$10% accuracy compared to the real fluence value, as the position of the device relative to the beam spot can not be exactly determined. Our aim was to achieve the main objectives of the test, as described in Section 7.1, using a simple test setup that would utilise only commercial off-the-shelf components. This was the main driver behind the selection of the metrics to be measured during the test. More particularly, these were the modulator-induced attenuation, the photocurrent, the leakage current and the absorption spectrum of the REAMs, all measured for voltage levels covering

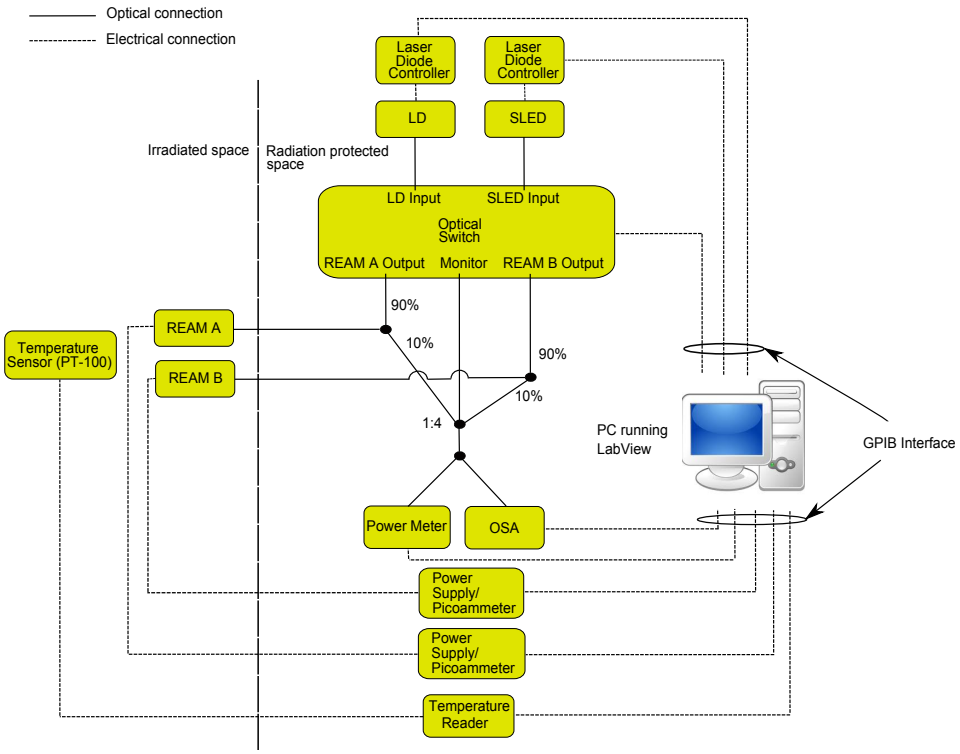

Figure 7.1: Measurement setup.

most of the operating voltage range - i.e. between -0.6 and 3.6 V. All the measured quantities were being measured continuously during irradiation.

The setup used to carry out the measurements is shown in Fig. 7.1. The unpackaged REAM devices and a PT-100 sensor to monitor the environmental temperature were placed into the irradiation environment. The rest of the setup was placed in the counting room that is protected from irradiation, located at a distance of ∼20 m from the irradiation space. Two 20 m single mode optical fibers were used to connect the REAMs to the rest of the setup. A Covega SLD-1108 1550 nm SLED and a Fitel FOL15DCWB 1553 nm DFB Laser Diode (LD) were used to illuminate the two REAMs. It should be noted that although the REAM specifications provided by the manufacturer are quoted at 1550 nm, the performance

of the devices at the LD operating wavelength (1553 nm) in terms of insertion loss and extinction ratio was within <1 dB of their 1550 nm values; the REAMs actually performed slightly better at 1553 nm. The SLED and LD were current- and temperature-stabilized. The SLED was used to carry out online measurement of the absorption spectrum of the REAMs over a wide wavelength range. The LD was mainly used to increase the reliability of the setup in case the SLED failed and to cross-check the results of the spectral measurements. It is also the device to be used in the architecture of our interest, where a single-wavelength LD would be used to illuminate the REAMs. A JSDU SB-Series fiber-optic switch was used to connect the LD and SLED to REAM A, "monitor" channel and REAM B devices shown in Fig. 7.1 in a sequential manner, i.e. only one light source was connected to only one out of the three used switch outputs at any point in time. Two outputs of the switch were connected to the REAM devices via 90/10 splitters. In both cases the output of the switch was connected to the 90% input and the REAM to the "common" of the splitter to maximise the optical power injected to the REAM and minimise the power directly coupled from the LD/SLED to the measurement instruments. Indeed, good isolation of >40 dB was measured between the 90% and the 10% inputs in all cases. The 10% outputs of the splitters routing back the light reflected by the REAMs and the "monitor" output of the switch were connected to three out of the four inputs of a 1:4 coupler. The fourth input remained unconnected. The "common" of the coupler was connected, again via a 90/10 splitter to General Purpose Interface Bus (GPIB) controlled optical power meter and Optical Spectrum Analyzer (OSA). The losses of all system components, as well as of the assembled system were measured before the irradiation test. These measurements, along with the measurments carried out when the LD/SLED were connected to the "monitor" channel were used to deduce the absorption characteristics of the REAM. Each of the REAMs was connected electrically to a picoammeter/voltage source to control

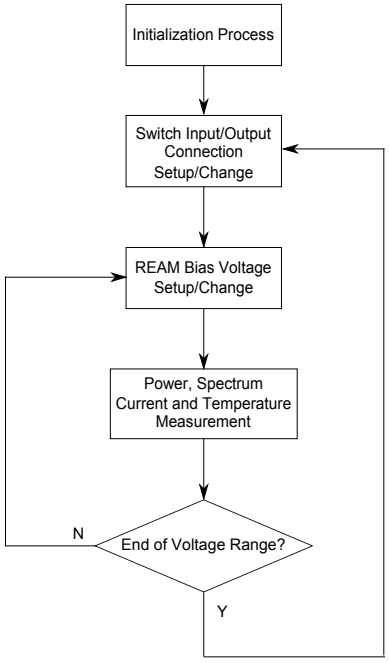

Figure 7.2: Measurement process.

the reverse bias voltage and measure the photocurrent or dark current (under no illumination) flowing through the device under test (DUT).

As Fig. 7.1 shows the laser diode controllers, the picoammeters/voltage sources, the temperature reader, the power meter, the OSA and the switch were all connected to a PC running LabView through its GPIB interface. The measurement process was fully automated. A process diagram of the measurement algorithm is shown in Fig. 7.2. After the initialization process, that included parameter setting for the laser diode controllers, the measurement process was conducted iteratively. The LabView program controlling the process consisted of two nested loops; the outer loop changed the switch input/output connectivity, while the inner loop modified the reverse bias voltage of the measured REAM. The reverse bias voltage was changed in steps of 0.2 V from -0.6 V to 3.6 V. The measurement process allowed measurement of all the metrics of interest - the REAM-induced attenuation, absorp-

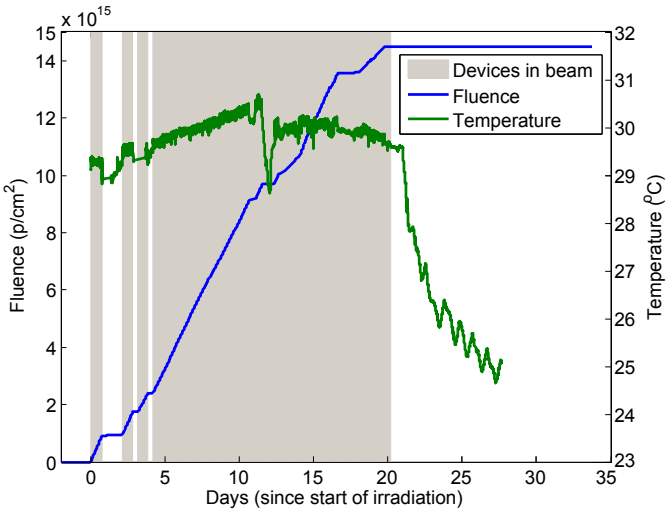

Figure 7.3: Fluence and temperature vs. time.

tion spectrum, photocurrent and dark current - all as a function of the applied bias voltage. Each outer-loop iteration was designed to last no more that 20 minutes, so that the change in the environmental variables for a single voltage sweep does not significantly affect the measurement. As Fig. 7.2 shows the measurement process was designed as an infinite loop. The program included an interruption process (not shown in the figure) that could be invoked by the user.

As one of the primary aims of the test was to investigate the radiation resistance limits of the REAMs, the measurement process was designed as an infinite loop. This feature along with the online modulator performance monitoring allowed the continuation of the test for as long as it was necessary to cause device failure. The two REAMs were irradiated for a period of 20 days; a period long enough to cause device failure. Measurements were continuously taken over 27 days except for short intervals of unintended interruption. The measurements continued after the end of irradiation to investigate any possible annealing effects. Fig. 7.3 shows the evolution of the environmental variables, i.e. the fluence levels the devices were exposed to and the temperature in the irradiation space over this time period. As

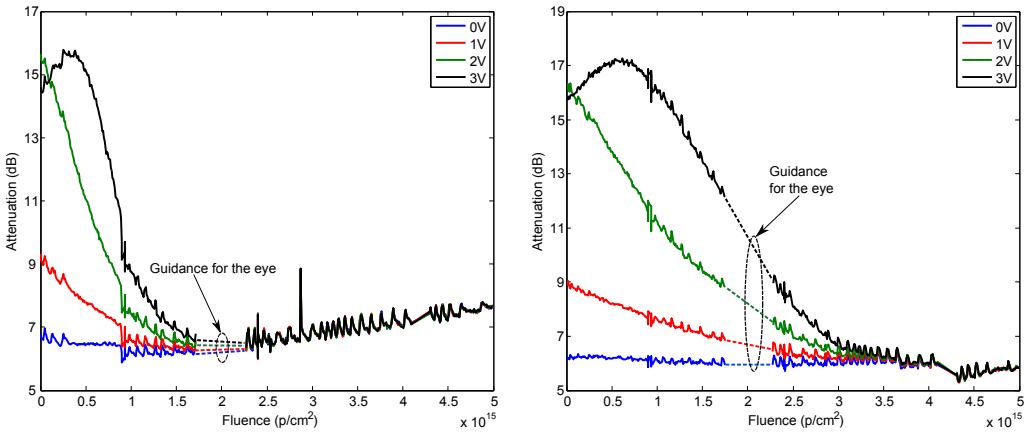

Figure 7.4: Modulator-induced attenuation vs. fluence - (a): REAM A, (b): REAM B.

the diagram shows the fluence increased gradually from 0 to the level of $\sim$14x10^{15} 24 GeV p/cm^2. The diagram also demonstrates the time periods over which the devices were in- and out-of-beam. The environmental temperature was measured to fluctuate between 29^o C and 31^o C during irradiation and it decreased to $\sim$25^o C after that period.

7.3 Component-Level Analysis

In Chapter 6 the principles of operation of EAMs were outlined. As a reminder we briefly repeat that EAMs are devices that modulate light through the variation of absorption of semiconductor material when an external electric field is applied. There are two possible underlying physical mechanisms that can be utilised to cause this effect; the Franz-Keldysh Effect (FKE) in the bulk active layer or the Quantum Confined Stark Effect (QCSE) in Multiple Quantum Wellss (MQWs) [201]. The modulators used in this work are based on QCSE.

It is obvious that for an EAM to be operational, the modulator-induced atten-

uation has to follow the variations of the externally applied voltage. Moreover, the higher the variation of the attenuation, the more efficient the modulation of light. Therefore an initial assessment of the impact of irradiation on REAM performance can be carried out by examining the evolution of attenuation at different reverse bias voltage levels as a function of fluence. Fig. 7.4.(a) and 7.4.(b) show the attenuation at 0, 1, 2 and 3 V measured using the LD, for REAM A and B, respectively. For both REAMs, the attenuation levels converge with increasing fluence, i.e. the modulation efficiency decreases. Beyond a fluence of $\sim$3x10^{15} 24 GeV p/cm^2 the induced attenuation is no longer influenced by the applied reverse bias voltage for either of the modulators, thus the modulators have stopped being operational. This finding explains why previous studies did not observe any significant performance degradation with irradiation, as the fluence levels used in previous studies were below 0.5x10^{15} p/cm^2. No annealing was observed after the end of irradiation.

Although Fig. 7.4.(a) and 7.4.(b) provide useful information related to the radiation resistance of the REAMs, this information is not sufficient to explain the mechanism behind the radiation-induced performance degradation. Based on this information we cannot conclude whether the degradation is caused by a change in the wavelength of the excitonic absorption peak, a lowering of the absorption maximum or a different cause. The snapshots of the evolution of the REAM absorption spectrum for different values of reverse bias voltage as fluence levels increase, measured using the SLED and shown in Fig. 7.5 to 7.8, provide more insight into the degradation mechanism.

The principle of operation of QCSE-based modulators, discussed in Chapter 6, is again demonstrated graphically using the measured spectra of REAM A and B in Fig. 7.5.(a) and 7.5.(b), respectively. As shown in the figures, the change in the induced attenuation at a fixed wavelength for varying voltage levels, is caused by a move of the exciton absorption peak to longer wavelengths, its broadening and a

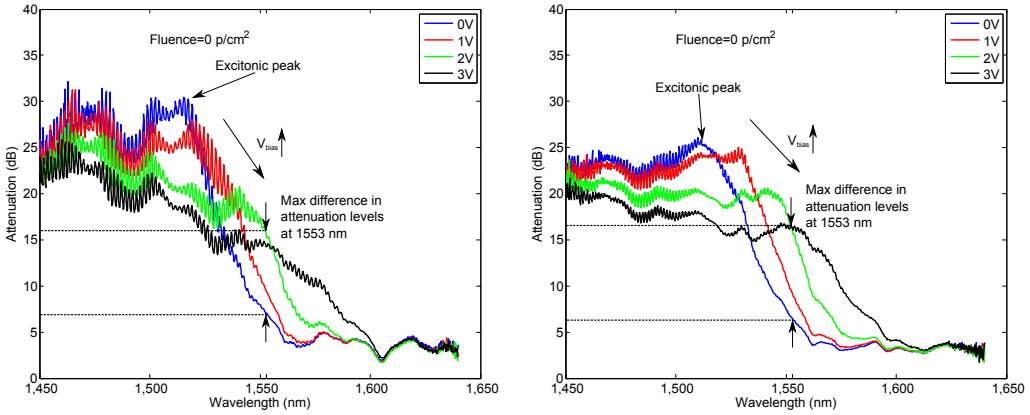

Figure 7.5: REAM Spectrum - before start of irradiation - (a): REAM A, (b): REAM B.

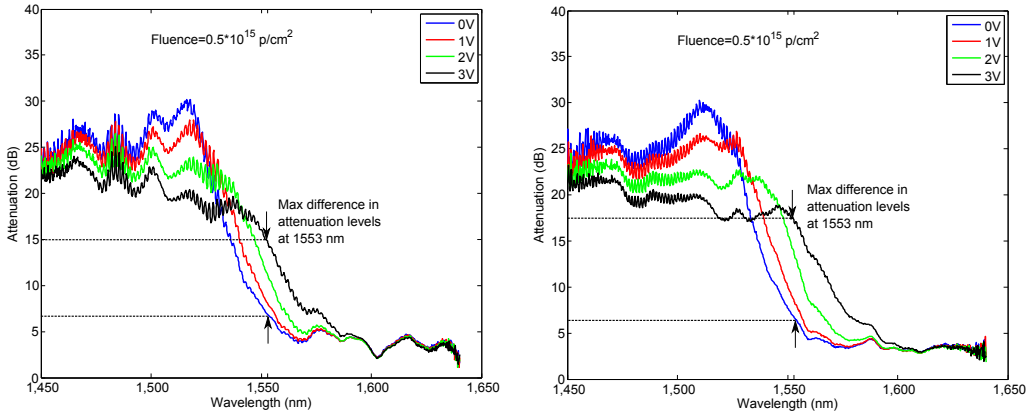

Figure 7.6: REAM Spectrum - Fluence=$0.5 * 10^{15}$ p/cm^2 - (a): REAM A, (b): REAM B.

reduction of its strength with increasing reverse bias voltage [201]. Following this description of QCSE, Fig. 7.5 to 7.8 show clearly why the induced attenuation levels at a specific wavelength for different reverse bias voltages - presented in Fig. 7.4.(a) and 7.4.(b) - converge. For both REAMs it is observed that although the shape of the spectrum remains largely unaffected by irradiation at 0 V it is obvious that it stops responding to changes in the applied reverse bias voltage with increasing

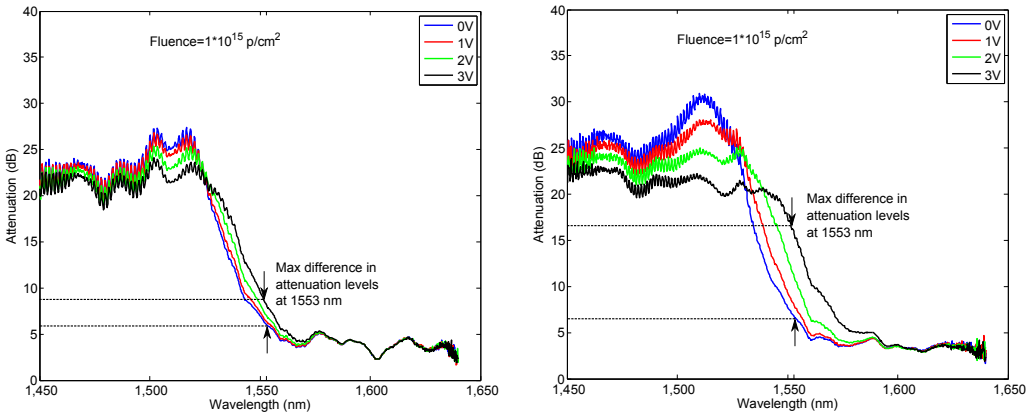

(a) (b)

Figure 7.7: REAM Spectrum - Fluence=$1*10^{15}$ p/cm^2 - (a): REAM A, (b): REAM B.

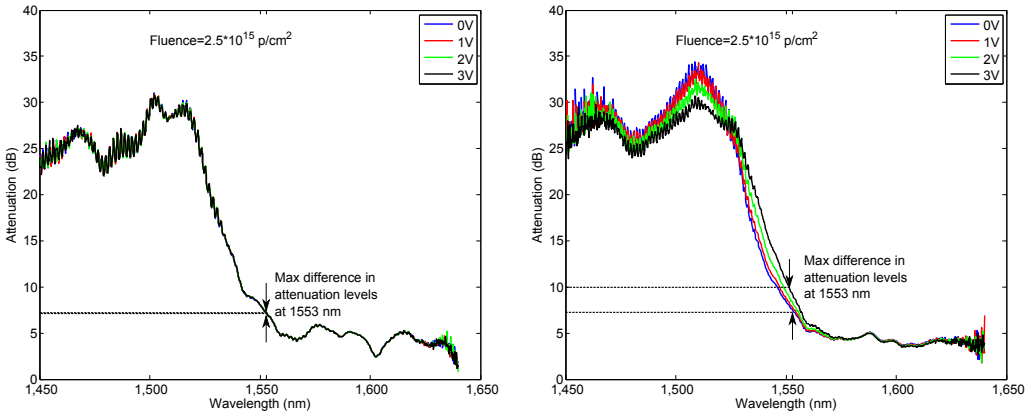

(a) (b)

Figure 7.8: REAM Spectrum - Fluence=$2.5 * 10^{15}$ p/cm^2 - (a): REAM A, (b): REAM B.

fluence. Thus the excitonic peak broadening and move to longer wavelengths is no longer observed with increasing voltage. To our best knowledge this effect is reported here for the first time in EAMs. A possible explanation for the observed behavior is the modification of the p-i-n structure in which the quantum wells are embedded due to donor and acceptor compensation as a result of the irradation [217]. As the doping concentration within the device changes due to displacement

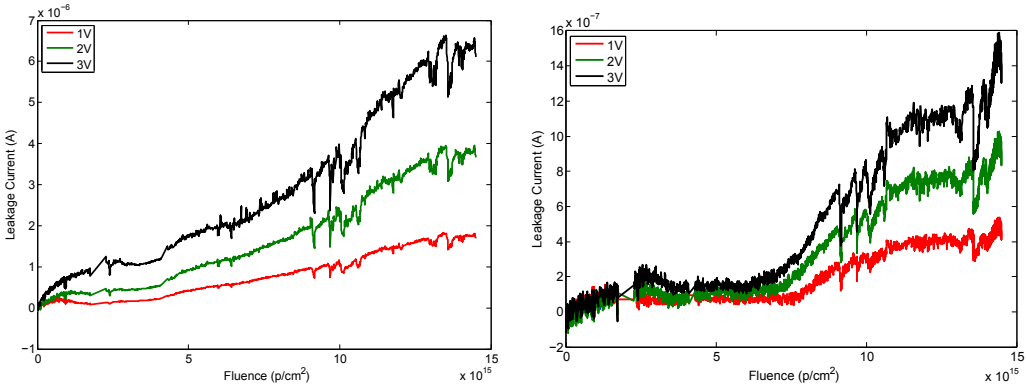

(a) (b)

Figure 7.9: Leakage current vs. fluence - (a): REAM A, (b): REAM B.

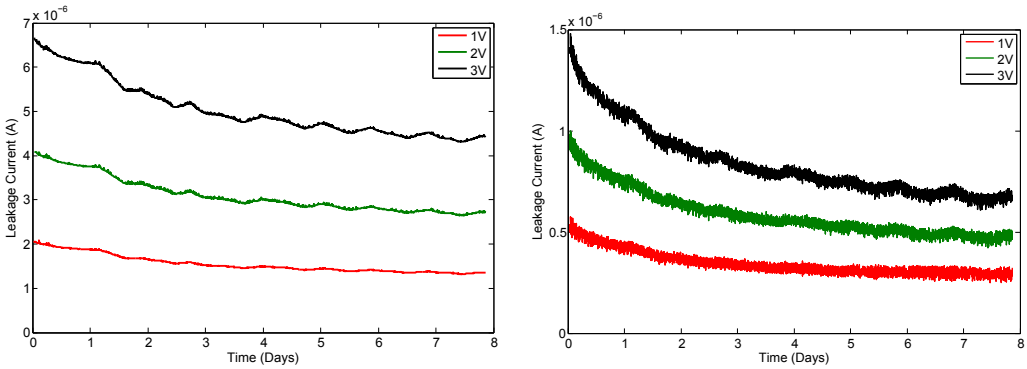

(a) (b)

Figure 7.10: Leakage current annealing vs. time - (a): REAM A, (b): REAM B.

damage, the electric field distribution with the application of an external voltage also changes. Consequently the electric field applied to the quantum well region may be significantly weaker.

Leakage current is an important parameter as its value is directly related to power consumption that should be kept minimum for devices installed on-detector. The evolution of leakage current as a function of fluence for different reverse bias voltage levels is shown in Fig. 7.9.(a) and 7.9.(b) for REAM A and B, respectively. Irradiation led to a significant increase in leakage current for both devices, from

values ranging in the order of tens of nA to several μA for both REAMs by the end of irradiation for a voltage level of 3 V. More precisely leakage current at the end of irradiation reached 6 μA for REAM A and 1.6 μA for REAM at 3 V. These values of leakage current would lead to a power consumption increase of $\sim$10% at 3 V assuming normal REAM operation - i.e. ignoring the REAM responsivity decrease because of irradiation and using the link budget calculations of Chapter 6 to evaluate the required incident optical power to the REAMs. On the other hand, contrary to the modulator-induced attenuation case, annealing was observed for leakage current as shown in Fig. 7.10.(a) and 7.10.(b). After a radiation-induced increase of almost three orders of magnitude, leakage current at 3 V decreased by 30% for REAM A and 50% for REAM B after 5 days (120 hours) of annealing at room temperature.

7.4 System-Level Analysis

Following the discussion on the impact of radiation on REAMs from a component-level perspective that was carried out in Section 7.3, we can now move on to analyze the effects of radiation at the system level. Our goal is to link the previously discussed parameters, related to modulator performance, to metrics that can be used to assess network performance. The ultimate aim of the analysis is to conclude whether the architecture described in Chapter 6 and reproduced in Fig. 7.11 can be utilised as a single, unified architecture at the HL-LHC. The tools used to achieve this goal are similar to the ones used in Chapters 5 and 6; the use of power budget and the calculation of the relevant power penalties caused by various impairments [159]. In this case we consider the impairments caused by the radiation-induced modulator performance degradation.

In Chapter 6 it was shown that EAMs influence the power budget primarily via

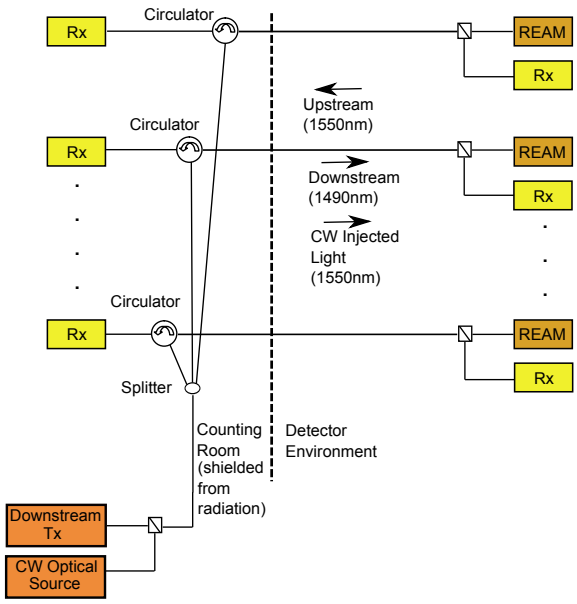

Figure 7.11: Network architecture.

two parameters; their insertion loss and their extinction ratio. The insertion loss was defined as the residual loss of the modulator when a "1" is transmitted, while the extinction ratio as the ratio of the optical power at the binary "1" (P_1) to the power at the binary "0" (P_0) level [209], $ER = \frac{P_1}{P_0}$. In Chapters 5 and 6 it was also explained that the impact of a non-perfect extinction ratio can be taken into account during link budget calculations using the extinction ratio power penalty, defined as the additional power required - in terms of average transmitted power - to achieve the same performance as in the case where a perfect extinction ratio is used [159]. The extinction ratio power penalty δ_{ex} can be calculated using the following equation [159]:

$$\delta_{ex} = \frac{1 + r_{ex}}{1 - r_{ex}} \tag{7.1}$$

where $r_{ex} = \frac{1}{ER}$. The impact of the insertion loss and the extinction ratio can be embedded into one performance indicator that we are going to term "overall

power penalty" $\alpha_{ream,overall}$ and define as:

$$\alpha_{ream,overall} = \alpha_{ream,ins} + \alpha_{ream,ER} \tag{7.2}$$

where $\alpha_{ream,ins}$ is the REAM insertion loss and $\alpha_{ream,ER}$ the REAM extinction ratio power penalty.

The overall power penalty, as well as the extinction ratio power penalty, at 1553 nm as functions of fluence are shown in Fig. 7.12.(a) and 7.12.(b) for REAM A and B, respectively. The figures also show the LHC fluence levels for ten years of operation, as well as the HL-LHC qualification fluence levels for the inner (Tracker) and outer (Calorimeter) detector layers. The HL-LHC qualification fluence levels set here are based on the limits defined for the Versatile Link project [21]. As the Versatile Link limits are typically expressed in 20 MeV neutrons, appropriate conversion factors were used to calculate the 24 GeV proton equivalent fluence. More precisely, [218] reports that 20 MeV neutrons are 1.9 times less damaging than 300 MeV/c pions, that in turn are 8.3 times more damaging than 0.8 MeV neutrons for devices fabribated in similar material systems. In [219] is also reported that 0.8 MeV neutrons are 8.4 times less damaging than 24 GeV protons, for the same material systems. Combining these results, we derive a 1.9 conversion factor between 20 MeV neutrons and 24 GeV protons - with the protons being more damaging. The same methodology has been used to calculate the LHC fluence levels [8] shown in the figures.

The results presented in Fig. 7.12.(a) and 7.12.(b) clearly show that although the increase of the overall power penalty is negligible at LHC and HL-LHC Calorimeter fluence levels, it is very high for HL-LHC Tracker fluence levels. For both devices, the overall power penalty has increased by more than 10 dB. In Chapter 6 we showed that a 10 dBm CW light source can be used to serve 16 or 32 users, depending on

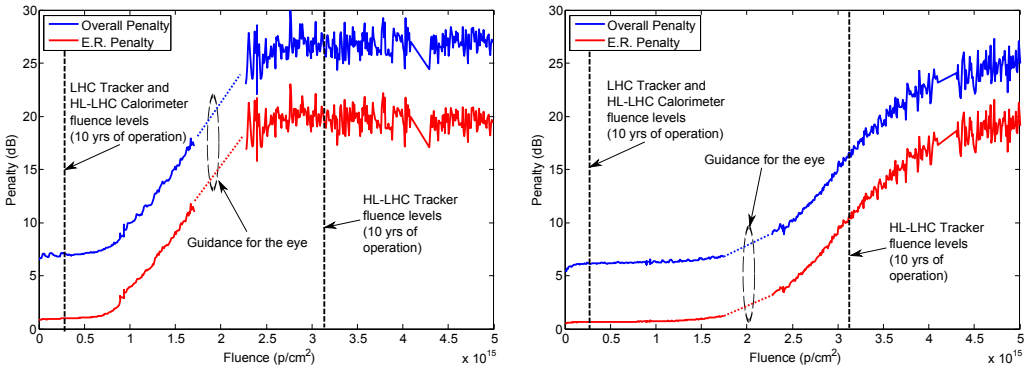

Figure 7.12: Overall and extinction ratio (ER) power penalty vs. fluence at 1553 nm - (a): REAM A, (b): REAM B.

the sensitivity of the upstream receiver. A 10 dB increase of the power penalty would lead to a reduction in the number of users sharing the same CW light source by a factor of at least 8 resulting in 2 or 4 users being served. Moreover as Fig. 7.12.(a) and 7.12.(b) show most of the overall power penalty increase is caused by an increase in the extinction ratio power penalty. This implies that the extinction ratio has reached low values, thus the modulators may no longer be operational and an increase in the power of the CW light source would not alleviate the problem.

To investigate the feasibility of an alternative solution, we used the absorption spectrum measurements, carried out with the SLED to calculate the extinction ratio evolution with increasing fluence under two different scenarios; in the first scenario the CW light source wavelength is assumed to be set to the optimum wavelength of operation, that minimises the overall power penalty before irradiation and then it is held fixed. In the second scenario, the CW light source wavelength is assumed to track the optimum wavelength of operation minimising the overall power penalty. The results of the calculation are shown in Fig. 7.13.(a) and 7.13.(b) for REAM A and B respectively. The fluence qualification levels for the LHC Tracker and for the HL-LHC Tracker and Calorimeter are also displayed. We set the

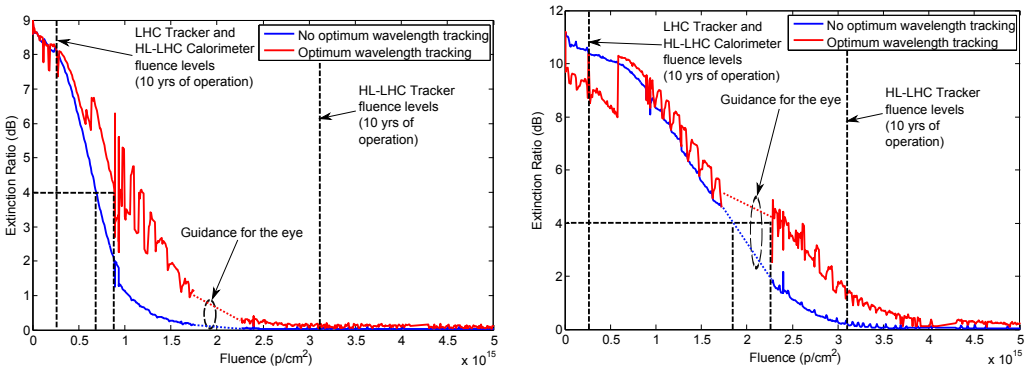

Figure 7.13: Extinction ratio vs. fluence with and without use of optimum wavelength tracking mechanism - (a): REAM A, (b): REAM B.

minimum extinction ratio threshold at 4 dB as below this value the extinction ratio power penalty rises rapidly, even with small variations of the extinction ratio value [159]. As the results show the extinction ratio falls below the 4 dB extinction ratio threshold for fluences below 2x10^{15} p/cm^2 for both REAMs, in the first scenario. The use of an optimum wavelength tracking mechanism can deliver a performance improvement of ∼30% in terms of the maximum operating fluence. However, in all cases the minimum extinction ratio threshold is well below the 3.1x10^{15} p/cm^2 fluence level expected in the inner detector layers of the HL-LHC. Thus a REAM-based architecture can only be used at the outer detector layers and does not appear to be an appropriate solution for the inner detector layers of the HL-LHC.

7.5 Conclusions

In this chapter a study of the impact of irradiation on QCSE-based EAMs is reported, at fluence levels never studied before. As previous studies focused on lower fluence levels, the radiation hardness limits of REAMs were not well established. Our study shows that the modulation efficiency of the devices close to their des-

ignated wavelength degrades significantly for fluence levels above 0.5x10^{15} 24 GeV p/cm^2 and are no longer operational at ∼2.5x10^{15} 24 GeV p/cm^2. Irradiation causes convergence of modulator-induced attenuation levels for different voltage levels and an increase in leakage current. One fundamental difference in the behavior of these two parameters is the fact that annealing has been observed for the leakage current, but not for the attenuation levels. Online spectrum measurements were carried out that provide insight into the degradation mechanism. The absorption spectrum retains its shape even for fluences above ∼2.5x10^{15} 24 GeV p/cm^2, indicating that the quantum well structure remained intact, but it becomes gradually less responsive to variations of the externally applied voltage with increasing fluence. A possible explanation for this effect is the modification of doping concentrations due to irradiation that changes the electric field distribution within the device.

The impact of the component-level performance degradation on network performance was also investigated. We showed that although the overall power penalty caused by REAM operation remains stable at LHC Tracker and HL-LHC Calorimeter fluence levels, it increases significantly at HL-LHC Tracker fluence levels. The increase in the power penalty is mainly attributed to the increase in the extinction ratio power penalty and much less on the insertion loss, that shows comparatively small variation during irradiation. We investigated the benefits of using an optimum wavelength tracking mechanism on extinction ratio. We showed that this mechanism delivers moderate increases in the maximum radiation levels at which our network can operate. The maximum operating fluence level achieved is still lower than the HL-LHC Tracker qualification fluence level. Thus, a network architecture based on REAMs, such as the one described in Chapter 6, does not meet the radiation hardness requirements of the HL-LHC Tracker. However, REAMs can operate in the less hostile HL-LHC Calorimeter environment, where they can possibly provide benefits in terms of speed and power consumption, compared to

directly modulated lasers. A possible avenue to increase REAM radiation hardness is appropriate device design and the benefits of this approach remain a future direction of research.

Chapter 8

Conclusions

As stated in the Introduction of this thesis (Chapter 1), the fundamental goal throughout our research was to generate new knowledge with respect to ways advances in optical network and optoelectronic technologies can be used to benefit the particle physics community. This goal was pursued within a certain framework that provided the platform for our research; the LHC upgrade. It was also made clear that to achieve this broad objective the focus of our efforts would be on a particular technology - PONs. We would explore how to best utilize this technology to upgrade the "last tier" of links, i.e. those residing between the last information-processing stage and the accelerator. At the same time the radiation hardness of any optoelectronic components suggested for use close to the particle collision point would be investigated. Research on the radiation hardness of optoelectronic components whose radiation resistance limits had not been clearly established in the past would be of particular interest to the particle physics community, therefore it would serve well the fundamental goal of our research.

Having described the work in detail, it is now time to revisit the research goals and reflect on how well these have been met. It is time to summarize the work

and evaluate it and identify the main contributions and discuss ways to improve it. These suggestions for improvement pave the way for future research with the potential of multiplying the impact of the work carried out in this thesis and its benefits to the particle physics community.

8.1 Work Summary

It is quite common for engineering and scientific projects to start with a requirements definition phase; this is exactly how this work started. During this stage the relationship between accelerator and network operating parameters was explored. This knowledge was then used to project the impact of the LHC upgrade to the requirements of the links of our interest. The requirements for a single, unified architecture, able to accommodate all types of traffic transmitted over the "last tier" of links were then defined. Consequently, a systematic survey of the literature on PONs was conducted. This review of the literature essentially defined the PON "architectural space" and identified the "standard" network design options at our disposal. This solid background work was necessary to move on to the next step; that of network design.

The first network design that was generated was that of a TDM PON targeting timing, trigger and control applications. A point-to-multipoint architecture was matching well the data rate requirements, as most of the information in the downstream direction is broadcast, while the required upstream data rate is not very high for such applications. One of the main challenges, however, was to verify that the strict timing requirements could be met. This was achieved using an FPGA-based demonstrator of the network. A TDM-based architecture could meet the upstream bandwidth requirements for TTC applications, but not those for data readout. A different solution would have to be applied in that case. A closer examination of the

"standard" network design options led to a network design based on WDM. The network design of our choice was based on a reflective architecture, using modulators at the detector side. For the downstream direction spectrum slicing or the use the broadcast AWG were identified as possible choices. The limitations of the network design were theoretically investigated. The outcome of this research was that a PON based on the standard design choices would be a costly and complex solution, while meeting the performance requirements of a unified architecture would be challenging. For that reason a simpler architecture was designed. Main features of the architecture were the fact that it matched well the highly asymmetric, upstream intensive nature of traffic in particle physics applications and the use of REAMs at the detector side. A number of experiments were carried out testing the most critical parts of the architecture to demonstrate that the architecture is a suitable candidate that can meet the performance requirements. The final step, that is of equal, if not greater, interest to the particle physics community as the architecture itself, was that of testing the radiation resistance limits of the REAMs. Two devices were irradiated using unprecedented levels of radiation. The radiation resistance limits of the devices were established. The measurements during irradiation provided new insight into the radiation damage mechanism and the network-level analysis assessed the impact of radiation on network performance.

A comparison between the work description and the research goals highlights the main contributions of the research presented in this thesis.

The first main contribution is the design of a fixed-latency TDM PON for timing, trigger and control applications. This network architecture increases the infrastructure efficiency through its point-to-multipoint architecture and its bidirectionality. At the same time it offers ample bandwidth; more than the required by the targeted applications.

The systematic research within the PON "architectural space" to identify an

appropriate architecture that can meet the requirements of a unified network architecture at the HL-LHC is another major contribution of this Thesis. Although the resulting architecture appears - at least currently - too complex and too costly to be deployed, its limitations are much better understood. The literature review along with the WDM PON design process can form a guideline for further research in the future, in case there are new technologies removing the current limitations. Furthermore the long-standing question about the applicability of WDM PONs in high energy physics applications has been answered. People can now argue for or against the use of WDM PONs with knowledge of their limitations and the design alternatives.

The design of the simplified architecture based on the use of REAMs essentially provided an efficient way to use REAMs at the front-end. Optical modulators are devices that always attracted the attention of the particle physics community, due to their potential radiation hardness. The experiments showed that the architecture can meet the network performance requirements and paved the way for the radiation tests.

The results of the irradiation tests resolve another long-standing query; whether EAMs are immune to very high levels of radiation or not. It is another example of how the research presented in this thesis established the limitations of a certain technology. Discussions on optimal choices regarding network and optoelectronic technologies suitable for the "last-tier" of links of the HL-LHC will from now on be based much more on data than they used to be and design decisions will be taken with much more confidence that the optimum solution has been found. New technologies can be tracked and compared against the current solutions easier, as the work presented in this thesis outlines the technical challenges that need to be resolved in a systematic way and can be used as a template for any future effort for technology evaluation.

8.2 Future Work

Researchers around the world consider the extension of their work by other people a gratifying and rewarding experience. It is the best evidence that their research is alive and evolving, not left behind or unusable. It would not have been possible for science to advance if researchers did not build on previous findings. The impact of the work presented on this thesis could be amplified greatly if other people took this research forward and built on it. At this stage we can discuss possible ways to do exactly this; improve and extend our work.

One of the possible future research topics is to investigate further the REAM performance degradation mechanism due to irradiation with the purpose of altering the device design to increase its resistance to radiation. Our irradiation tests have shown that the QCSE mechanism remained unaffected by irradiation even at high fluence levels. Therefore it may be possible to design a device that remains operational at HL-LHC tracker radiation levels. In such a case the simple architecture presented in Chapter 6 could be used to increase infrastructure efficiency at the HL-LHC. Further research can be carried out to investigate whether the REAM can be used as a transmitter and receiver at the same time, thus further simplifying the front-end. The use of REAMs as transceivers has already been suggested in the past but only for RF signals [220]. Investigating whether the same concept can be applied to baseband signals using appropriate line coding and filtering techniques is a possible research area.

In case the radiation hardness of REAMs cannot be improved by appropriate device design, then the focus of the research must shift to other optoelectronic components. One promising component regarding its radiation hardness is the Mach-Zehnder modulator. Its radiation resistance at HL-LHC levels has not been yet investigated thoroughly. Further research will also be required to ensure that

the low mass, low power and polarization-insensitivity requirements of the HL-LHC can be met. The use of Mach-Zehnder modulators in a reflective configuration can be a challenge and could be part of the research. An architecture similar to that suggested in Chapter 6 could be utilized to use Mach-Zehnder modulators at the front-end.

In Chapter 5 it has been stated that injection-locking can have a significant beneficial impact on the properties of the slave laser. Thus it may be a means to "remotely upgrade" currently used lasers or upgrade the current infrastructure using lasers that are injection-locked to improve their performance characteristics.The impact of injection-locking on the performance of lasers whose performance degraded due to irradiation can also be investigated. The architecture suggested in Chapter 6 can be used in this case too, to increase infrastructure efficiency.

Another possible future research avenue is to further investigate methods to resolve the issues that limit the applicability of WDM PON architectures to particle physics applications. The most promising candidate architectures, i.e. the use of remotely seed modulators or injection-locked lasers at the front-end, require the use of a remote CW light source. This source should be shared between many users. However, as discussed in Chapter 5, the high upstream data rate requirement calls for the use of a high quality signal in terms of SNR. To that end, following up advances in QD-LDs may be a good practice. Such sources could provide the required high-power, multiple wavelength signal whose SNR does not degrade after the spectrum-slicing process. In fact, any source providing high-quality signal at a low cost can be the solution to this problem.

Finally other ways to improve the WDM PON architecture and increase the benefits it offers in terms of infrastructure efficiency can become topics of further research. One such way would be to place the AWG inside the detector; currently this network design would be considered controversial. There would be both sup-

porters and opponents of such a move. The main argument of the opponents is that the AWG would introduce a single point of failure within a hostile environment. Any failure at this point would lead to a relatively large segment of the detector being "lost". Ways to decrease this probability to acceptable levels would increase the perceived value of the WDM PON as a suitable candidate in the particle physics community. Appropriate redundancy or protection schemes that are technology agnostic could also open the way for the exploration of other technologies such as OCDMA PONs - in case the related technologies become more mature and less expensive.

The discussion of possible ways to extend and improve the research presented in this thesis is only limited by the creativity of the researcher and could go on for much longer. The purpose of the current discussion, however, is not to exhaust all the possibilities that exist. It is mainly to show that there are indeed many possible extensions to the current research and that its impact can be enhanced. The author believes that the research goals we have set at the beginning of this thesis have been met to a large extent. At the same time it is worth repeating that there is no larger gratification to a researcher than seeing other people building on their research and we would encourage any such move. It is hoped that the research reported in this thesis will provide a platform for such.

Bibliography

[1] G. Kane and A. Pierce, *Perspectives on LHC Physics*. Singapore: World Scientific, 2008.

[2] N. P. Hessey, "Overview and Electronics Needs of ATLAS and CMS High Luminosity Upgrades," CERN, Geneva, Tech. Rep. ATL-UPGRADE-PROC-2008-001; ATL-COM-UPGRADE-2008-003, Oct. 2008.

[3] L. Evans, *The Large Hadron Collider: a marvel of technology*. Lausanne, Switzerland: EPFL Press, 2009.

[4] (2013, Jan). [Online]. Available: http://startswithabang.com/wp-content/uploads/2008/05/lhc-sim.jpg

[5] R. K. Bock and A. Vasilescu, *The Particle Detector Briefbook*. Berlin, Germany: Springer, 1998.

[6] (2013, Jan). [Online]. Available: https://cms-docdb.cern.ch/cgi-bin/PublicDocDB/ShowDocument?docid=5581

[7] J. Christiansen. (2008, Jul) Introduction to electronics. [Online]. Available: http://cds.cern.ch/record/1035285?ln=en

[8] R. Adolphi *et al.*, "The CMS experiment at the CERN LHC," *J. Instrum.*, vol. 3, p. S08004, 2008.

[9] (2013, Jan). [Online]. Available: http://www.dtc.umn.edu/mints/home.php

[10] Dr. Jan Troska, Private Communication, Nov. 2009.

[11] G. Aad *et al.*, "The ATLAS Experiment at the CERN Large Hadron Collider," *J. Instrum.*, vol. 3, p. S08003, 2008.

[12] A. Alves *et al.*, "The LHCb Detector at the LHC," *J. Instrum.*, vol. 3, p. S08005, 2008.

[13] W. C. Riegler. (2009, Jul.) Summer student lecture programme course, detectors. [Online]. Available: http://cds.cern.ch/record/1187564?ln=en

[14] J. Christiansen. (2008, Jul.) Summer student lecture programme course, introduction to electronics. [Online]. Available: http://cds.cern.ch/record/1035285?ln=en

[15] (2009, Feb.) Slhc, the high-luminosity upgrade (public event). [Online]. Available: http://cdsweb.cern.ch/record/1163932

[16] O. S. Bruning *et al.*, "Lhc luminosity and energy upgrade: A feasibility study," CERN, Geneva, Tech. Rep. CERN-LHC-Project-Report-626, Dec. 2002.

[17] Dr. Duccio Abbaneo, Private Communication, Dec. 2009.

[18] F. Close. (2009, Jul) Introduction to particle physics (for non particle physicists). [Online]. Available: http://cds.cern.ch/record/1187531?ln=en

[19] A. De Roeck *et al.* (2006) LHC luminosity upgrade: detector challenges. CERN. Geneva. [Online]. Available: https://cdsweb.cern.ch/record/892904?ln=en

[20] N. P. Hessey, "Overview and Electronics Needs of ATLAS and CMS High Luminosity Upgrades," in *Topical Workshop on Electronics for Particle Physics (TWEPP)*, Naxos, Greece, 2008, p. 5.

[21] J. Troska. Versatile Link Technical Specification, part 2.1. [Online]. Available: https://edms.cern.ch/file/1140665/1/VTRx_Spec_v2.0.pdf

[22] A. Strässner, "Development of new readout electronics for the ATLAS LAr Calorimeter at the sLHC," CERN, Geneva, Tech. Rep. ATL-LARG-PROC-2009-016. ATL-COM-LARG-2009-041, Oct. 2009.

[23] G. Hall, "Design of a trigger module for the CMS Tracker at SLHC," in *Topical Workshop on Electronics for Particle Physics (TWEPP)*, Paris, France, 2009, pp. 243–248.

[24] P. Moreira *et al.*, "The GBT Project," in *Topical Workshop on Electronics for Particle Physics (TWEPP)*, Paris, France, 2009, pp. 342–346.

[25] J. Troska, S. Detraz, S. Papadopoulos, I. Papakonstantinou, S. Rui Silva, S. Seif el Nasr, C. Sigaud, Stejskal, C. Soos, and F. Vasey, "The Versatile Transceiver Proof of Concept," in *Topical Workshop on Electronics for Particle Physics (TWEPP)*, Paris, France, Sep. 2009.

[26] K. Fouli and M. Maier, "OCDMA and Optical Coding: Principles, Applications, and Challenges [Topics in Optical Communications]," *IEEE Commun. Mag.*, vol. 45, pp. 27–34, 2007.

[27] J. Armstrong, "OFDM for Optical Communications," *J. Lightw. Technol.*, vol. 27, pp. 189–204, 2009.

[28] J. M. Senior, *Optical fiber communications: principles and practice.* Englewood Cliffs, NJ: Prentice-Hall, 2009.

[29] C. F. Lam, *Passive Optical Networks: Principles and Practice; electronic version.* San Diego, CA: Elsevier, 2007.

[30] L. Hutcheson, "FTTx: Current Status and the Future," *IEEE Commun. Mag.*, vol. 46, pp. 90–95, 2008.

[31] L. G. Kazovsky *et al.*, "Next-Generation Optical Access Networks," *J. Lightw. Technol.*, vol. 25, pp. 3428–3442, 2007.

[32] C.-H. Lee *et al.*, "Fiber to the Home Using a PON Infrastructure," *J. Lightw. Technol.*, vol. 24, pp. 4568–4583, 2006.

[33] D. J. Shin *et al.*, "Hybrid WDM/TDM-PON with wavelength-selection-free transmitters," *J. Lightw. Technol.*, vol. 23, pp. 187–195, 2005.

[34] A. Kaszubowska *et al.*, "Multifunctional operation of a fiber Bragg grating in a WDM/SCM radio over fiber distribution system," *IEEE Photonics Technol. Lett.*, vol. 16, pp. 605–607, 2004.

[35] H. Rohde *et al.*, "Next generation optical access: 1 Gbit/s for everyone," in *35th European Conf. on Optical Communication (ECOC)*, Vienna, Austria, 2009, pp. 1–3.

[36] C. K. G. and O. Andrew. (1998) The size and growth rate of the internet. [Online]. Available: http://firstmonday.org/htbin/cgiwrap/bin/ojs/index.php/fm/rt/printerFriendly/620/541

[37] P. W. Shumate, "Fiber-to-the-Home: 1977-2007," *J. Lightw. Technol.*, vol. 26, pp. 1093–1103, 2008.

[38] D. Gutierrez, K. Kim, S. Rotolo, F. An, and L. Kazovsky, "FTTH standards, deployments and research issues," in *Proc. of JCIS*, Salt Lake City, UT, 2005, pp. 1358–1361.

[39] K. Grobe and J.-P. Elbers, "PON in adolescence: from TDMA to WDM-PON," *IEEE Commun. Mag.*, vol. 46, pp. 26–34, 2008.

[40] K. Tanaka *et al.*, "IEEE 802.3av 10G-EPON Standardization and Its Research and Development Status," *J. Lightw. Technol.*, vol. PP, p. 1, 2009.

[41] F. Effenberger and T. S. El-Bawab, "Passive Optical Networks (PONs): Past, present, and future," *Optical Switching and Networking*, vol. 6, pp. 143–150, Jul. 2009.

[42] E. Säckinger, *Broadband circuits for optical-fiber communication; electronic version.* Newark, NJ: Wiley, 2005.

[43] E. Sackinger *et al.*, "15 mW, 155 Mb/s CMOS burst-mode laser driver with automatic power control and end-of-life detection," in *IEEE Int. Solid-State Circuits Conf. (ISSCC), Dig. of Tech. Papers*, 1999, pp. 386–387.

[44] N. Ishihara *et al.*, "3.3 V, 5O Mb/s CMOS transceiver for optical burst-mode communication," in *43rd IEEE Int. Solid-State Circuits Conference (ISSCC), Digest of Technical Papers*, 1997, pp. 244–245, 466.

[45] H. Nakamura, "Fast response burst-mode transmitter for 10-Gbit/s-class PON Systems," in *Proc. 7th Int. Conf. on Optical Internet (COIN)*, 2008, pp. 1–2.

[46] H. Nakamura *et al.*, "AC-Coupled Burst-Mode Transmitter Using Baseline-Wander Common-Mode-Rejection Technique for 10-Gbit/s-Class PON Systems," *J. Lightw. Technol.*, vol. 27, pp. 336–342, Feb. 2009.

[47] C.-C. Chen *et al.*, "A 1.25 Gbps burst-mode receiver IC with extended dynamic range," in *IEEE Symp. Proc. Dig. of Papers Radio Frequency integrated Circuits (RFIC)*, 2005, pp. 625–628.

[48] M. Nakamura *et al.*, "A burst-mode optical receiver with high sensitivity using a PIN-PD for a 1.25 Gbit/s PON system," in *Proc. Tech. Dig. Optical Fiber Communication Conf. (OFC/NFOEC)*, vol. 5, 2005, p. 3.

[49] P. Ossieur *et al.*, "DC-coupled 1.25 Gbit/s burst-mode receiver with automatic offset compensation," *Electron. Lett.*, vol. 40, pp. 447–448, 2004.

[50] ——, "Analysis of optimum avalanche gain of burst-mode receivers for PON applications," *IEEE Photonics Technol. Lett.*, vol. 17, pp. 884–886, 2005.

[51] ——, "Sensitivity penalty calculation for burst-mode receivers using avalanche photodiodes," *J. Lightw. Technol.*, vol. 21, pp. 2565–2575, 2003.

[52] C. Su *et al.*, "Theory of burst-mode receiver and its applications in optical multiaccess networks," *J. Lightw. Technol.*, vol. 15, pp. 590–606, 1997.

[53] C. A. Eldering, "Theoretical determination of sensitivity penalty for burst mode: fiber optic receivers," *J. Lightw. Technol.*, vol. 11, pp. 2145–2149, 1993.

[54] J.-W. Kwon *et al.*, "AC-coupled burst-mode OLT SFP transceiver for gigabit ethernet PON systems," *IEEE Photonics Technol. Lett.*, vol. 17, pp. 1519–1521, 2005.

[55] Y. Ota and R. G. Swartz, "Burst-mode compatible optical receiver with a large dynamic range," *J. Lightw. Technol.*, vol. 8, pp. 1897–1903, 1990.

[56] M. Nakamura *et al.*, "1.25-Gb/s burst-mode receiver ICs with quick response for PON systems," *IEEE J. Solid-State Circuits*, vol. 40, pp. 2680–2688, 2005.

[57] P. Ossieur *et al.*, "A 1.25-gb/s burst-mode receiver for GPON applications," *IEEE J. Solid-State Circuits*, vol. 40, pp. 1180–1189, 2005.

[58] S. Yamashita *et al.*, "Novel cell-AGC technique for burst-mode CMOS preamplifier with wide dynamic range and high sensitivity for ATM-PON system," *IEEE J. Solid-State Circuits*, vol. 37, pp. 881–886, 2002.

[59] K. Nishimura *et al.*, "A 1.25-Gb/s CMOS burst-mode optical transceiver for ethernet PON system," *IEEE J. Solid-State Circuits*, vol. 40, pp. 1027–1034, 2005.

[60] Q. Le *et al.*, "A burst-mode receiver for 1.25-Gb/s ethernet PON with AGC and internally created reset signal," *IEEE J. Solid-State Circuits*, vol. 39, pp. 2379–2388, 2004.

[61] N. Suzuki *et al.*, "Demonstration of 10.3-Gbit/s burst-mode CDR employing 0.13 um SiGe BiCMOS quad-rate sampling IC and data-phase decision-algorithm for 10Gbps-based PON systems," in *Proc. 34th European Conf. on Optical Communication (ECOC)*, Brussels, Belgium, 2008, pp. 1–2.

[62] M. Nogawa *et al.*, "A 10 Gb/s burst-mode CDR IC in 0.13 μm CMOS," in *IEEE Int. Solid-State Circuits Conf. (ISSCC) Dig. of Tech. Papers*, vol. 1, 2005, pp. 228–595.

[63] M. Ishikawa *et al.*, "A study of an over-sampling burst-mode CDR with gated VCO for 10Gbps PON systems," in *Proc. 7th Int. Conf. on Optical Internet (COIN)*, 2008, pp. 1–2.

[64] J. Lee and M. Liu, "A 20Gb/s Burst-Mode CDR Circuit Using Injection-Locking Technique," in *Proc. Dig. of Tech. Papers, IEEE International Solid-State Circuits Conference (ISSCC)*, 2007, pp. 46–586.

[65] M. Mcgarry *et al.*, "Ethernet passive optical network architectures and

dynamic bandwidth allocation algorithms," *IEEE Commun. Surv. Tutor.*, vol. 10, pp. 46–60, 2008.

[66] J. E. Prat, *Next-Generation FTTH Passive Optical Networks: Research towards unlimited bandwidth access.* Berlin, Germany: Springer, 2008.

[67] M. P. McGarry *et al.*, "Ethernet PONs: a survey of dynamic bandwidth allocation (DBA) algorithms," *IEEE Commun. Mag.*, vol. 42, pp. S8–15, 2004.

[68] B. Skubic *et al.*, "A comparison of dynamic bandwidth allocation for EPON, GPON, and next-generation TDM PON," *IEEE Commun. Mag.*, vol. 47, pp. S40–S48, 2009.

[69] J. Zheng and H. T. Mouftah, "Media access control for Ethernet passive optical networks: an overview," *IEEE Commun. Mag.*, vol. 43, pp. 145–150, 2005.

[70] G. Kramer *et al.*, "IPACT a dynamic protocol for an Ethernet PON (EPON)," *IEEE Commun. Mag.*, vol. 40, pp. 74–80, 2002.

[71] M. Ma *et al.*, "A bandwidth guaranteed polling MAC protocol for Ethernet passive optical networks," in *Proc. INFOCOM 2003. 22nd Annual Joint Conference of the IEEE Computer and Communications Societies*, vol. 1, San Francisco, CA, 2003, pp. 22–31.

[72] S. Choi and J. Huh, "Dynamic bandwidth allocation algorithm for multimedia services over Ethernet PONs," *ETRI JOURNAL*, vol. 24, pp. 465–468, Dec. 2002.

[73] C. M. Assi *et al.*, "Dynamic bandwidth allocation for quality-of-service over Ethernet PONs," *IEEE J. Sel. Areas Commun.*, vol. 21, pp. 1467–1477, 2003.

[74] K. Ennser *et al.*, "Extending reach of passive optical networks through optical amplification," in *11th Int. Conf. on Transparent Optical Networks (ICTON)*, Azores, Portugal, 2009, pp. 1 –4.

[75] R. P. Davey *et al.*, "Long-Reach Passive Optical Networks," *J. Lightw. Technol.*, vol. 27, pp. 273–291, 2009.

[76] B. Zhu and D. Nesset, "GPON reach extension to 60 km with entirely passive fibre plant using Raman amplification," in *Proc. 35th European Conf. on Optical Communication (ECOC)*, Vienna, Austria, 2009, pp. 1–2.

[77] D. P. Shea and J. E. Mitchell, "Long-Reach Optical Access Technologies," *IEEE Network*, vol. 21, pp. 5–11, 2007.

[78] A. V. Tran *et al.*, "Feed-forward control of SOA gain for power equalization in optical burst switching networks," *Opt. Commun.*, vol. 266, pp. 500 – 504, 2006.

[79] J. Park *et al.*, "FTTH Deployment Status & Strategy in Korea: GW-PON Based FTTH Field Trial and Reach Extension Strategy of FTTH in Korea," in *Proc. IEEE Global Telecommunications Conf. (GLOBECOM)*, 2008, pp. 1–3.

[80] R. Davey *et al.*, "Options for future optical access networks," *IEEE Commun. Mag.*, vol. 44, pp. 50–56, 2006.

[81] M. K. Weldon *et al.*, "Next-generation access networks: A preview," *Bell Lab. Tech. J.*, vol. 13, pp. 1–10, 2008.

[82] C.-H. Lee *et al.*, "WDM-PON experiences in Korea [Invited]," *J. Opt. Netw.*, vol. 6, pp. 451–464, May 2007.

[83] S. Kamei, "Recent progress on athermal AWG wavelength multiplexer," in *Proc. Conf. on Optical Fiber Communication (OFC)*, San Diego, CA, 2009, pp. 1–3.

[84] H. Terui *et al.*, "Reduction of Second-Order Temperature Dependence of Athermal AWG With Resin-Filled Groove by Pressure Control," *IEEE Photonics Technol. Lett.*, vol. 21, pp. 1426–1428, 2009.

[85] J. Ingenhoff, "Athermal AWG devices for WDM-PON architectures," in *Proc. IEEE Lasers and Electro-Optics Society (LEOS)*, 2006, pp. 26–27.

[86] Y. Liu *et al.*, "Directly-modulated athermal transmitter for uncooled WDM systems," in *Proc. 31st European Conf. on Optical Communication (ECOC)*, vol. 3, Glasgow, UK, 2005, pp. 581–582.

[87] H. Sano *et al.*, "Athermal and tunable operations of 850 nm VCSEL with thermally actuated cantilever structure," in *Proc. 35th European Conf. on Optical Communication (ECOC)*, Vienna, Austria, 2009, pp. 1–2.

[88] A. Banerjee *et al.*, "Wavelength-division-multiplexed passive optical network (WDM-PON) technologies for broadband access: a review [Invited]," *J. Opt. Netw.*, vol. 4, pp. 737–758, Nov. 2005.

[89] L. A. Coldren *et al.*, "Tunable semiconductor lasers: a tutorial," *J. Lightw. Technol.*, vol. 22, pp. 193–202, 2004.

[90] J. Harris, J. S., "Tunable long-wavelength vertical-cavity lasers: the engine of next generation optical networks?" *IEEE J. Quantum Electron.*, vol. 6, pp. 1145–1160, 2000.

[91] G. S. Li *et al.*, "Electrically-pumped directly-modulated tunable VCSEL for

metro DWDM applications," in *Proc. 27th European Conf. on Optical Communication (ECOC)*, vol. 2, Amsterdam, The Netherlands, 2001, pp. 220–221.

[92] J. Buus and E. J. Murphy, "Tunable lasers in optical networks," *J. Lightw. Technol.*, vol. 24, pp. 5–11, 2006.

[93] R. Szweda, "VCSEL applications diversify as technology matures," *III-Vs Review*, vol. 19, pp. 34 – 38, 2006.

[94] M. S. Leeson and S. Sun, "Spectrum slicing for low cost wavelength division multiplexing," in *Proc. 2nd ICTON Mediterranean Winter ICTON-MW 2008*, 2008, pp. 1–4.

[95] R. D. Feldman, "Crosstalk and loss in wavelength division multiplexed systems employing spectral slicing," *J. Lightw. Technol.*, vol. 15, pp. 1823–1831, 1997.

[96] G. J. Pendock and D. D. Sampson, "Transmission performance of high bit rate spectrum-sliced WDM systems," *J. Lightw. Technol.*, vol. 14, pp. 2141–2148, 1996.

[97] V. Arya and I. Jacobs, "Optical preamplifier receiver for spectrum-sliced WDM," *J. Lightw. Technol.*, vol. 15, pp. 576–583, 1997.

[98] M. S. Leeson, "Pulse position modulation for spectrum-sliced transmission," *IEEE Photonics Technol. Lett.*, vol. 16, pp. 1191–1193, 2004.

[99] A. J. Keating and D. D. Sampson, "Reduction of excess intensity noise in spectrum-sliced incoherent light for WDM applications," *J. Lightw. Technol.*, vol. 15, pp. 53–61, 1997.

[100] D. K. Jung *et al.*, "Wavelength-division-multiplexed passive optical network based on spectrum-slicing techniques," *IEEE Photonics Technol. Lett.*, vol. 10, pp. 1334–1336, 1998.

[101] D. Fattal *et al.*, "Design of an efficient light-emitting diode with 10 GHz modulation bandwidth," *Appl. Phys. Lett.*, vol. 93, pp. 243 501–243 501–3, 2008.

[102] S. S. Wagner and T. E. Chapuran, "Broadband high-density WDM transmission using superluminescent diodes," *Electron. Lett.*, vol. 26, pp. 696–697, 1990.

[103] S. Woodward *et al.*, "A spectrally sliced PON employing Fabry-Perot lasers," *IEEE Photonics Technol. Lett.*, vol. 10, pp. 1337–1339, Sep. 1998.

[104] J. S. Lee *et al.*, "Spectrum-sliced fiber amplifier light source for multichannel WDM applications," *IEEE Photonics Technol. Lett.*, vol. 5, pp. 1458–1461, 1993.

[105] N. Kashima, "Dynamic properties of FP-LD transmitters using side-mode injection locking for LANs and WDM-PONs," *J. Lightw. Technol.*, vol. 24, pp. 3045–3058, 2006.

[106] J.-H. Moon *et al.*, "Effects of Back-Reflection in WDM-PONs Based on Seed Light Injection," *IEEE Photonics Technol. Lett.*, vol. 19, pp. 2045–2047, 2007.

[107] X.-F. Cheng *et al.*, "Impact of Facet Reflectivity and Operation Condition on Injection-Locking Fabry-Perot Laser Diodes with Spectrum Sliced ASE Noise in WDM-PON," in *Proc. Conf. on Lasers and Electro-Optics, (CLEO)*, 2007, pp. 1–2.

[108] G.-R. Lin *et al.*, "Comparison on Injection-Locked FabryPerot Laser Diode With Front-Facet Reflectivity of 1Transmission in WDM-PON System," *J. Lightw. Technol.*, vol. 27, pp. 2779–2785, Jul. 2009.

[109] H. D. Kim *et al.*, "A low-cost WDM source with an ASE injected Fabry-Perot semiconductor laser," *IEEE Photonics Technol. Lett.*, vol. 12, pp. 1067–1069, 2000.

[110] S.-M. Lee *et al.*, "Dense WDM-PON based on wavelength-locked Fabry-Pe´rot laser diodes," *IEEE Photonics Technol. Lett.*, vol. 17, pp. 1579–1581, 2005.

[111] D. J. Shin *et al.*, "Low-cost WDM-PON with colorless bidirectional transceivers," *J. Lightw. Technol.*, vol. 24, pp. 158–165, 2006.

[112] X. Cheng *et al.*, "Study on Spectrum Sliced ASE Source for Injection-locking of Fabry-Prot Laser Diodes," in *10th IEEE Int. Conf. on Communication systems., (ICCS)*, Singapore, 2006, pp. 1 –5.

[113] Z. Xu *et al.*, "High-speed WDM-PON using CW injection-locked Fabry-Pérot laser diodes," *Opt. Express*, vol. 15, pp. 2953–2962, 2007.

[114] Y. J. Wen and C.-J. Chae, "WDM-PON upstream transmission using Fabry-Perot laser diodes externally injected by polarization-insensitive spectrum-sliced supercontinuum pulses," *Opt. Commun.*, vol. 260, pp. 691 – 695, 2006.

[115] Z. Xu *et al.*, "10 Gb/s WDM-PON upstream transmission using injection-locked Fabry-Perot laser diodes," in *Proc. Conf. on Optical Fiber communication/National Fiber Optic Engineers Conf. (OFC/NFOEC)*, 2006, pp. 3 pp.–.

[116] W.-S. Tsai *et al.*, "Bidirectional dense wavelength-division multiplexing passive optical network based on injection-locked vertical-cavity surface-emitting lasers and a data comparator," *Opt. Eng.*, vol. 45, no. 9, p. 095003, 2006.

[117] S. Hann *et al.*, "Direct-modulated upstream signal transmission using a self-injection locked F-P LD for WDM-PON," in *Proc. 31st European Conf. on Optical Communication (ECOC)*, vol. 3, 2005, pp. 451–452.

[118] E. K. Lau *et al.*, "Enhanced Modulation Characteristics of Optical Injection-Locked Lasers: A Tutorial," *IEEE J. Sel. Topics. Quantum Electron.*, vol. 15, pp. 618–633, 2009.

[119] J. Wang *et al.*, "Enhancement of modulation bandwidth of laser diodes by injection locking," *IEEE Photonics Technol. Lett.*, vol. 8, pp. 34–36, 1996.

[120] E. K. Lau *et al.*, "Strong optical injection-locked semiconductor lasers demonstrating > 100-GHz resonance frequencies and 80-GHz intrinsic bandwidths," *Opt. Express*, vol. 16, pp. 6609–6618, 2008.

[121] F. Payoux *et al.*, "Gigabit optical access using WDM PON based on spectrum slicing and reflective SOA," in *Proc. 31st European Conf. on Optical Communication (ECOC)*, vol. 3, Glasgow, UK, 2005, pp. 455–456.

[122] L. Xu and H. Tsang, "Colorless WDM-PON Optical Network Unit (ONU) Based on Integrated Nonreciprocal Optical Phase Modulator and Optical Loop Mirror," *IEEE Photonics Technol. Lett.*, vol. 20, pp. 863–865, May 2008.

[123] G. Berrettini *et al.*, "Colorless WDM-PON Architecture for Rayleigh Backscattering and Path-Loss Degradation Mitigation," *IEEE Photonics Technol. Lett.*, vol. 21, pp. 453–455, 2009.

[124] N. J. Frigo *et al.*, "A wavelength-division multiplexed passive optical network with cost-shared components," *IEEE Photonics Technol. Lett.*, vol. 6, pp. 1365–1367, 1994.

[125] W. Lee *et al.*, "Bidirectional WDM-PON based on gain-saturated reflective semiconductor optical amplifiers," *IEEE Photonics Technol. Lett.*, vol. 17, pp. 2460–2462, 2005.

[126] J.-H. Yu *et al.*, "Remodulation schemes with reflective SOA for colorless DWDM PON," *J. Opt. Netw.*, vol. 6, pp. 1041–1054, 2007.

[127] Y. Takushima *et al.*, "Design Issues in RSOA-based WDM PON," in *Proc. IEEE Photonics Global at Singapore Conf. (IPGC)*, Singapore, 2008, pp. 1–4.

[128] S. Y. Kim *et al.*, "Enhanced performance of RSOA-based WDM PON by using Manchester coding," *J. Opt. Netw.*, vol. 6, pp. 624–630, 2007.

[129] S. Jang *et al.*, "A bidirectional RSOA based WDM-PON utilizing a SCM signal for down-link and a baseband signal for up-link," in *Proc. Conf. on Optical Fiber Communication/National Fiber Optic Engineers Conf. (OFC/NFOEC)*, 2007, pp. 1–3.

[130] K. Y. Cho, Y. J. Lee, H. Y. Choi, A. Murakami, A. Agata, Y. Takushima, and Y. C. Chung, "Effects of reflection in rsoa-based wdm pon utilizing remodulation technique," *IEEE/OSA Journal of Lightwave Technology*, vol. 27, no. 10, pp. 1286–1295, 2009.

[131] P. J. Urban *et al.*, "Mitigation of Reflection-induced Crosstalk in a WDM Access Network," in *Proc. Conf. on Optical Fiber Communication/National Fiber Optic Engineers Conf. (OFC/NFOEC)*, 2008, pp. 1–3.

[132] K. Cho *et al.*, "Demonstration of RSOA-based WDM PON Operating at Symmetric Rate of 1.25 Gb/s with High Reflection Tolerance," in *Optical Fiber Communication/National Fiber Optic Engineers Conf., (OFC/NFOEC)*, San Diego, CA, 2008, pp. 1 –3.

[133] A. Murakami *et al.*, "Enhanced reflection tolerance of upstream signal in a RSOA-based WDM PON by using Manchester coding," in *Proc. of SPIE, Conf. on Optical Transmission, Switching, and Subsystems V*, vol. 6783, Wuhan, China, 2007, Proceedings Paper, pp. 67 832I1–67 832I5.

[134] E. Wong *et al.*, "Directly Modulated Self-Seeding Reflective Semiconductor Optical Amplifiers as Colorless Transmitters in Wavelength Division Multiplexed Passive Optical Networks," *J. Lightw. Technol.*, vol. 25, pp. 67–74, 2007.

[135] K. Y. Cho *et al.*, "10-Gb/s Operation of RSOA for WDM PON," *IEEE Photonics Technol. Lett.*, vol. 20, pp. 1533–1535, 2008.

[136] B. Schrenk *et al.*, "Colourless FSK/ASK Optical Network Unit based on a Fabry Prot type SOA/REAM for symmetrical 10 Gb/s WDM-PONs," in *35th European Conf. on Optical Communication (ECOC)*, Vienna, Austria, 2009, pp. 1–2.

[137] I. T. Monroy *et al.*, "Monolithically integrated reflective SOA-EAcarrier remodulator for broadband access nodes," *Opt. Express*, vol. 14, pp. 8060–8064, 2006.

[138] Z. Xu *et al.*, "Broadcast capable 40-Gb/s WDM passive optical networks," in *Proc. 35th European Conf. on Optical Communication (ECOC)*, Vienna, Austria, 2009, pp. 1–2.

[139] M. Chacinski *et al.*, "Electroabsorption Modulators Suitable for 100-Gb/s Ethernet," *IEEE Electron Device Lett.*, vol. 29, pp. 1014–1016, Sept. 2008.

[140] Y. Yu *et al.*, "80 Gb/s ETDM transmitter with a traveling-wave electroabsorption modulator," in *Proc. Tech. Dig. Optical Fiber Communication Conf. OFC/NFOEC*, vol. 3, 2005, p. 3 pp.

[141] Y. Tian *et al.*, "A WDM passive optical network enabling multicasting with color-free ONUs," *Opt. Express*, vol. 16, pp. 10 434–10 439, 2008.

[142] X. Zhou and J. Yu, "Multi-Level, Multi-Dimensional Coding for High-Speed and High-Spectral-Efficiency Optical Transmission," *J. Lightw. Technol.*, vol. 27, pp. 3641–3653, 2009.

[143] J. Shin and N. Dagli, "Ultra-low voltage GaAs/AlGaAs Mach-Zehnder intensity modulators," in *Proc. IEEE Avionics, Fiber-Optics and Photonics Technology Conf.*, 2008, pp. 55–56.

[144] S. Dahlfort, "Comparison of 10 Gbit/s PON vs WDM-PON," in *Proc. 35th European Con. on Optical Communication (ECOC)*, Vienna, Austria, 2009, pp. 1–2.

[145] M. Hajduczenia and H. J. A. da Silva, "Next generation PON systems - Current status," in *Proc. 11th Int. Conf. on Transparent Optical Networks (ICTON)*, Azores, Portugal, 2009, pp. 1–8.

[146] V. Chakravarthy *et al.*, "TDCS, OFDM, and MC-CDMA: a brief tutorial," *IEEE Commun. Mag.*, vol. 43, pp. S11–S16, 2005.

[147] G. Parsaee and A. Yarali, "OFDMA for the 4th generation cellular networks," in *Canadian Conf. on Electrical and Computer Engineering*, vol. 4, 2004, pp. 2325–2330.

[148] J. Armstrong, "OFDM: From Copper and Wireless to Optical," in *Proc. Conf. on Optical Fiber communication/National Fiber Optic Engineers Conf. (OFC/NFOEC)*, 2008, pp. 1–27.

[149] J. A. C. Bingham, "Multicarrier modulation for data transmission: an idea whose time has come," *IEEE Commun. Mag.*, vol. 28, pp. 5–14, 1990.

[150] N. Ujiie, "Application to a High-Energy Physics Experiment of the Optical-Transmission Readout System," *IEEE Trans. Nucl. Sci.*, vol. 39, pp. 875–879, Aug. 1992.

[151] N. Ujiie *et al.*, "A Time-Extended Optical Readout Transmission Scheme to a High-Density Detector System," *Nucl. Instrum. Meth. A*, vol. 342, pp. 186–192, Mar. 1994.

[152] A. Aloisio, F. Cevenini, and V. Izzo, "An approach to DWDM for real-time applications," *IEEE Trans. Nucl. Sci.*, vol. 51, pp. 526–531, Jun. 2004.

[153] E. Heine *et al.*, "Developments for a passive optical node network for deployment in deep sea enabling time synchronous data readout," *Nucl. Instrum. Meth. A*, vol. 602, pp. 146–149, Apr. 2009.

[154] F. Ameli *et al.*, "The data acquisition and transport design for NEMO phase I," *IEEE Trans. Nucl. Sci.*, vol. 55, pp. 233–240, Feb. 2008.

[155] H. Lohner, "Deep-sea research infrastructure for high-energy neutrino astronomy," *Nucl. Instrum. Meth. A*, vol. 617, pp. 495–498, May 2010.

[156] (2013, Apr). [Online]. Available: http://ttc.web.cern.ch/ttc/

[157] W.-P. Huang *et al.*, "Optical Transceivers for Fiber-to-the-Premises Applications: System Requirements and Enabling Technologies," *J. Lightw. Technol.*, vol. 25, pp. 11 –27, Jan. 2007.

[158] M. Bonilla *et al.*, "Techno-economical comparison between GPON and EPON networks," in *Innovations for Digital Inclusions, 2009. K-IDI 2009. ITU-T*, Mar del Plata, Argentina, 2009, pp. 1 –5.

[159] G. P. Agrawal, *Fiber-optic communication systems; 3rd ed.* New York, NY: Wiley, 2002.

[160] (2010, Sep). [Online]. Available: http://www.oesolution.com/

[161] (2010, Sep). [Online]. Available: http://www.xilinx.com/support/documentation/data_sheets/ds022-1.pdf

[162] (2010, Sep). [Online]. Available: http://www.xilinx.com/support/documentation/application_notes/xapp195.pdf

[163] J. Kim and D.-K. Jeong, "Multi-gigabit-rate clock and data recovery based on blind oversampling," *IEEE Commun. Mag.*, vol. 41, pp. 68 – 74, Dec. 2003.

[164] A. Borghesani, "Optoelectronic Components for WDM-PON," in *Proc. 9th Int. Conf. on Transparent Optical Networks (ICTON)*, vol. 1, Rome, Italy, 2007, pp. 305–308.

[165] C. Da Via *et al.*, "Lightwave analogue links for LHC detector front-ends," *Nucl. Instrum. Meth. A*, vol. 344, pp. 199 – 211, 1994.

[166] A. Baird *et al.*, "Analog lightwave links for detector front-ends at the LHC," *IEEE Trans. Nucl. Sci.*, vol. 42, pp. 873 –881, Aug. 1995.

[167] R. Macias *et al.*, "Advance validation of radiation hardness and reliability of lasers for CMS optical links," *IEEE Trans. Nucl. Sci.*, vol. 52, pp. 1488 – 1496, Oct. 2005.

[168] J. Troska *et al.*, "Radiation Damage Studies of Lasers and Photodiodes for Use in Multi-Gb/s Optical Data Links," *IEEE Trans. Nucl. Sci.*, vol. 58, pp. 3103 –3110, Dec. 2011.

[169] N. Deng *et al.*, "A WDM Passive Optical Network With Centralized Light Sources and Multicast Overlay," *IEEE Photonics Technol. Lett.*, vol. 20, pp. 114 –116, Jan. 2008.

[170] Y. Gu *et al.*, "A carrier-reuse WDM-PON architecture with multicast/broadcast capability," in *7th Int. Conf. on Information, Communications and Signal Processing (ICICS)*, Macau, China, 2009, pp. 1 –5.

[171] J. Cho and others., "Broadcast Transmission in WDM-PON using a Broadband Light Source," in *Optical Fiber Communication and the National Fiber Optic Engineers Conf., (OFC/NFOEC)*, Anaheim, CA, 2007, pp. 1 –3.

[172] (2010, May). [Online]. Available: http://www.denselight.com/product1.htm

[173] J. Kani *et al.*, "Design and demonstration of Gigabit spectrum-sliced WDM systems employing directly modulated super luminescent diodes," in *Optical Fiber Communication Conf (OFC/NFOEC), Tech. Dig.*, vol. 3, 2005, p. 3.

[174] K.-Y. Liou and G. Raybon, "Operation of an LED with a single-mode semiconductor amplifier as a broad-band 1.3- mu;m transmitter source," *IEEE Photonics Technol. Lett.*, vol. 7, pp. 1025 –1027, Sep. 1995.

[175] T. Pham *et al.*, "Bidirectional 1.25-Gbps WDM-PON with broadcasting function based on fabry-perot light source and RSOA," in *Conf. on Optical Fiber Communication (OFC)*, San Diego, CA, 2009, pp. 1 – 3.

[176] N. Kim and M. Kang, "Traffic Share-Based Multicast Scheduling for Broad-

cast Video Delivery in Shared-WDM-PONs," *Lightwave Technology, Journal of*, vol. 25, pp. 2814 –2827, Sept. 2007.

[177] F. Payoux *et al.*, "WDM PON with a single SLED seeding colorless RSOA-based OLT and ONUs," in *European Conf. on Optical Communications (ECOC)*, 2006, pp. 1 – 2.

[178] F. Fresi *et al.*, "Single RSOA based ONU for RZ symmetrical WDM PONs at 2.5 Gb/s," in *Int. Conf. on Photonics in Switching (PS)*, 2008, pp. 1 –2.

[179] G. Talli and P. D. Townsend, "Hybrid DWDM-TDM long-reach PON for next-generation optical access," *J. Lightw. Technol.*, vol. 24, pp. 2827–2834, 2006.

[180] A. Aloisio, F. Cevenini, and V. Izzo, "An approach to DWDM for real-time applications," *IEEE Trans. Nucl. Sci.*, vol. 51, pp. 526 – 531, Jun. 2004.

[181] D. Calvet, "A review of technologies for the transport of digital data in recent physics experiments," *IEEE Trans. Nucl. Sci.*, vol. 53, pp. 789 – 794, Jun. 2006.

[182] S. Anvar, "Data acquisition architecture studies for the KM3NeT deep sea neutrino telescope," in *IEEE Nuclear Science Symposium Conf. Record, (NSS)*, 2008, pp. 3558 –3561.

[183] C. Da Via *et al.*, "Large scale application of multi-quantum-well reflective modulators for analogue lightwave links," in *Conf. on Lasers and Electro-Optics, Europe, (CLEO Europe)*, Amsterdam, The Netherlands, 1994, p. 305.

[184] (2010, Aug). [Online]. Available: http://www.afwtechnologies.com.au/pm_filter_wdm.html#1310-1550

[185] (2010, May). [Online]. Available: http://www.oequest.com/getproduct/16939/cat/0/page/1

[186] (2010, Aug). [Online]. Available: http://www.oequest.com/getproduct/19518/cat/0/page/1

[187] (2010, May). [Online]. Available: http://www.oequest.com/

[188] (2010, May). [Online]. Available: http://www.corning.com/WorkArea/showcontent.aspx?id=41261

[189] (2010, May). [Online]. Available: http://www.exalos.com/productlist/download.php?pdf=/productinfo/datasheet/EXS1510-2111.pdf

[190] (2010, May). [Online]. Available: http://www.oequest.com/getproduct/17214/cat/1098/page/1

[191] (2010, Jun.). [Online]. Available: http://www.ciphotonics.com/cip_semiconductor_2.htm

[192] (2010, May). [Online]. Available: http://www.oequest.com/getproduct/19456/cat/1164/page/1

[193] (2010, May). [Online]. Available: http://www.us.anritsu.com/downloads/files/AD14113A_E_04_20030506.pdf

[194] (2010, Aug.). [Online]. Available: http://www.ciphotonics.com/PDFs_Sept09/R_EAM_1550_LS_C.pdf

[195] D. Zimmerman and L. Spiekman, "Amplifiers for the masses: EDFA, EDWA, and SOA amplets for metro and access applications," *J. Lightw. Technol.*, vol. 22, pp. 63 – 70, Jan. 2004.

[196] F. Xiong *et al.*, "Multimode-injection-locked Fabry-Perot laser diode as remote seeding light for WDM-PONs," in *Photonics Global Conference (PGC)*, 2010, pp. 1 –3.

[197] Q. Nguyen *et al.*, "30 Gbit/s downstream capacity of cost-effective colourless WDM-PON based on injection-locked Fabry-Perot lasers," *Electron. Lett.*, vol. 45, pp. 948 –949, 2009.

[198] W. Holloway *et al.*, "Multiwavelength source for spectrum-sliced WDM access networks and LAN's," *IEEE Photonics Technol. Lett.*, vol. 9, pp. 1014 –1016, Jul. 1997.

[199] K. Liu and W. Wang, "Misalignment distortion penalty in moderate-speed directly modulated WDM systems and its reduction using fiber Bragg grating lasers," *IEEE Photonics Technol. Lett.*, vol. 9, pp. 1649 –1651, Dec. 1997.

[200] C. Li *et al.*, "Channel capacity optimization of chirp-limited dense WDM/WDMA systems using OOK modulation and optical filters," in *IEEE Int. Conf. on Communications (ICC)*, vol. 2, 1991, pp. 580 –584.

[201] G. Li and P. Yu, "Optical intensity modulators for digital and analog applications," *J. Lightw. Technol.*, vol. 21, pp. 2010 – 2030, Sep. 2003.

[202] F. Dorgeuille and F. Devaux, "On the transmission performances and the chirp parameter of a multiple-quantum-well electroabsorption modulator," *IEEE J. Quantum Electron.*, vol. 30, pp. 2565 –2572, Nov. 1994.

[203] Z. Huan *et al.*, "Spectral Analysis using Linearly Chirped Gaussian Pulse Stacking," *Chinese Phys. Lett.*, vol. 26, Jul. 2009.

[204] (2010, Aug). [Online]. Available: http://www.gemfire.com/Main/Products/AWG/gemfireawg.html

[205] M. Fox, *Optical properties of solids.* Oxford, UK: Oxford Univ. Press, 2001.

[206] J.-S. Lee, "Signal-to-noise ratio of spectrum-sliced incoherent light sources including optical modulation effects," *J. Lightw. Technol.*, vol. 14, pp. 2197 –2201, Oct. 1996.

[207] (2012, Feb). [Online]. Available: http://www.ciphotonics.com/

[208] D. Yin *et al.*, "Laser diode comb spectrum amplification preserving low RIN for WDM applications," in *Asia Communications and Photonics Conf. and Exhibition (ACP)*, vol. 2009-Supplement, Nov. 2009, pp. 1 –7.

[209] G. Ghione, *Semiconductor Devices for High-Speed Optoelectronics.* Cambridge, UK: Cambridge University Press, 2009.

[210] (2012, Dec). [Online]. Available: https://www.oequest.com/getproduct/19435/cat/0/page/1

[211] I. Dawson *et al.*, "Irradiation tests of optoelectronic components for LHC inner-detectors," *Nucl. Instrum. Meth. A* , vol. 387, pp. 369–376, 1997.

[212] G. Cervelli, K. Gill, R. Grabit, M. Persello, G. Stefanini, and F. Vasey, "Radiation hardness of electro-optic asymmetric Fabry-Perot modulators," *NUCL INSTRUM METH A*, vol. 400, pp. 435–446, 1997.

[213] P. Goetz *et al.*, "Effects of proton irradiation on InGaAs/AlGaAs multiple quantum well modulators [for free-space optical communication]," in *IEEE Aerospace Conf. Proc.*, vol. 3, 2001, pp. 1523 –1529.

[214] (2010, Feb). [Online]. Available: https://irradiation.web.cern.ch/irradiation/irrad3.htm

[215] M. Glaser *et al.*, "Radiation test facilities in the new PS East Hall at CERN," in *5th European Conf. on Radiation and Its Effects on Components and Systems, (RADECS)*, 1999, pp. 136 –141.

[216] ——, "Dosimetry Assessments in the Irradiation Facilities at the CERN-PS Accelerator," *IEEE Trans. Nucl. Sci.*, vol. 53, pp. 2016 –2022, Aug. 2006.

[217] C. Claeys and E. Simoen, *Radiation effects in advanced semiconductor materials and devices*. Berlin, Germany: Springer, 2002.

[218] K. Gill *et al.*, "Radiation hardness qualification of InGaAsP/InP 1310 nm lasers for the CMS Tracker optical links," *IEEE Trans. Nucl. Sci.*, vol. 49, pp. 2923 – 2929, Dec. 2002.

[219] ——, "Radiation damage and annealing in 1310nm InGaAsP/InP lasers for the CMS tracker," in *Photonics for Space Environments VII*, vol. 4134, San Diego, CA, 2000, Proceedings Paper, pp. 176–184.

[220] D.-S. Shin *et al.*, "Low-Detuning Operation of Electroabsorption Modulator as a Zero-Bias Optical Transceiver for Picocell Radio-Over-Fiber Applications," *IEEE Photonics Technol. Lett.*, vol. 20, pp. 951 –953, Jun. 2008.